

DISSERTATION

COMMUNITY RISK DUE TO WILDLAND URBAN INTERFACE FIRES: A TOP-DOWN
PERSPECTIVE

Submitted by

Akshat Chulahwat

Department of Civil and Environmental Engineering

In partial fulfillment of the requirements

For the Degree of Doctor of Philosophy

Colorado State University

Fort Collins, Colorado

Summer 2021

Doctoral Committee:

Advisor: Hussam Mahmoud

Bruce Ellingwood

John van de Lindt

Camille Stevens-Rumann

Copyright by Akshat Chulahwat 2021

All Rights Reserved

ABSTRACT

COMMUNITY RISK DUE TO WILDLAND URBAN INTERFACE FIRES: A TOP-DOWN PERSPECTIVE

Recent wildfire events, in the United States and around the world, have resulted in thousands of homes destroyed and many lives lost, leaving communities and policy makers, with the question as to how to manage wildfire risk. Wildland urban interface fires have demonstrated the unrelenting destructive nature of these events and signify the need to address the problem. This is particularly important given the prevalent trend of increased fire frequency and intensity. Current approaches to managing wildfires focus on fire suppression and managing fuel build-up in wildlands. Frequent suppression of small scale fires has led to the absence of a natural reduction mechanism, which in turn, results in low frequency high intensity fires. This phenomena has been termed as the Wildfire paradox and it reinforces the ideology that wildfires are inevitable and are actually beneficial; therefore focus should to be shifted towards minimizing potential losses to communities. However, reliance on these strategies alone has clearly proven inadequate. This requires the development of vulnerability-based frameworks that can be used to provide holistic understanding of risk. Mitigation strategies geared towards complete containment of wildfires within the wildlands are unrealistic. Therefore, the primary goal has to be on making communities resilient, with the purpose of minimizing potential losses. There is a paucity of information regarding the interplay between communities and wildfires. Unlike other hazards, for which there exists significant knowledge base, quantification of WUI fires is still an unanswered question for us. To better understand what factors govern the impact of WUI fires, tools to assess and quantify the risk of wildfires to communities are required.

In this study, a probabilistic approach for quantifying community vulnerability to wildfires by applying concepts of graph theory is devised. A directed graph is developed to model wildfire

inside a community by incorporating different fire propagation modes. Four modes are considered in this study - Convection, Radiation and Embers, and individual ignition models for each are formulated. Through these modes the graph model accounts for relevant community-specific characteristics including wind conditions, community layout, individual structural features, and the surrounding wildland vegetation. The graph model is then used to evaluate vulnerability of each component of the community using shortest path algorithms. The framework is utilized to study the infamous 1991 Oakland fire in an attempt to unravel the complexity of community fires. Centrality measures from graph theory are used to identify critical behavior patterns and evaluate the effect of fire mitigation strategies.

Using the vulnerability framework developed, the risk of communities is further quantified. Risk is generally defined by three components - (1) Hazard intensity (2) Degree of exposure and (3) Exposed elements. In context of wildfires, the risk is formulated by combining the following three components - probability of wildland ignition, probability of fire reaching the community and vulnerability of community. Four different communities across the United States are selected and risk analysis is conducted for the months May-September to understand the correlation between community risk and community characteristics. Unlike current practice, the results are shown to be community-specific with substantial dependency of risk on meteorological conditions, environmental factors, and community characteristics and layout. For the final part of this study, an intervention optimization is formulated and applied to the four communities to observe the effect of different intervention measures on community risk. The findings show the need for exploring unique viable solutions to reduce risk for communities independently, as opposed to embracing a generalized approach, which is currently the case.

ACKNOWLEDGEMENTS

I would like to express my sincerest gratitude to my advisor, Professor Hussam Mahmoud, without whom this thesis would never have been possible. His constant guidance and support all these years, not just academically but also on a personal level, has brought me to this point in life, and for that I will always be grateful to him. This Ph.D. under his mentorship has been an exceptional experience for me.

I would like to thank all the committee members, Professor Bruce Ellingwood, Professor John van de Lindt and Professor Camille Stevens-Rumann for their insightful suggestions and support. I would like to acknowledge the Department of Civil and Environmental Engineering at Colorado State University and its dedicated staff, who have helped me over the years numerous times. I would also like to thank all the friends that I made during this endeavor. Every one of them has helped and inspired me.

Finally, I would like to thank my dearest parents who have supported me every step of the way and provided encouragement when I needed it the most. They have always been my inspiration to keep going.

DEDICATION

I would like to dedicate this thesis to my dearest parents

TABLE OF CONTENTS

ABSTRACT	ii
ACKNOWLEDGEMENTS	iv
DEDICATION	v
LIST OF TABLES	viii
LIST OF FIGURES	ix
Chapter 1 Introduction	1
1.1 Motivation	4
1.2 Research Significance	5
1.3 Research Objective and Scope	6
Chapter 2 Literature Review	10
2.1 Background	10
2.2 Analytical Methods	11
2.3 Numerical Methods	14
2.4 Experimental Methods	16
2.5 Code Provision and Guidelines	17
Chapter 3 Wildland Propagation Model	21
3.1 Effect of Wind	23
3.2 Effect of Topography	24
3.3 Ember Spotting	26
3.4 Wildland Model Validation and Calibration	28
Chapter 4 Community Propagation Model	31
4.1 Convection Model	34
4.2 Radiation Model	39
4.2.1 View Factors Calculation	41
4.2.2 Radiation Matrix	43
4.2.3 Radiation Ignition	49
4.3 Ember Spotting Model	51
4.4 Community Model Validation	57
Chapter 5 Community Vulnerability and General Observations	59
5.1 Introduction	59
5.2 Vulnerability Evaluation	59
5.2.1 Shortest Path Algorithm	62
5.2.2 Polar Fragility	66
5.3 Intervention Framework	68
5.4 Community Analysis Results	70
5.4.1 Community inherent vulnerability	71
5.4.2 Effect of Individual Ignitable Elements	72

5.4.3	Effect of Fire Intervention	78
5.4.4	Effect of Wildlands	80
5.4.5	Identifying Flow Paths	82
5.4.6	Computational resources and observations	84
Chapter 6	Risk Assessment and Intervention Strategy Optimization	88
6.1	Risk Framework	88
6.1.1	Background and modeling details	89
6.1.2	Wildland Ignition Probability	92
6.1.3	Community Susceptibility	96
6.1.4	Wildland Propagation Probability	96
6.2	Case Study: Risk Analysis of Archetypal Communities in United States . .	102
6.3	Intervention Strategy Optimization	107
6.3.1	Intervention Framework	107
6.3.2	Optimization Framework	110
6.3.3	Optimization Tests	114
Chapter 7	Conclusions and Future Work	118
Bibliography	121
Appendix	136

LIST OF TABLES

4.1	Classification of ignitable elements based on their ignition capacity	33
4.2	Convection model parameter values	37
4.3	Radiation model parameter values	50
4.4	Relative access probabilities for different type of ignitable elements	52
4.5	Ember model parameter values	56
5.1	Details for each community layout	72
5.2	Kendall rank correlation (τ) for degree centrality of region O_I at different wind speeds	76
5.3	Kendall rank correlation (τ) for degree centrality of region O_{II} at different wind speeds	76
5.4	Computational details for the test cases	85
6.1	Details for each community layout	90
6.2	Pearson correlation values between risk (R), vulnerability of community (V) and probability of wildland ignition (P_i), for each community	105
6.3	Effectiveness of different intervention measures	108

LIST OF FIGURES

1.1	Different stages involved in wildland urban interface fires	7
1.2	Components of proposed framework	7
3.1	Different states of cells considered in the Cellular Automata model	22
3.2	Segmentation of cell space based on wind direction	24
3.3	A sample simulation showing effect of wind speed and direction on fire propagation	25
3.4	Topography layout of test scenario	26
3.5	A sample simulation showing effect of topography on fire propagation	26
3.6	A sample simulation showing effect of ember spotting on fire propagation. (a) Fire propagation patterns with time (b) Ember generation and landing patterns	28
3.7	Fire Front shapes obtained from [106] under (a) absence of wind and (b) wind from west to east	29
3.8	Fire Front shapes obtained from proposed algorithm under (a) absence of wind and (b) wind from west to east	30
4.1	A sample representation of actual community layout (Fort Collins, Colorado, USA) as a graph network. The nodes of each element define its specific boundary and the edges represent the potential fire propagation paths (Map data ©OpenStreetMap contributors [107])	32
4.2	Variation of convection threshold distance (radial axis in m) for different wind directions (polar axis in degrees) for two cases of different node heights - (i) 2.5 m and (ii) 5 m, when the angle between the source and target ignitable element is 90°	36
4.3	Variation of flame length (x-axis) with varying wind speeds (y-axis) for two cases of different node heights - (i) 2.5 m and (ii) 5 m	38
4.4	Procedure shown for calculating net radiative heat flux exchange between two ignitable elements such that element m is ignited.	43
4.5	Ember ignition probabilities as a function of distance x for different values of volume $V_n^{(i)}$ and wind speed v_w	57
5.1	Procedure for evaluating probability of ignition for any source node s inside the community due to the wildlands Ω (©OpenStreetMap contributors [107])	61
5.2	Calculation of vulnerability of destination element (D) due to source element S for a part of an actual community Hacienda Heights, Los Angeles, CA. (a) Fire pathways shown for wind direction $\theta = 300^\circ$ (b) Fire pathway shown for wind direction $\theta = 60^\circ$ (c) Fragility curve to represent variation in vulnerability of element D for different wind directions (θ) and wind speed v_w (©OpenStreetMap contributors [107])	67
5.3	Active and Passive intervention formulations applied to the graph theory model	70

5.4	Region of Oakland affected by the 1991 wildfire along with the point of origin. Two regions are selected for analysis (a) Region O_I with wind direction $\theta = 225^\circ$ and (b) Region O_{II} with wind direction $\theta = 300^\circ$. For both regions vulnerability for each element is calculated from the source in their respective layouts. Significantly high vulnerability of all elements observed in both layouts in absence of any fire mitigation (©OpenStreetMap contributors [107])	71
5.5	Eigenvector centrality of region O_{II} for wind directions (a) $\theta = 300^\circ$ (b) $v_w = 60^\circ$ (c) $v_w = 180^\circ$ (©OpenStreetMap contributors [107])	73
5.6	Bonacich centrality of region O_{II} for (a) $\beta = 0.75$ (b) $\beta = 0.50$ (c) $\beta = 0.25$ (d) $\beta = 0.10$ (©OpenStreetMap contributors [107])	74
5.7	Degree centrality of region O_I for wind speeds (a) $v_w = 29.058$ m/s (b) $v_w = 10$ m/s (c) $v_w = 5$ m/s (d) $v_w = 1$ m/s (©OpenStreetMap contributors [107])	75
5.8	Degree centrality of region O_{II} for wind speeds (a) $v_w = 29.058$ m/s (b) $v_w = 12.5$ m/s (c) $v_w = 10$ m/s (d) $v_w = 5$ m/s (e) $v_w = 1$ m/s (©OpenStreetMap contributors [107])	76
5.9	Transitivity of region O_I for (a) $v_w = 29.058$ m/s and (b) $v_w = 0$ m/s (©OpenStreetMap contributors [107])	77
5.10	Transitivity of region O_{II} for (a) $v_w = 29.085$ m/s and (b) $v_w = 0$ m/s. The magnified snapshot shows certain ignitable elements with low area to exhibit high transitivity values (©OpenStreetMap contributors [107])	78
5.11	Vulnerability distributions obtained for $N = 100$ iterations at different intervention strengths (μ) for (a) region O_I (b) region O_{II} . The lower and upper edges of the box correspond to the 25th and 75th percentile, the center dot represents the median and circular markers represent the outliers	79
5.12	Effect of fire intervention (mitigation) showed for (a) region O_I and (b) region O_{II} of Oakland at intervention strength $\mu = 50\%$ for different wind speeds to highlight significance of intervention strategy. Vulnerability distributions are calculated for $N = 100$ iterations at each wind speed and the efficiency of strategy η is measured as the standard deviation for each distribution	80
5.13	Vulnerability distribution of region O_I for source locations observed during 1991 Oakland fire (Reconstructed from [129]) (©OpenStreetMap contributors [107])	82
5.14	Total community vulnerability shown at each element when that specific element is considered as a source. With each iteration the element which results in maximum community vulnerability is added to the list of sources. The figures show the change in community vulnerability for region O_I as sources are added for iteration (a) $i = 1$ (b) $i = 2$ (c) $i = 3$ (d) $i = 4$ (e) $i = 5$ (©OpenStreetMap contributors [107])	83
5.15	Maximum probability flow paths at wind speed $v_w = 29.058$ m/s, considering only short-range propagation modes - radiation and convection, for regions (a) Hacienda Heights ($v_w = 300^\circ$) (b) Oakland region O_I (c) Oakland region O_{II} (©OpenStreetMap contributors [107])	84
5.16	Community layout showing spatial discretization (Map data ©OpenStreetMap contributors [107])	87
6.1	Community layouts for (a) Austin (Texas) (b) Jackson (Wyoming) (c) Oakland (California) (d) Steamboat (Colorado) (Map data ©OpenStreetMap contributors [107])	91
6.2	Sample wildfire ignition data from WFAS Archives	92

6.3	Probability of ignition (P_i) in months May-September for years 2007, 2012 and 2017 for Austin (Texas)	94
6.4	Probability of ignition (P_i) in months May-September for years 2007, 2012 and 2017 for Jackson (Wyoming)	94
6.5	Probability of ignition (P_i) in months May-September for years 2007, 2012 and 2017 for Oakland (California)	95
6.6	Probability of ignition (P_i) in months May-September for years 2007, 2012 and 2017 for Steamboat Springs (Colorado)	95
6.7	An example of Vulnerability map for Austin (Texas)	97
6.8	An example of Vulnerability map for Jackson (Wyoming)	98
6.9	An example of Vulnerability map for Oakland (California)	98
6.10	An example of Vulnerability map for Steamboat Springs (Colorado)	99
6.11	Community vulnerability (V) in months May-September for years 2007, 2012 and 2017 for Austin (Texas)	99
6.12	Community vulnerability (V) in months May-September for years 2007, 2012 and 2017 for Jackson (Wyoming)	100
6.13	Community vulnerability (V) in months May-September for years 2007, 2012 and 2017 for Oakland (California)	100
6.14	Community vulnerability (V) in months May-September for years 2007, 2012 and 2017 for Steamboat Springs (Colorado)	101
6.15	WUI fire risk in months May-September for years 2007, 2012 and 2017 for Austin (Texas)	103
6.16	WUI fire risk in months May-September for years 2007, 2012 and 2017 for Jackson (Wyoming)	103
6.17	WUI fire risk in months May-September for years 2007, 2012 and 2017 for Oakland (California)	104
6.18	WUI fire risk in months May-September for years 2007, 2012 and 2017 for Steamboat (Colorado)	104
6.19	Polar fragilities for (a) Austin (Texas) (b) Jackson (Wyoming) (c) Oakland (California) (d) Steamboat Springs (Colorado) at wind speed $V_w = 15$ m/s	107
6.20	List of different intervention strategies Λ	113
6.21	Optimal cases for different importance factor combinations for Steamboat Springs (Colorado)	114
6.22	Vulnerability, intervention cost and total fitness digram shown for Austin	116
6.23	Vulnerability, intervention cost and total fitness digram shown for Jackson	116
6.24	Vulnerability, intervention cost and total fitness digram shown for Oakland	117
6.25	Vulnerability, intervention cost and total fitness digram shown for Steamboat	117

Chapter 1

Introduction

Wildfire intensity and occurrence rate have been observed to increase alarmingly in recent years [1]. The consequences of these wildfires, particularly when interacting with communities, have been dire and have resulted in substantial socio-economic losses all over the world [2, 3]. In the U.S. alone, the year 2018 has experienced the most catastrophic wildfire season on record in California, resulting in 7,579 fires that burned a total of 1,667,855 acres (674,957 ha), the largest amount of burned acreage recorded in a fire season. The fires have caused more than \$2.975 billion (2018 USD) in damages, including \$1.366 billion in fire suppression costs. Even in 2017, the year before that, exhibited similar pattern of events both in frequency and intensity, such as the Tubbs Fire, which was named the most destructive fire before the Camp Fire of 2018, the Thomas fire, which caused over US \$2.2 billion in damages and US \$230 million in suppression costs and the North Bay fire, which included 14 wildfires across California, burned over 245,000 acres, torched 8,800 homes and claimed the lives of 42 people, making it one of the most deadly wildfires in the history of the state. The infamous 2016 Canada McMurray Fire, which burned through 1,500,000 acres, causing destruction of approximately 2,400 homes and forcing an excess of 88,000 people to flee their homes. Classified as the costliest disaster in Canadian history, the corresponding economic losses reached approximately C(\$9 billion). These events are just few examples of the level of destruction observed in wildfire events in the last few years. There are numerous other wildfire events that have left a mark on the world, including the recent Attica wildfires in Greece [4] and the 2018 Australian bushfires, among others. The most surprising of all are the multiple fires in a small Swedish town Lapland of Jokkmokk, which lies in the Arctic circle [5]. The recent devastating nature of these events is a testimonial to the fact that not only the intensity of wildfires are on the rise [6–8], but also the fire season is elongating as well [9, 10]. As of now, the yearly federal expenditures on managing wildfires easily exceeds US\$1 billion per year [1], and is only expected to rise given the prevalent trend. The collective damages incurred

in the U.S. due to wildfires in the year 2017 amounted to approximately US \$18 billion. The UN Intergovernmental Panel on Climate Change (IPCC), comprised of 192 nations, recently released the landmark report that forewarns the immediate need to take action to curb the rise in climate change. Therefore, there is a present need to devise proper strategies to mitigate the impact of wildfire. Suppression and management of fuel build-up in wildlands has been the primary focus for managing wildfires, which has proven to be insufficient [11–14].

There are several wildfire protection programs, such as Firewise, aimed at the community level to inform residents of useful fire protection measures. These commonly include managing defensible spaces around houses, using fire retardant materials and using automatic fire suppression systems. While significant efforts are placed every year on increasing population awareness towards fire mitigation practices, no clear quantitative design policies exist. Currently, wildfire suppression is aimed at severe fire suppression that has led to reduction in controlled small-scale fires, which aid in reducing wildland density and provide an ecological balance. In the absence of any natural reduction mechanism and given the limited fuel management strategies, rapid growth in wildland ecology has resulted in significant increase in high intensity wildfires [12, 15]. Population residing in the wildland urban interface is on the rise and expected to further increase [16], which has led to significant increase in exposure of communities to wildfires. A recent study [17] showed that almost 84% of the wildfire incidents are a result of human actions, which correlates with the previous statement. In light of these developments, a shift in wildfire management paradigm is required such that mitigation efforts are geared towards wildland urban interface as well. Appropriate attention needs to be placed on communicating and regulating community risk as well [12, 18].

Most studies on wildfires are biased towards wildlands. There is paucity of literature on dynamics of community wildfire propagation. Many researchers believe more attention should be paid to fire regulation needs, in addition to wildland management, for communities to coexist with nature. Calkin et al. [12] discussed this paradigm for controlling wildfire risk. Wildfires are a part of nature, both inevitable and necessary, pointing to only one foregone conclusion - Wildfire management needs to be driven by regulating vulnerability of communities [12, 18] by making

communities resilient to wildfire events. The concept of “Resilience,” in the context of civil engineering, is generally described as the ability of a community to withstand external shocks to its infrastructure components and recover from such shocks efficiently and effectively. With the increasing intensity of natural hazards every year, the focus of research community has shifted towards assessing resilience of communities to these events. Such that informed decisions can be made to create robust communities which experience minimal damage and can be recovered efficiently. Resilience comprises of two components - (1) Initial damage phase and (2) Recovery phase. The former relates to the damage incurred by a community due to a specific type of hazard and the latter relates to the recovery of critical infrastructures within a community with time. Since each hazard has a different impact on community, resilience for each hazard needs to be quantified separately by formulating damage models for corresponding hazards. There have been several comprehensive frameworks established for different hazards such as - earthquakes [19], floods [20], hurricanes [21, 22], tornadoes [23–25] and Tsunamis [26]. However, wildfire risk has not been quantified yet in such manner, which makes it difficult to assess resilience of communities to wildfires.

The full realization of wildfire risk assessment and management requires the use of advanced analytical and numerical tools. The most accurate tools are arguably those that are based on computational fluid dynamics (CFD). However, CFD models are computationally very expensive and their use in very large problems (i.e. community level analysis) is currently not feasible. With advances in computational infrastructure, in the near future, the use of CFD models will become a reality. However, with the risk of wildland urban interface (WUI) fires on rise each year, communities cannot afford to wait for the computational technology to match the complexity of the problem. With this in mind, the pressing need lies in exploring alternative directions for quantifying and studying WUI risk of communities.

1.1 Motivation

Wildfires are a natural phenomena, similar to other natural hazards. However, only recently (spring 2018) the Wildfire Disaster Funding Act (H.R. 2862) was passed by congress, in which wildfires were classified as a natural hazard just like hurricanes, floods, and earthquakes [27]. An abundance of detailed knowledge exists on risk quantification of other hazards [28, 29]. In case of earthquakes, for example, we understand the underlying factors that govern infrastructure damage potential. For instance the depth of focus from the epicenter, the fault rupture mechanism, and the proximity of the infrastructure to fault lines are all factors that affect the damage potential. Some other factors include type of soil, water content within the soil, among several others. Damage potential from wildfires lack the same level of details as other hazards. Even though wildfires can be classified as a natural disaster they do not necessarily behave in a similar fashion as other hazards. Wildfire is the only natural hazard in which the intensity of the hazard increases with time in proportion to the volume of damage caused. The ignitable structures act as fuel to the ongoing fire and result in an increase in spread. The yearly funding appropriated to any hazard is limited. Given the rise in population living near the wildland urban interface [16, 30, 31] and the changing climate it is essential that optimized allocation of funding is considered for mitigation procedures. In order to do that an unanswered question still remains - Have we quantified the underlying factors involved in wildfire events and do we understand their importance relative to each other?

Wildfire mitigation is primarily focused on complete fire suppression and control [32], which ultimately results in high expenditure [33, 34]. Emphasis on public lands within and adjacent to communities provides some relief but falls short of the level of mitigation required to impact the susceptibility of communities [33]. Essentially, current management practices have continued with the approach that has led us to the wildfire paradox by framing the WUI fire disaster as a wildfire control problem, instead of focusing on the susceptibility of structures to the inevitability of wildfire exposure. Several researchers [32, 33, 35, 36] have found that the characteristics of a home determine home ignition potential to a great extent as compared to its immediate surroundings. In addition, some researchers [37] have also found that community layout is a critical factor gov-

erning the likelihood of household ignition. There are other factors as well, pertaining to built environment properties, such as - housing density, fuel load and moisture, weather and some others [38]. Primary responsibility for preventing home destruction lies with homeowners rather than public land managers. Adequate metrics are required to quantify the ignition potential of individual households within a community such that informed mitigation decisions can be made, both, by the authorities and household owners and to provide better understanding of the factors governing wildfire behavior.

1.2 Research Significance

With the increasing communities at the wildland urban interface the concern for developing fire resilient communities is ever pressing. There are several models on quantifying wildfire risk in context of wildlands. However, currently there does not exist any computationally efficient model to quantify risk of communities to WUI fires. Even urban planning and structural guidelines incorporate limited form of design requirements for wildfires. Wildfires are dissimilar to other hazards such as earthquakes, floods and tsunamis. For any natural hazard event, the source of disturbance has an independent effect on each structure. Generally, with some exceptions, the performance of any one structure under the hazard does not affect the performance of other structures under the same hazard. In case of wildland urban interface fires, the probability of a house catching fire is strictly dependent on the probability of other houses around it getting ignited. Each individual structure when ignited not only propagates the fire to neighboring structures but also generate embers, which further increase the likelihood of other structures igniting.

This propagation behavior of WUI fires inside a community can be considered similar to that of systemic transmission of diseases in a social network. Graph theory has been widely utilized to understand disease transmission [39–45], which has provided unparalleled advances in the field. Similarly, a graph theory model might be able to provide a better understanding of global behavior of WUI fires in communities as well. There are Computational Fluid Dynamics models that are able to successfully capture the wildfire dynamics within a community, however, their significant

computational requirement restricts their application to practical purposes. Graph models, on the other hand, have been known to be sufficiently efficient in terms of practical applications.

1.3 Research Objective and Scope

There has been prolific increase in studies focused on quantifying community resilience following extreme events in the U.S. including major efforts through the NIST-funded Center of Excellence for Community Resilience Planning led by Colorado State University (CSU), of which this study is part of. Measured by the recovery process, resilience studies have focused on infrastructures, social, or economic recovery [46–48]. However, a prerequisite for any resilience analysis is quantification of structural damage caused by the hazard. Various analytical, numerical, and experimental methods have been utilized to obtain such quantification under various hazards. While this quantification in the case of structural fire does exist [49,50], proper tools for community level assessment under fire, whether caused by earthquakes or wildfires, are still lacking. As such, the focus of this study is to provide a computationally efficient platform for studying the interaction of wildland urban interface (WUI) fires with communities to quantify wildfire risk, which is an essential ingredient for any future resilience analysis.

A WUI fire is a special case of wildfire which initiates in the wildlands but continues to proceed into a community. The general steps involved in a WUI fire can be classified into - (1) Wildfire initiation in the wildlands (2) Wildfire propagation from the internal regions of wildland to the wildland-urban interface (3) Ignition of ignitable areas inside community; and (4) Propagation of fire to different parts of community (Fig. 1.1). In accordance with this classification, the study is primarily conducted in two major parts - (1) Propagation within wildlands and (2) Propagation inside communities (Fig. 1.2). However, the study is kept biased towards the latter since there is an abundance of research related to the former.

For the first component, theory of Cellular Automata (CA) is used to formulate a two-dimensional dynamic wildfire propagation model. In doing so, the propagation mechanism of wildfire is modeled by a set of rules in CA to account for short- and long-range heat transfer mechanisms and the

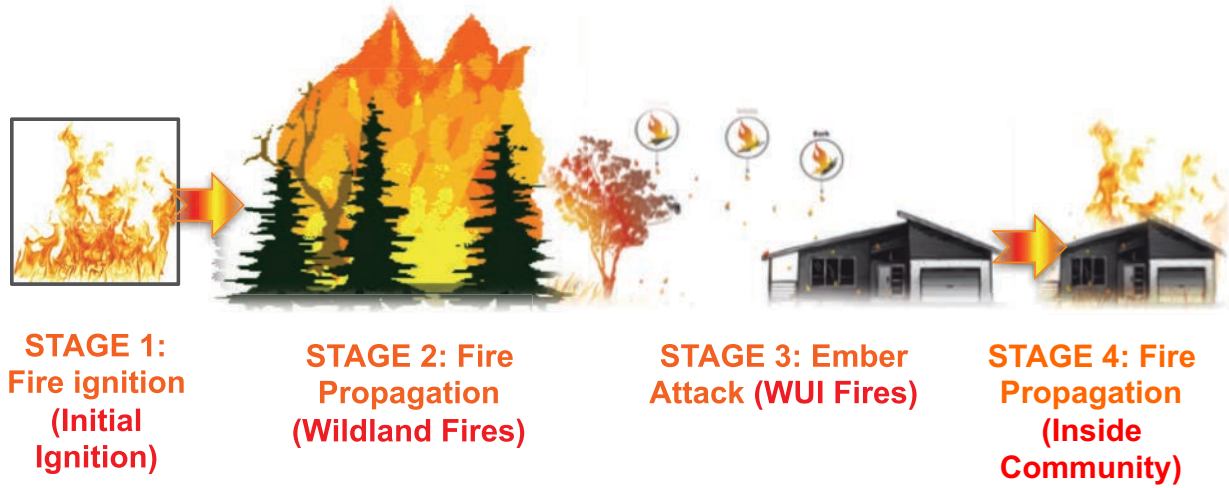


Figure 1.1: Different stages involved in wildland urban interface fires

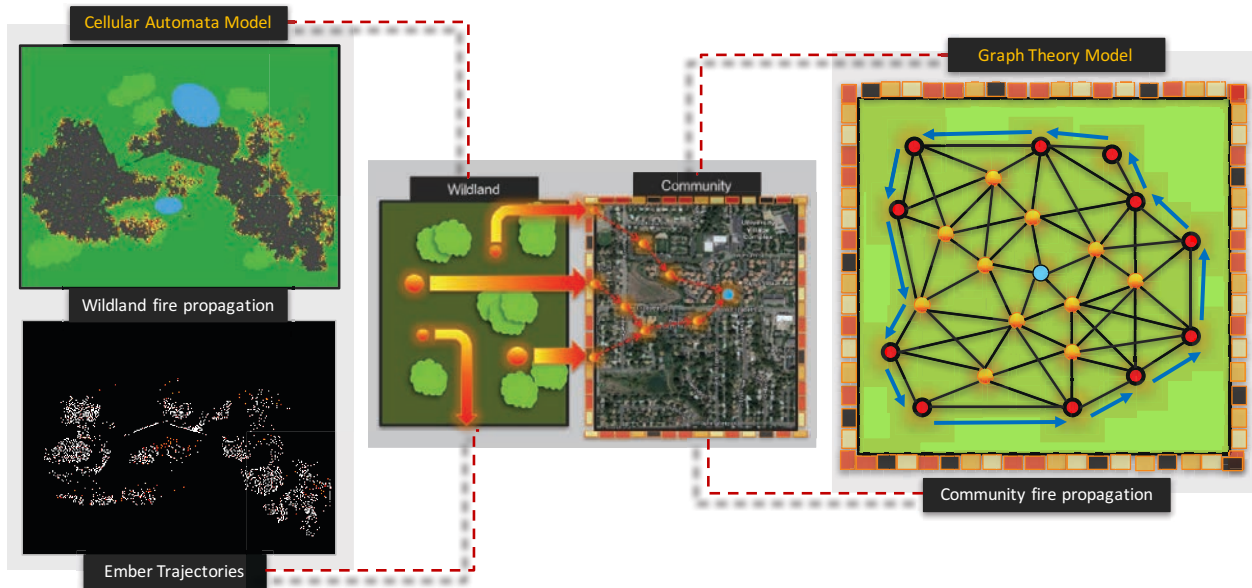


Figure 1.2: Components of proposed framework

rules are defined so as to include the effect of external factors, including but not limited to, wind conditions (direction and speed), topography and vegetation properties. To model the behavior of wildfire inside communities concepts of graph theory [39–41] are used. A directed graph for community in question is developed to model wildfire inside a community by incorporating different fire propagation modes. The model accounts for relevant community-specific characteristics including wind conditions, community layout, individual structural features, and the surrounding wildland vegetation. Vulnerability of individual components of community is evaluated using concepts of shortest path such that overall exposure of a community can be evaluated. Effect of fire mitigation measures within communities are also incorporated to account for community response. The framework is tested to draw out meaningful conclusions on the behavior pattern of WUI fires and the role of individual components in a community. Finally, the community propagation model is utilized to evaluate risk of some communities in US to wildfires.

Chapter 2 provides a background of the analytical, numerical and experimental methods developed in fire research on wildfire propagation. Various code provisions and guidelines for wildfire mitigation, currently implemented in US, are also discussed. Chapter 3 provides the theoretical development of a probabilistic wildland fire propagation model based on concepts of Cellular Automata. Implementation of both short- and long-range propagation mechanisms in the wildland model are described. In addition, effects of fuel density, wind conditions and topography are incorporated into the model. Chapter 4 describes the development of a probabilistic community wildfire propagation model based on concepts of graph theory. Individual sub-models for different modes of heat propagation are described that form the basis for the proposed graph model. In Chapter 5, the steps involved in evaluating individual ignitable element vulnerability, as well as, entire community vulnerability are discussed using the graph formulated in the previous chapter. A new type of fragility to quantify vulnerability of different parts of communities to wildfires is introduced. Results of tests conducted on parts of different communities in Oakland, which includes - vulnerability analysis of community under similar conditions as 1991 Oakland fire, study of wildfire propagation dynamics using graph Centrality measures and studying the effects of fire intervention

and wildlands on community vulnerability are also shown. In Chapter 6 the framework for evaluation of risk is discussed, along with the individual components involved in it. The results from risk analysis on four different communities across United States are shown and discussed, followed by a theoretical foundation to incorporate and quantify the effects of fire mitigation/intervention measures inside communities, such that wildfire vulnerability can be captured more accurately. An optimization framework is combined with the intervention framework to explore and better understand optimal intervention measures in communities for different communities.

Chapter 2

Literature Review

2.1 Background

There exist several models on wildfires, all of which can be namely classified into three categories – Analytical, Numerical and Empirical. Each type possesses certain strengths and limitations. For instance, analytical models are computationally efficient since they are an approximate mathematical representation of the actual behavior. These are specifically advantageous for emergency planning purposes as they can be employed as preliminary tools; however, they cannot be used in comprehensive analysis, where local or minute behaviors are of interest. Numerical models on the other hand involve modeling the fundamental physics of the problem, which in case of wildfire is best described by coupled dynamic fluid-flow and thermodynamic equations. As a result, these can be highly accurate but are mostly non user-friendly and can result in impractical processing time. These models are specifically used for research purposes. Currently, all numerical wildfire models suffer from exaggerated computation time, making them impractical for high number of simulations. The empirical models as the name suggests are strictly data based. These models are fundamentally easy to use; however, their applicability is restricted to cases similar to the reference data used for calibration.

Other than these 3 primary classifications hybrid models have also been developed which share traits with more than one classification. The data-driven models are a recent addition to wildfire research and can be considered as hybrid models. Data-driven models utilize extensive data to calibrate approximate models, which can be either a numerical or analytical, to increase their accuracy. The strict dependency of these models on data hinders their widespread application in investigating wildfires since one of the major problems in quantifying fire behavior up till now has been lack of pertinent physical data. Another class of hybrid models consist of a cross between analytical and numerical models, such that only a certain portion of the behavior is modeled using

physical principles and the rest is compensated using mathematical concepts. These models have a lower dependency on data than empirical models and at the same time do not have impractical computation requirements. The main concern with these types of models is their respective formulation, which therefore requires careful deliberation to arrive to effective formulations.

There exist several wildfire propagation models that are currently being used by fire management agencies and researchers all over the world. These models encompass different types (as discussed above) ranging from empirical to completely analytical. Some prominent examples include - Rothermel's wildland fuel model [51], National bushfire model [52], BehavePlus [53], FlamMap [54, 55], FARSITE [56], FSPro [57], WIFIRE [58] and others [59, 60]. These models are widely accepted and entail several aspects of wildfires; however, the models either entirely focus on wildlands or pertain to a localized aspect of fire propagation in communities. While robust computational fluid dynamic (CFD) models exist for simulating structure-fire interactions on a community scale [61], their complexity and computational demand prevent their widespread application. The physics involved in modeling wildfire propagation is computationally expensive, as it pertains to solving simultaneous fluid-thermodynamic differential equations. The lack of requisite data for wildfires further prevents better understanding and modeling of wildfires let alone their interaction with communities. With advances in computational infrastructure, in the near future, the use of CFD models will become a reality. Other fire propagation models have been explored in the past using concepts of graph theory, both for wildlands [62–64] and urban settings [65, 66]. These models provide a better alternative to the ones discussed, however, their focus has been either on wildlands entirely or on urban fires, as a result, they do not incorporate all factors involved in WUI fires.

2.2 Analytical Methods

Rothermel's wildland fuel spread model [51] is considered as one of the most widely used fire propagation models and has been successfully utilized in various simulation programs. The model is based on extending the work by Frandsen [67] and comprises a mathematical expression

for predicting the rate of fire growth. In the model, conservation of energy principle is applied to a unit volume of fuel ahead of an advancing fire in a homogeneous fuel bed. The model is complete in the sense that no prior knowledge of a fuel's burning characteristics is required and only the inputs describing the physical and chemical makeup of the fuel and the environmental conditions in which it is expected to burn are needed. The general inputs taken by the formula are fuel loading, fuel depth, fuel particle surface-area-to-volume ratio, fuel particle heat content, fuel particle moisture and mineral content, and the moisture content. The model has been subjected to some direct verification tests such as in logging slash assembled fuel beds [68] for both prescribed and wild grass fires [69]. Stevenson and others [70] were also able to match observations and predictions of spread rate in mixed chaparral-like fuels using Rothermel's model in conjunction with an area-growth computer algorithm.

Albini [59] presented a mathematical model to predict maximum spot fire distances. This work has laid the foundation for several other models, such as the BEHAVE model of USDA [53], which uses a simplified modification of Albini's work. Albini's spotting model hinges on the concept that, regardless of the source, all firebrand trajectories are similar except for the first phase of the trajectory in which the lofting height (initial firebrand height) is attained. In order to implement the simplified method for calculating lofting heights from wind-driven surface fires, Albini modeled fireline intensity pulses that cast firebrands aloft using a best-fit frequency spectrum, which measures the thermal energy in a pulse. Albini proposed a simpler model, called the 'lofting energy model' [71], which is a simplification of the previous model. The two parameters are fuel-dependent and must be computed for each condition of fuel type and moisture. The lofting energy model estimates mean thermal energy per foot of fireline at the front of wind-driven surface fires spreading at a uniform rate under suitable burning conditions.

Knight and Coleman [52] used Huygen's principle to model the spread of the perimeter of a wildfire as part of the National Bushfire Model. They suggested that a perimeter of a fire can be regarded as a continuous curve or as a discrete number of points approximating such curve. This is also known as the fire front in several studies. Each point on the perimeter can be considered

as a point source, which expands as a small ellipse. The parameters of each ellipse are a function of the local fuel type, slope, meteorological conditions and the time step. According to Huygens' principle, the envelope of these ellipses describes the new perimeter. Problems with this approach arise when the terrain and fuel are discontinuous, causing the perimeter to become complex and develop concavities. Some other studies have also used Huygens' principle for the propagation of a fire shape [56, 72–77]. However, these models require intensive measures to correct crossing segments on the fire edge and to merge multiple fronts [52, 56, 78]. To alleviate this problem, Finney [62] approached the propagation modeling as a search for the minimum time for fire to travel among nodes in a two-dimensional network. The paths producing minimum travel time between nodes are then interpolated to reveal the fire perimeter positions at an instant in time. These fire perimeters and their fire behavior characteristics (e.g. spread rate and fireline intensity) are essentially identical to the products of perimeter expansion techniques. Travel time methods offer potential advantages for some modeling applications, because they are more readily parallelized for computation than methods for expanding fire fronts and require no correction for crossed fronts or merging separate fires. Cohen [33] proposed a model to understand the effects of fire radiation on structures. They developed a thermal radiation and ignition model to estimate structure ignition potential using various types and densities of vegetation and flame-to-structure distances. Model results indicated that ignitions from flame radiation are unlikely to occur from burning vegetation beyond 40 meters (131.23 ft) of a structure and thinning vegetation within 40 meters (131.23 ft) reduces the effect of ignition significantly. Woycheese and others [79] also proposed an analytical model to determine fire brand propagation. They considered factors such as plume velocity fields, brand size and shape distributions, time varying wind velocities, combustion rates and terrain effects. The study assumed brands to be spherical in nature and utilized the concept of mechanics to determine the equations for maximum brand propagation distance. Several other analytical models have been formulated and tested over the years. These models have formed the basis for several numerical models and have led to the advancement in the field of WUI fires analysis.

2.3 Numerical Methods

Recent advancement in computational methods and numerical techniques have resulted in an increase in the application of numerical methods in almost all fields of science. The advantages of using numerical methods lie in the fact that they are cost effective and can be a substitute to experimental studies, providing a better perspective in some cases. In light of the high uncertainties in the risk poses by WUI fires, several numerical models have been developed in the last decade to emulate real-time behavior of fire. The most successful fire propagation models at present are the ‘Fire Dynamic Simulator’ (FDS) [61] and its extension - the ‘Wildland-Urban Interface Fire Dynamic Simulator’ (WFDS), developed by the National Institute of Standards and Technology (NIST). The FDS is a computational fluid dynamics model of fire-driven fluid flow. The software solves numerically a large eddy simulation form of the Navier–Stokes equations that is appropriate for low-speed, thermally driven flow, with an emphasis on smoke and heat transport from fires. Smoke generated during wildfires is a source of concern for the community as it impedes fire suppression efforts. Thus, it is important to consider behavior of smoke while considering a plan of action against any wildfires and community evacuation. NIST developed a smoke visualization tool ‘Smokeview’ [80] to visualize the data from FDS. It utilizes numerical simulations generated by the FDS to calculate the changing distribution of smoke, fire gases, and temperature. BehavePlus [53] is another fire behavior software which accounts for a variety of fire parameters such as rate of spread, spotting distance, scorch height, tree mortality. In addition, fire environment parameters such as fuel moisture and wind adjustment factor are also included. BehavePlus is part of a suite of fire behavior systems that includes FlamMap [54, 55], FARSITE [56], and FSPro [57]. The FlamMap fire mapping and analysis system does fire behavior calculations for each point on the landscape with fuel moisture and wind constant in time. The FARSITE fire area simulator models fire growth under conditions that vary in both space and time. The fire behavior at a point (pixel) depends on the fire spreading from adjoining pixels and the conditions at the time it burned. The FSPro fire spread probability system performs hundreds or thousands of separate fire growth simulations from weather sequences based on climatology. Under the Landscape Fire

and Resource Management Planning Tools Prototype Project, or LANDFIRE Prototype [81], a large field-referenced database was compiled to act as the training data for multi-faceted goals, including 1) developing predictive landscape models, 2) generating satellite image catalogs and biophysical gradient layers to serve as spatial predictors for mapping vegetation and wildland fuel characteristics, 3) developing vegetation and fuel map unit classifications, 4) developing vegetation dynamics models for simulating vegetation development over time, and 5) implementing a landscape succession model (LANDSUMv4) for simulating historical fire regimes and vegetation reference conditions.

The challenges found when developing quantitative fire models are associated with providing accurate mathematical representations of the multi-physics phenomena that constitute the fire dynamics. In addition, data pertaining to fire behavior that is required to inform the model are quite sparse. A possible approach to overcome the limitations found in numerical simulations of fires is data assimilation (DA), which combines computer simulation tools with sensor observations through iteratively correcting the numerical model by the observed data to improve the prediction abilities of the numerical models. The use of DA in other fields of science, especially for weather prediction, has been proven successful and has started to gain popularity in modeling fire as well. Finney et al. [57] developed a data ensemble simulation system (FSPro) that can account for uncertainties in long-range weather conditions and two-dimensional wildland fire spread. The study comprised of modeling fuel moisture based on energy release component while developing a U.S. fire danger rating index and modeling the index variation throughout the fire season using time series analysis of historical weather data. To account for uncertainties in wind, wind speed and direction was stochastically sampled from joint probabilities of historical wind data for the date range of the fire simulation period. The simulations performed were found to be in consistent agreement with the reference cases. Some other data-assimilation fire models have also been developed and successfully applied such as – Rochoux et al. [60], Zhang et al. [82] and WIFIRE by Altintas et al. [58]. With the success of these models, soon fire models will also acquire the prediction accuracy of weather models as well. However, in order to achieve that substantial data

is required regarding the behavior of fire and its other parameters, thus experimental studies are quite vital at this stage of research in wildfires.

2.4 Experimental Methods

In order to quantify WUI fires, significant and comprehensive data are required. Thus, experimental studies of fire are quite crucial in understanding the behavior and for developing preventive measures. Over the years, urban fires have been investigated in detail; however, WUI fires have not been given the necessary attention. In the last decade, significant number of experimental studies have been conducted. Rollo [83] correlated the relationship between wind speed and building configuration with the transportation characteristics of various sizes of fire brand material developed by Cheney and Sullivan [84]. Given the variables of wind direction, wind speed, and topography, their study assessed the behavior of a single-story mono-pitch base model on an unobstructed horizontal ground plane subjected to a scaled 7 m (23 ft) vertical wind profile ranging between 28-35 *Km/hr* (17.4-21.75 mph). Cohen performed large-scale testing during the International Crown fire modeling experiments from 1997-2001. From these experiments, it was determined that when a clear defensible space of 36 m (120 ft) was maintained, radiative exposure was insufficient to ignite wooden exterior walls from crown fires, i.e. only firebrands or local combustible material (e.g. mulch) could ignite a structure. Reinhardt et al. (2006) used destructive measurement techniques to measure canopy fuels on plots in five interior west conifer stands. The work was geared at quantifying important fuel parameters such as bulk density, canopy fuel load, and vertical profiles of canopy fuels. The experimental results were compared with several computational methods to test the validation. Murphy et al. [85], Safford et al. [86] and Calkin [12] showed that fuel treatments that reduced the fire intensity beyond the high-intensity zones were not effective in reducing WUI losses.

Various experimental studies on WUI fires have also been conducted by researchers at NIST. These studies have paved way for many other experimental work all over the world. For example, the NIST, in collaboration with the University of Florida and the US Forest Service Southern Re-

search Station, tested 34 species of ornamental shrubs at NIST's Large Fire Laboratory (LFL) to quantify and rank their flammability. Wind-tunnel experiments were conducted on the specimens to characterize the potential of disk [87, 88] and cylinder-shaped [89] firebrands to ignite different types of fuel beds such as - surface fuels and structural fuels. The cylinder-shaped firebrand dimensions were based on Douglas fir tree burn experiments previously conducted in NIST's LFL and Korean pine trees at the Building Research Institute (BRI) in Japan [90]. It was shown that if the firebrands were burning, then both types of firebrands would induce ignition in the fuel bed. Following these experiments, further studies were conducted to determine the range of conditions for firebrand ignition of common building materials [91]. A simple and efficient firebrand generator was developed by NIST, which is also referred to as the 'NIST Dragon' [89], that produces glowing firebrands. The output capacity of the generator was validated to that of the results produced for Douglas tree burns as well as Korean pine trees [90]. The generator has been used in several other experimental studies by NIST and has also been used to study firebrand ignition in the large-scale wind tunnel (5 m (16.4 ft) wide, 4 m (13.12 ft) tall) at Japan's BRI. The success of NIST Dragon has motivated researchers all around the world to develop a similar mechanism for firebrand testing. The conditions simulated by the firebrand experiments are now being adopted to simulate real time WUI fire scenarios. In addition to NIST, other agencies - United States Forest Services (USFS) and the Insurance Institute for Business and Home Safety (IBHS) have also been highly active in this field. Recent experimental studies have identified clear vulnerabilities of WUI structures to low intensity fires and firebrands, including roofing components, eaves, vents, wood piles, mulch, fences, decks, and so on [12, 92, 93]. These unique full-scale and reduced-scale test methods have provided and continue to provide the proper means by which future building codes and standards for fire protection of structures can be developed.

2.5 Code Provision and Guidelines

Codes and standards are useful for regulatory bodies to adopt in order to help mitigate potential WUI home ignitions and the impact on communities. There are several standards and codes that

were developed to address the problem of WUI fires; however, none extensively covers all aspects of the problem. There is currently no standardized method of risk assessment that can be applied nationwide to WUI communities in the U.S. [94]. Some of the most prominent codes and standards include:

- o NFPA 1141: Standard for fire protection infrastructure for land development in wildland, rural, and suburban areas [95]
- o NFPA 1142: Standard on water supplies for suburban and rural firefighting [96]
- o NFPA 1144: Standard for reducing structure ignition hazards from wildland fire [97]
- o NFPA 1143: Standard for wildland fire management [98]
- o ICC International Wildland-Urban Interface Code [99]
- o California Building Code Chapter 7A: Materials and Construction Methods for Exterior Wildfire Exposure [100]

The standards set by NFPA 1141 - 1144, the ICC WUI code and CA CBC can partially be used by planners, developers, and communities. NFPA 1141 covers - means of access, building access and separation, fire protection, water supply, community safety, emergency preparedness and fire protection during construction. NFPA 1142 primarily deals with regulation of water supplies required in rural areas, but also includes regulations related to WUI to some extent. NFPA 1143 applies to wildland fire management. NFPA 1144 is the most useful for home and property owners as it deals with assessment of fire hazards in the structure ignition zone, building design, location and construction and fuel loads around the defensible space. Section 701A of the 2009 California Building Code includes a wide variety of topics regarding prevention of WUI fires such as - protection against intrusion of embers under roof coverings or into attics through attic ventilation, ignition-resistant exterior construction, use of tempered glass windows, and multiple decking requirements [100]. The California building code is viewed to be the most flexible and comprehensive of all standards in the U.S. to mitigate the effects of WUI fires. An in-depth investigation

of the 2007 San Diego fires showed that houses built between 2001 to 2004 following CA Building Code standards were much less likely to burn, with 2-3% of those houses exposed to WUI fires burning, as opposed to 13-17% of exposed homes built before 2001 burning. Many other standards have also been developed which primarily deal with testing of materials and components of structures in WUI-prone communities. The American Standards of Testing and Materials (ASTM) has been a proponent for developing such standards, some of which are listed below.

- o ASTM E108 - Standard Test Methods for Fire Tests of Roof Coverings [101]
- o ASTM E84 - Standard Test Method for Surface Burning Characteristics of Building Materials [102]
- o ASTM E2726 – Standard Test Method for Evaluating the Fire-Test-Response of Deck Structures to Burning Brands [103]
- o ASTM D2898 – Standard Practice for Accelerated Weathering of Fire-Retardant-Treated Wood for Fire Testing [104]
- o UL 790 - Standard Test Methods for Fire Tests of Roof Coverings [105]
- o Testing Standards CA SFM 12.7A-1, Exterior Wall Siding and Sheathing [100]
- o Testing Standards CA SFM 12.7A-2, Exterior Windows [100]
- o Testing Standards CA SFM 12.7A-3, Under Eaves [100]
- o Testing Standards CA SFM 12.7A-4, Decking [100]

Firewise is a program of the National Fire Protection Association, co-sponsored by the USFS, DOI, and the National Association of State Foresters (NASF), developed to aid homeowners in preventing WUI fires. Firewise aims at a more hands on approach by the community itself through promoting involvement of homeowners through taking individual responsibility for protecting their homes from the risk of wildfire [98]. Firewise describes the goal of teaching residents about

wildfire and about smart practices around their homes that can reduce the risk of destruction. The program started in 1986 as a national project and gradually evolved to become a national program in 2002. It encourages local solutions for wildfire safety by involving homeowners, community leaders, planners, developers, firefighters, and others in an effort to protect people and properties from wildfire risks. These codes and standards provide some degree of protection from WUI fires; however, these are all qualitative in nature. To develop effective measures, the behavior of WUI fire needs to be better understood and quantified through simplified tools such that advancements in quantitative standards can be made.

Chapter 3

Wildland Propagation Model

In order to quantify and understand wildfire risk to communities, it is essential to first understand the propagation mechanisms in wildlands, since they are a critical part of WUI fires. In this study, a Cellular Automata (CA) model is proposed and developed to simulate wildfire propagation in wildlands (Fig. 3.1). Theory of Asynchronous CA, which is a discrete element modeling technique, is utilized to create an approximate analytical model as a function of certain probabilistic parameters that account for the uncertainties associated with the problem and can be tuned by on-site data to improve the model's accuracy as per user's discretion. CA was originally developed in the 1940s by Stanislaw Ulam and John Von Neumann, however its significance did not come to light until the 1970's, when British mathematician John Horton Conway created the 'Game of Life'. A cellular automaton consists of a regular grid of cells such that each cell can attain a finite number of states. On a two-dimensional grid of $N \times M$ cells, each cell $\{A(i, j, t) : i \in N, j \in M, t \in \mathbb{R}\}$ may be present at any of the finite number of states. At each time step t the next state of a cell $A(i, j, t + 1)$ is determined by its present state and the states of its local neighbors. CA models can be used to emulate both deterministic and probabilistic scenarios. A significant number of CA models have been developed in different fields of science ranging from astrophysics, ecology, and hydrology to structural engineering and many others.

The CA framework is implemented by dividing the layout of wildland area into a grid comprising of cells. The size of the cells will be a function of the scale of the location chosen for analysis. If the cells are chosen to be too small the computation cost would increase significantly, and if they are chosen too big the accuracy could be affected. The state of each cell is determined by its respective color. For instance, the fire blocks (Fig. 3.1) represent propagation of fire by means of different colored cells. The numbers on each cell represent the flame intensity and the flame cells are assigned increasing strength numbers as 1, 2 and 3. The yellow, orange and red cells are the different stages of flame intensity, and black cell represents burnt-out state. The green cells

represent the wildland vegetation and are the only ignitable elements in the model. For initial tests, only two types of vegetation are considered (Fig. 3.1). Dark green vegetation cells represent grass and the light green cells represent trees. The blue cells represent water, which stays unaffected by fire.

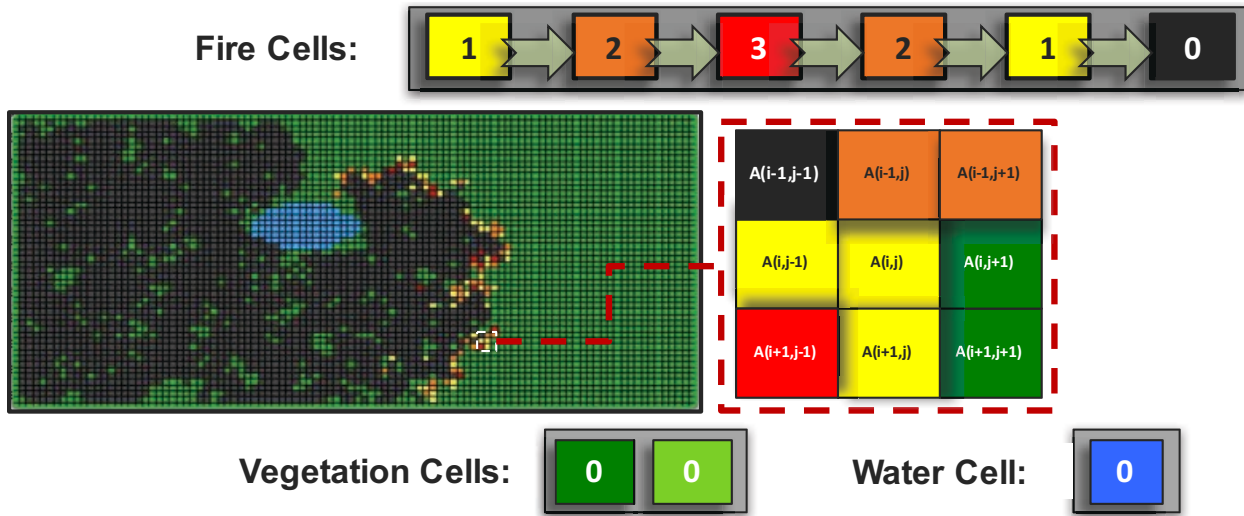


Figure 3.1: Different states of cells considered in the Cellular Automata model

The probability of ignition for each cell is calculated by Eq. 3.1, where $f(\cdot)$ is defined by Eq. 3.2. Using the probability of ignition the new state of each cell is given by Eq. 3.3, where $H(\cdot) \in [0, 1]$ is the Heaviside function, $rnd(\cdot) \in [0, 1]$ is a random number generator up to two decimal places and $I(\cdot)$ is the state value for fire progression (Fig. 3.1). For initial tests, it is assumed that each flame intensity lasts for only a unit time i.e. after each time step the flame changes its intensity based on its previous state. Each vegetation block has the chance to be ignited if at least one of the neighboring cells is ignited. The equation states that the probability of ignition of the center block is proportional to the number of cells ignited in its neighboring cells and is given by the summation of the flame strengths of the neighboring blocks scaled by λ_s , which is the expected probability of ignition due to short-range heat transfer when only one neighboring cell is ignited.

$$P_i(i, j, t + 1) = (f(A(x, y, t)) | x \in \{i, i + 1, i - 1\}, y \in \{j, j + 1, j - 1\}, (x, y) \neq (i, j)) \quad (3.1)$$

$$f(X_1, \dots, X_n) = \sum_{w=1}^n X_w \cdot \lambda_s \quad (3.2)$$

$$A(i, j, t + 1) = \begin{cases} H(P_i(i, j, t + 1) - rnd(i, j, t)) & \text{if } A(i, j, t) = 0 \\ I(A(i, j, t) + 1)_{I \in \{1 \rightarrow 2 \rightarrow 3 \rightarrow 2 \rightarrow 1 \rightarrow 0\}} & \text{if } A(i, j, t) > 0 \end{cases} \quad (3.3)$$

3.1 Effect of Wind

Wind conditions have a profound effect on wildfire propagation as it can not only alter the direction of propagation, but also the rate of propagation. For the proposed model, the effect of wind is segregated into two components – (1) wind speed (v_w) and (2) wind direction (θ). The CA fire propagation mechanism is modified to account for effect of wind by scaling the strength of neighboring cells. As shown in Fig. 3.2, the neighboring cells are divided into eight regions and m represent the boundaries of classification. Depending on the wind direction at time t the cells lying in the same region are scaled. For instance, if $\theta = 45^\circ$, the cell in region 4 is amplified ($A(x, y, t) = A(x, y, t) \cdot \lambda_w(x, y, t)$) and the cell in region 8 is reduced ($A(x, y, t) = \frac{A(x, y, t)}{\lambda_w(x, y, t)}$). Cell 4 is scaled up since it lies behind cell $A(i, j, t)$, and it will have a higher chance of igniting it, thereby increasing its contribution. On the other hand, cell 8 is scaled down as the wind will force the flame in cell 8 to move away from $A(i, j, t)$, thereby reducing its contribution. The scaling factor is defined by Eq. 3.4, where $g(\cdot)$ is a scaling function proportional to wind speed. As the wind speed increases, the probability of forward propagation increases while backward propagation decreases.

$$\lambda_w(x, y, t) = \begin{cases} g(v_w) & \text{if } A(x, y, t) \neq 0 \\ 1 & \text{otherwise} \end{cases} \quad (3.4)$$

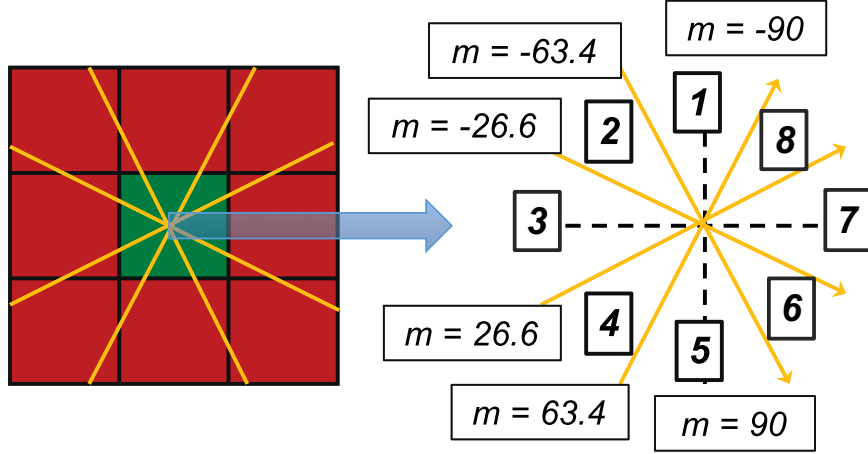


Figure 3.2: Segmentation of cell space based on wind direction

The effect of wind direction and speed on the wildfire propagation pattern is shown through a sample simulation in Fig. 3.3. Both wind direction and speed are varied in time and their respective values are shown on the top of the figures. As seen from the simulation, the fire starts out in the direction of wind since the wind speed is quite high at the beginning. As wind direction changes, the direction of fire deviates with it. When the wind speed is reduced sufficiently the fire spreads in all directions until the wind speed picks up again. When this pattern is repeated, and a non-uniform burn scar is observed from the simulation.

3.2 Effect of Topography

Topography, like wind, has a significant effect on fire propagation as well. The rate of fire propagation tends to decrease when going down slope and tends to increase when going up slope. A similar mechanism to the wind is utilized to account for the effect of variation in topography. Given the height for each cell from a specific reference point, based on the difference in heights between $A(i, j, t)$ and its neighboring cells ($A(x, y, t)$), the strength of the neighboring cells is modified as given by Eq. 3.5. The scaling factor $\lambda_t(x, y, t)$ is given by Eq. 3.6, where $h(x, y)$ and $h(i, j)$ are heights of neighboring and central cells and r_{th} is the threshold distance between them. When the difference in heights is negative i.e. the neighboring cell is below central cell the strength of neighbor cell is amplified, otherwise, the strength is reduced. The effect of topography is limited

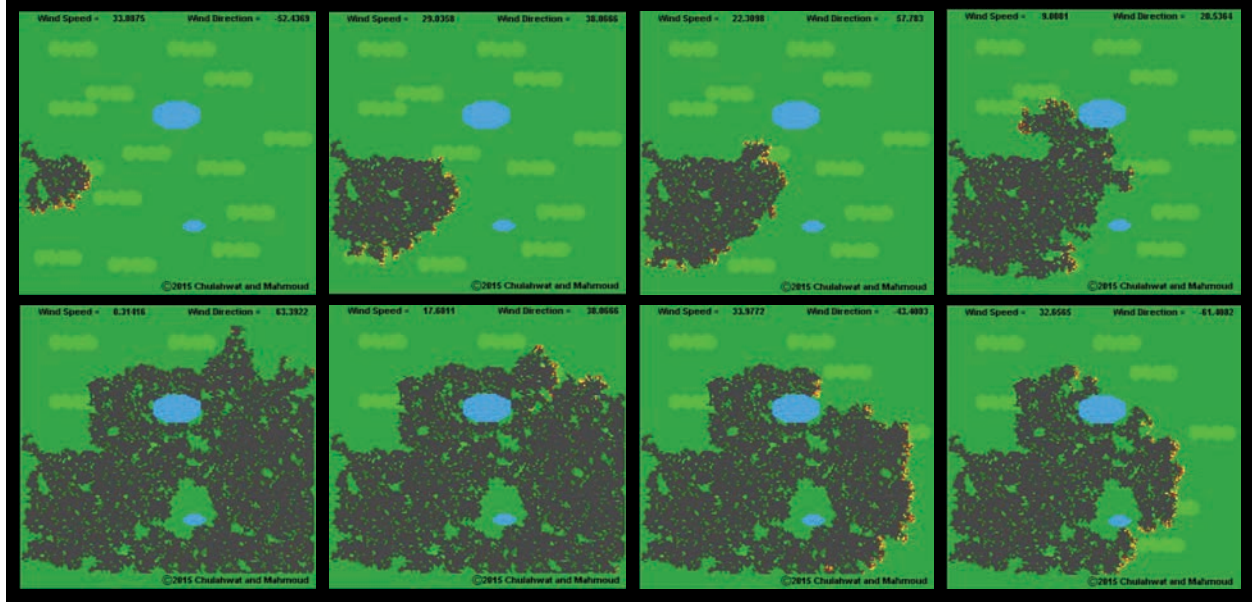


Figure 3.3: A sample simulation showing effect of wind speed and direction on fire propagation

by a threshold distance such that if the difference in height between the central and its neighboring cells is more than the threshold, then topography does not have an effect. The threshold distance ensures that the model is able to capture the presence of severe discontinuities in the topography.

$$A(x, y, t) = A(x, y, t) \cdot \lambda_t(x, y, t) \quad (3.5)$$

$$\lambda_t(x, y, t) = \begin{cases} e^{\frac{h(x,y)-h(i,j)}{r_{th}}} & \text{if } (A(x, y, t) \neq 0 \text{ and } (h(x, y) - h(i, j)) \leq r_{th}) \\ 1 & \text{otherwise} \end{cases} \quad (3.6)$$

The topographic profile of a test area is shown in Fig. 3.4, which also shows the fire initiation point and its expected route. A test simulation is presented in Fig. 3.5 to show the effect of differences in topography on wildfire propagation. For this simulation wind speed is assumed to be small to reduce its participation. The fire spreads out in all directions at first but eventually takes two directions - the upper and the lower paths shown in Fig. 3.5. The fire spreading along the top path eventually comes to a halt once it spreads completely, as it cannot spread to the lower regions from top. The fire which proceeded to the lower path keeps on spreading until it completely

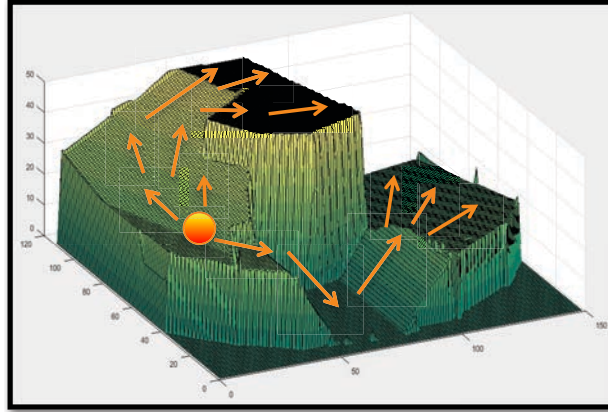


Figure 3.4: Topography layout of test scenario

covers the area. This test shows the restrictions introduced by a topographic profile on wildfire propagation and also the variation in propagation rates for wildfire as the fire travels faster going upslope than downslope.

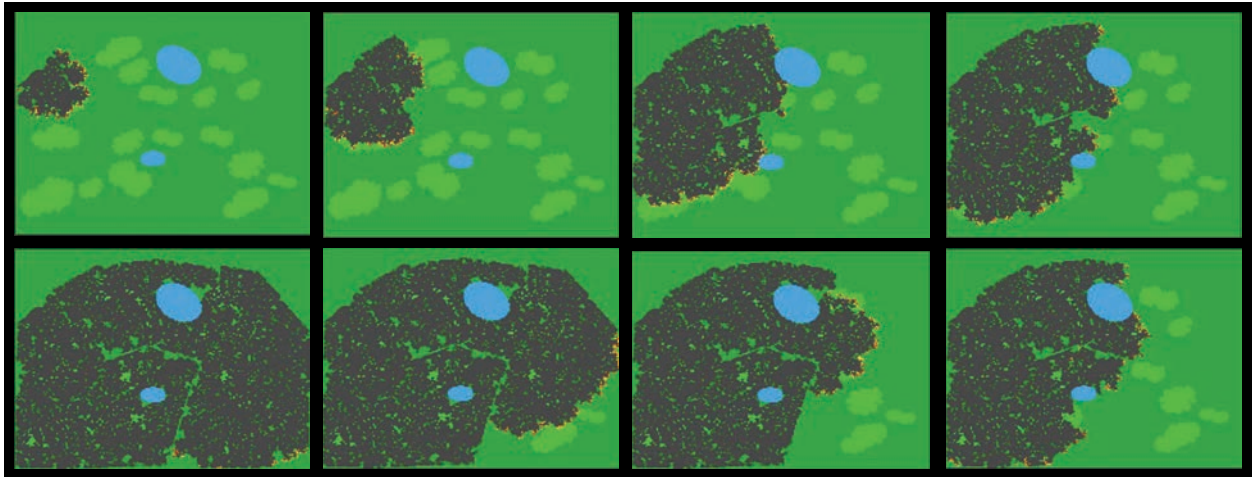


Figure 3.5: A sample simulation showing effect of topography on fire propagation

3.3 Ember Spotting

A wildfire propagates by short-range (convection, radiation and conduction) and long range (embers) heat transfer mechanism. The latter primarily includes embers generated from ignited sources, such as vegetation, houses, etc. Short-range mechanisms have been studied in sufficient

detail and have been incorporated in several models quite efficiently. However, the uncertainty associated with ember spotting is rather significant, and its complex mechanism, renders the implementation not so straight forward. Most studies ignore the spotting mechanism, which is an essential component to completely understand and model wildfire propagation. Embers are able to travel long distances and initiate fires at locations far away from the fire front, resulting in multiple fire-fronts and unpredictable fire propagation patterns. In the proposed algorithm, the embers are modeled probabilistically by assigning every cell a probability to generate embers. Once an ember is generated at a particular cell, its trajectory for it is calculated based on the uplift, wind direction and wind speed at that specific time. Each ember is treated as an individual particle and using kinematics the trajectory of each ember is calculated for next time step. At each time step, the trajectory for each ember is updated based on the conditions at that time. The wind speed and direction are a function of time, hence, the trajectory of embers may not be a straight path. Since in the proposed model all embers are tracked it is possible to update trajectories for each ember. While in flight, the embers can possibly collide with an incombustible object or they can collide with an ignitable object and ignite it, hence all embers are checked for collision at each time step while updating their respective trajectories.

Simulation results combining all the features of the proposed algorithm i.e. variation in wind, variation in topography and ember generation are shown in Fig. 3.6. For the generation of embers wind is a necessary condition, hence, a high wind velocity is considered. The topological profile of the area is considered the same as shown in Fig. 3.4. The first part of the simulation show the wildfire propagation patterns and the latter show the trajectories of the embers generated. The white spots are the landing locations of the embers and the orange spots are embers still in flight. The dark green vegetation cells represent short grass while light green vegetation represents trees. The embers are generated only from the light green cells since embers generated by grasses would be redundant as their flight distances would be quite small. In this simulation once the fire initiates it starts spreading and once it reaches a patch of trees it generates embers, which in turn initiate fire at some distance away. The direction of wind varies between -60° to 60° , as a result, the flight

path of the embers also changes accordingly. The embers generated tend to create new points of initiation resulting in faster propagation of fire. The embers generated by fire at lower elevations are seen to collide with the terrain and remain in the same area; however, once the fire reaches the highest elevation the embers generated are able to spread throughout the area.

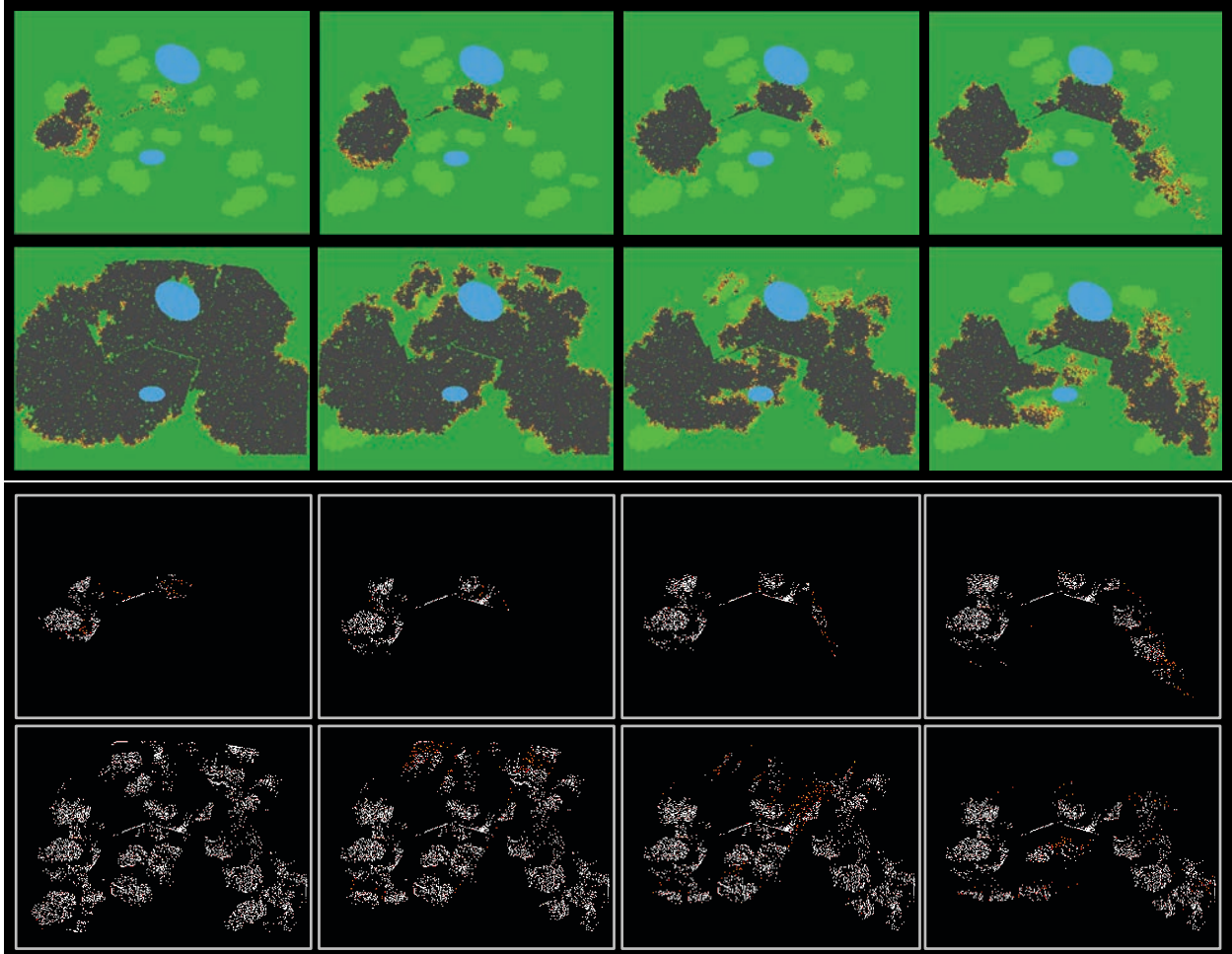


Figure 3.6: A sample simulation showing effect of ember spotting on fire propagation. (a) Fire propagation patterns with time (b) Ember generation and landing patterns

3.4 Wildland Model Validation and Calibration

A validation is conducted to ensure that the algorithm is producing acceptable results. Under the absence of wind, the shape of the fire front should be circular at all times, given that the

topography of the location and other factors such as fuel distribution are uniform. In the presence of wind; however, the circular fire front changes into an ellipse in the direction of wind. The seminal work by Karafyllidis and Thanailakis [106] presented one of the first CA based fire propagation models and the fire front shapes they obtained in presence and absence of wind are shown in Fig. 3.7. The proposed algorithm was tested under similar conditions, as shown in Fig. 3.8. The shape of the fire fronts obtained correlates well with the work by Karafyllidis and Thanailakis. This suggests that the CA rules selected for the propagation model are satisfactory. For this semi-quantitative validation, the proposed algorithm was tuned by adjusting the parameter λ_s to match the required shape. Since the proposed CA model is stochastic in nature it would require suitable calibration on a per case basis.

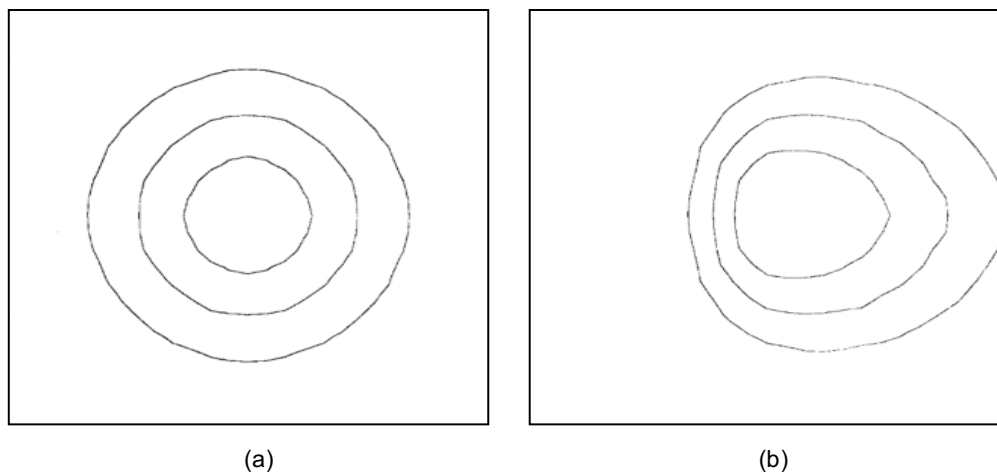


Figure 3.7: Fire Front shapes obtained from [106] under (a) absence of wind and (b) wind from west to east

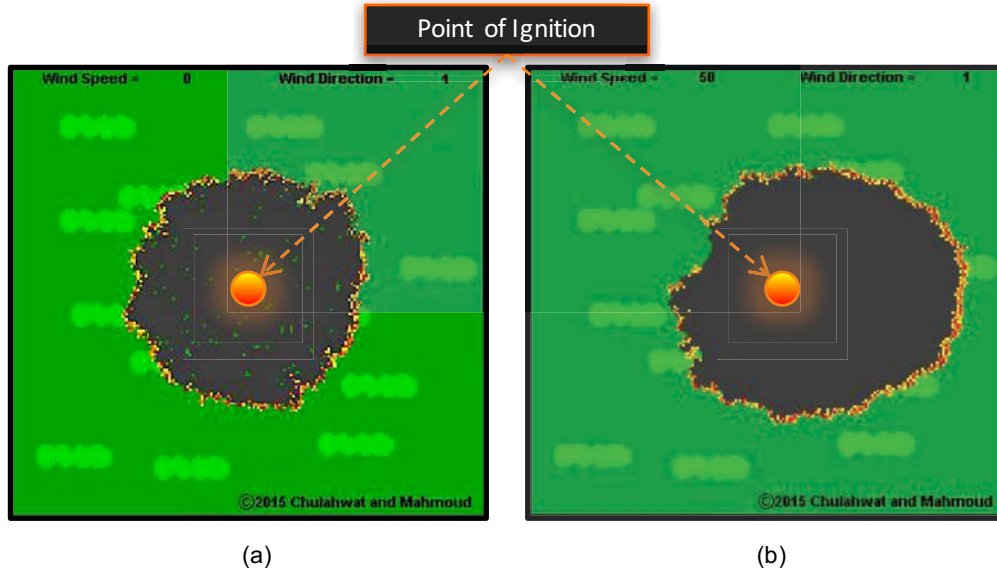


Figure 3.8: Fire Front shapes obtained from proposed algorithm under (a) absence of wind and (b) wind from west to east

Chapter 4

Community Propagation Model

The underlying propagation mechanisms for WUI fires are identical to wildland fires; however, the difference in topographic features creates explicit differences in behavior. The urban fire problem can be formulated analogous to a network flow problem in graph theory. A community comprises of ignitable, as well as, non-ignitable regions. Once a wildland fire reaches an urban interface it spreads into the community, propagating from one ignitable source to another (mostly in parallel). The discrete movement of wildfire can thus be modeled as a flow problem in graph theory. In this study, a graph model is presented (AGNI-NAR: '*Asynchronous Graph Nexus Infrastructure for Network Assessment of WUI Risk*'), which takes into account different modes of heat transfer to evaluate propagation probabilities between ignitable components, and subsequently, the vulnerability of a community. Once ignitable areas of the community in question are identified a suitable directed graph is developed. Each area/structure of a community is defined by multiple nodes that form a boundary, which can also be referred to as an 'ignitable element'. Even though parts of the area inside an ignitable element are ignitable, only the boundary of each ignitable element is defined by nodes. Each node does not represent a particular component, but rather a specific area within the element. For instance, a house represented by a boundary comprising of four nodes will have each node share one-fourth the area of the total house. A node is considered ignitable if even a small part of the area it covers is ignitable. Ideally, a high number of nodes can be used to model different components within an ignitable element, however that would increase the computational cost substantially.

The ignitable elements are utilized to form a directed graph, defined as $\mathcal{G} = (\mathcal{V}, \mathcal{E})$, where $\mathcal{V} = \{v_1, \dots, v_n\}$ defines the node set and $\mathcal{E} \subseteq \mathcal{V} \times \mathcal{V}$ defines the edge set. The adjacency matrix of the graph is defined as $A = [a_{(i,j)}] \in \mathbb{R}^{n \times n}$ associated to \mathcal{G} such that $a_{(i,j)} = (P_{tr}^{(i,j)})_{\{i \in \mathbb{Z}, j \in \mathbb{Z}\}}$, where $P_{tr}^{(i,j)} \in [0, 1]$ is the probability of fire transfer from ignitable node i to ignitable node j and \mathbb{Z} refers to set of integers. The nodes i and j are part of ignitable elements (same or different),

as the boundary of each element is described by node set $\mathcal{W}_{(m)}$ such that $\mathcal{V} = \cup_{m=1}^{N_w} \mathcal{W}_{(m)}$, where N_w is the total number of ignitable elements. A sample graph formulation is shown in Fig. 4.1 for a segment of city of Fort Collins (Colorado). Each element is comprised of multiple nodes, which forms the boundary. The edge weights assigned between the nodes define the wildfire propagation probabilities from one node to another. The elements in each community are classified into different categories to recognize ignitable elements. The classification is made into categories shown in Table 4.1 and each of which are further classified into sub-categories to improve the accuracy of the data. Each ignitable element classification can have minor categories. For instance, type 'Building' could be further classified into - residential, religious, commercial and others. Similarly, type 'Amenity' could encompass - entertainment, financial, transportation, education and others. An important thing to note is that while all 'Building' types can be considered ignitable, not all sub-classifications of type 'Amenity' would be ignitable. A detailed list of sub-categories is listed and defined in http://wiki.openstreetmap.org/wiki/Map_Features.

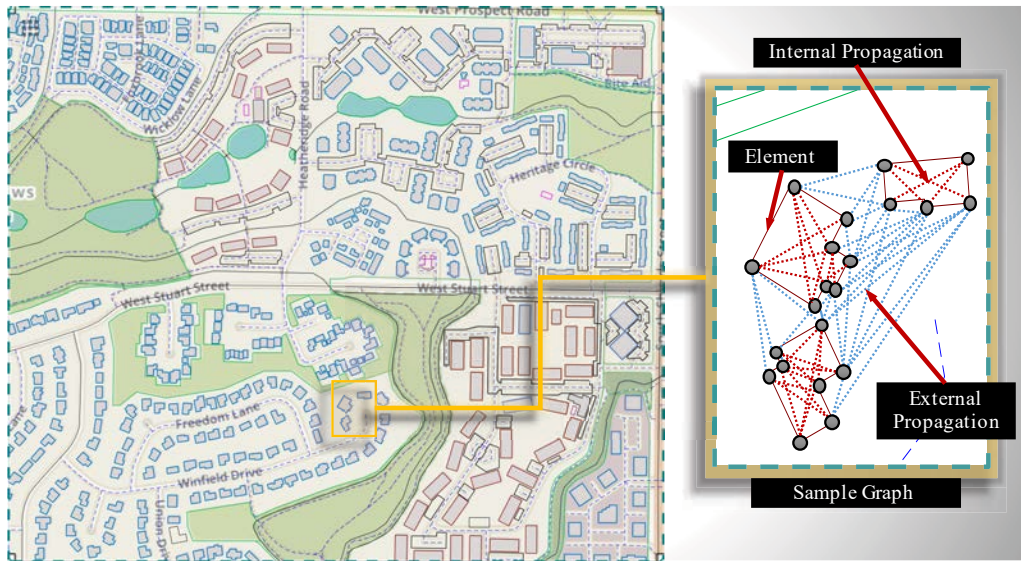


Figure 4.1: A sample representation of actual community layout (Fort Collins, Colorado, USA) as a graph network. The nodes of each element define its specific boundary and the edges represent the potential fire propagation paths (Map data ©OpenStreetMap contributors [107])

Table 4.1: Classification of ignitable elements based on their ignition capacity

Type	Landuse	Building	Amenity	Natural area	Leisure	Shop	Office	Route	Others
Ignition	Some	All	Some	All	All	All	All	None	None

The discrete vegetation in a community have an impact on wildfire behavior. Even though the vegetation patterns are not discretely modeled in the community layouts their effect is studied. A sensitivity analysis was conducted using Monte-Carlo simulation for $N = 100$ iterations. It is observed that for > 95 percentile cases, the mean vulnerability of the community converges to a single value. This suggests that for these layouts even if the location of vegetation around a house is unknown, the total risk of the community does not change drastically when effect of fire intervention is not considered. This can be attributed to the multiple paths available for the wildfire to propagate within a network. On the other hand, when fire intervention is applied, the effect of presence/absence of vegetation is inherently considered within the framework. The effect of vegetation would affect the fire graph network in general, and for best practice, the stray vegetation would have to be considered as separate nodes in the graph. To circumvent this problem in the future, satellite images can be used in conjunction with a custom image pattern recognition algorithm to identify stray vegetation, which can be overlaid on the GIS data to get an accurate representation of the community layout.

There are four primary modes of heat transfer from one ignitable elements to another that are observed during WUI fires. The four modes are incorporated using information from previous research studies on wildfire. These modes are classified into two types, based on the nature of source and target nodes, as - (1) Internal and (2) External propagation (Fig. 4.1). The former involves propagation within a particular ignitable element and the latter includes propagation from one ignitable element to another. The cumulative fire transfer probability along each edge from node i (under ignition) to node j is given by Eq. 4.1, such that internal propagation is governed dominantly by conduction mode [36], whereas, external propagation is governed by multiple modes [108]. When nodes i and j belong to the same ignitable element, the ignition transfer prob-

ability is given by conduction probability only - $P_{cond}^{(i,j)} \in \{0, 1\}$. The dependence of conduction propagation on material properties is not considered, hence $P_{cond}^{(i,j)} = 1$ for all cases. It is observed from preliminary tests that the effect of internal propagation of ignitable elements on the global vulnerability of the community is minimal, hence conduction is modeled in a simplified manner. In case of external propagation, three modes of heat transfer are considered - (1) Convection - $P_{conv}^{(i,j)} \in \{0, 1\}$ (2) Thermal radiation - $P_{rad}^{(i,j)} \in [0, 1]$ and (3) Ember spotting - $P_{ember}^{(i,j)} \in [0, 1]$, which account for majority of fire propagation in WUI fires [35]. The total probability of external propagation is derived from the individual mode probabilities (Eq. 4.2), which are evaluated based on their respective formulated models. $X_{conv}^{(i,j)}$, $X_{rad}^{(i,j)}$ and $X_{ember}^{(i,j)}$ are the events that an element is ignited by convection, radiation and ember modes. The three modes of external propagation are mutually independent to each other but not entirely mutually exclusive. The details for the other three models are discussed in the following sections.

$$P_{tr}^{(i,j)} = \begin{cases} \min(P_{total}^{(i,j)}, 1) & \text{if } \{j \notin \mathcal{W}_{(m)} : i \in \mathcal{W}_{(m)}\}_{m \in \mathbb{Z}} \\ P_{cond}^{(i,j)} & \text{if } \{j \in \mathcal{W}_{(m)} : i \in \mathcal{W}_{(m)}\}_{m \in \mathbb{Z}} \end{cases} \quad (4.1)$$

$$P_{total}^{(i,j)} = P(X_{conv}^{(i,j)} \cup X_{rad}^{(i,j)} \cup X_{ember}^{(i,j)}) \quad (4.2)$$

4.1 Convection Model

Convection is the transfer of heat from one place to another by movement of fluids. The convective heat transfer includes transfer of heat flux driven by winds generated from fire. Ideally, convection models have been developed to account for complex heat transfer mechanisms using computational fluid dynamics (CFD) models. The most renowned is the Wildfire Dynamic Simulator (WFDS) developed by NIST [61], which utilizes the concepts of Finite Element to solve complex coupled hydrodynamic and thermodynamic differential equations spatially. The computational requirement of solving these coupled differential equations is quite significant and herein lies the biggest limitation of such models, which has made their widespread application all but

impossible given the current state of computation technology. To provide a practical formulation convective heat transfer was modeled using the concept of flame contact. In this study, heat transfer by convection corresponds to ignition of an object due to direct influence of flames. The probability of convection is defined by the condition whether the flames from the source reaches the target or not. Ignition due to convection would occur only if the distance between the source and target is less than the flame length generated by the source. As given by Eq. 4.3, the probability is considered unity since it is reasonable to assume that if the flames touch an ignitable object the chances of ignition will be most likely. $d^{(i,j)}$ is the distance between source node i and target node j and $d_{conv}^{(i,j)}$ is the convection threshold distance, which is defined as the flame length generated by the source node i .

$$P_{conv}^{(i,j)} = \begin{cases} 1 & \text{if } d^{(i,j)} \leq d_{conv}^{(i,j)} \\ 0 & \text{if } d^{(i,j)} > d_{conv}^{(i,j)} \end{cases} \quad (4.3)$$

The convection threshold distance (or flame length) can be described as a function of the following - (i) flame height generated at the source node $h_f^{(i)}$ (ii) inclination of the flame with respect to the horizontal axis $\theta_f^{(i)} \in [0, 90^\circ]$ and (iii) effect of wind direction on the convection threshold distance $\theta^{(i)} \in [0, 360^\circ]$. The relation between these variables, shown in Eq. 4.4, defines the convection distance model, which includes the effect of uncertainty in wind direction in the form of a wind correlation coefficient $F_{cc}^{(i,j)} \in [0, 1]$, given by Eq. 4.5. Wind direction directly affects the evaluation of effective flame length. If the wind direction and direction of target node are not aligned the flame length is effectively reduced. Consider the case, if an east-west wind is blowing and the target node is to the east of the source then the flame length will be in the opposite direction resulting in zero effective flame length. To capture this effect the wind correlation coefficient is introduced. It attains a maximum value of unity when there is perfect correlation between the wind direction and the direction of edge from node i to j , given by $\phi^{(i,j)}$, and a value of zero if the wind direction is opposite to the direction of target node. The effect of wind correlation coefficient can be best explained using Fig. 4.2. While keeping wind speed constant, the flame length is eval-

uated for different wind directions for 2 cases of nodal heights. The wind correlation coefficient is used to capture the uncertainty associated with local changes in wind direction in context of flame length variation. All angles are measured anti-clockwise from the positive X-axis, including the wind direction, such that a N-S wind would be represented by $\theta^{(i)} = 270^\circ$ and S-N wind by $\theta^{(i)} = 90^\circ$.

$$d_{conv}^{(i,j)} = \frac{F_{cc}^{(i,j)} \cdot h_f^{(i)}}{\tan(\theta_f^{(i)})} \quad (4.4)$$

$$F_{cc}^{(i,j)} = \begin{cases} \cos(|\phi^{(i,j)} - \theta^{(i)}|) & \text{if } |\phi^{(i,j)} - \theta^{(i)}| < 90^\circ \\ 0 & \text{if } |\phi^{(i,j)} - \theta^{(i)}| \geq 90^\circ \end{cases} \quad (4.5)$$

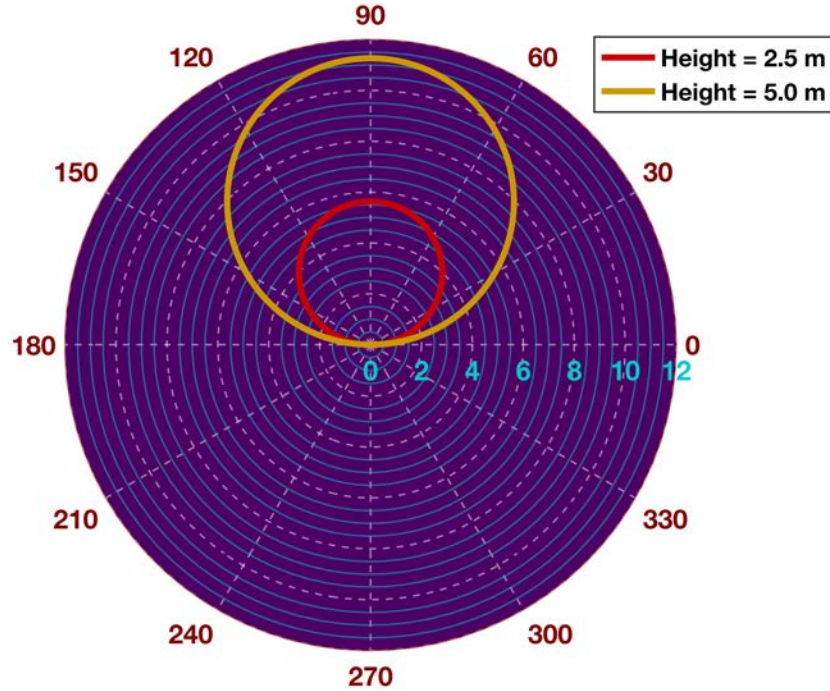


Figure 4.2: Variation of convection threshold distance (radial axis in m) for different wind directions (polar axis in degrees) for two cases of different node heights - (i) 2.5 m and (ii) 5 m, when the angle between the source and target ignitable element is 90°

As described above, the convection threshold distance is a function of flame height $h_f^{(i)}$ and flame angle $\theta_f^{(i)}$. The flame height is evaluated based on height of source node $h^{(i)}$, using Eq. 4.6, where α is a constant. The flame angle is heavily influenced by wind speed v_w as higher the wind speed the lower the inclination of flame will be with respect to horizontal axis. The flame angle is mapped linearly to wind speed such that $v_w^{min} \rightarrow \theta_{f,max}^{(i)}$ and $v_w^{max} \rightarrow \theta_{f,min}^{(i)}$, using Eq. 4.7. Since flame length is a function of flame angle, the length in turn is positively correlated to wind speed as well, as shown from Fig. 4.3. The plot shows variation in flame length with variation in wind speed while keeping the wind direction constant for two cases of different nodal heights. As observed from the figure, both wind speed and height of source nodes are positively correlated to flame length. All parameters used for the convection model are described in Table 4.2.

$$h_f^{(i)} = \alpha \cdot h^{(i)} \quad (4.6)$$

$$\theta_f^{(i)} = m \cdot v_w + b \quad (4.7)$$

Table 4.2: Convection model parameter values

Parameter	Definition	Value
α	Flame height constant	1.3
m	slope	-2.065
b	constant	90°
v_w^{min}	Minimum wind velocity	0 mph
v_w^{max}	Maximum wind velocity	65 mph
$\theta_{f,min}^{(i)}$	Minimum flame angle	30°
$\theta_{f,max}^{(i)}$	Maximum flame angle	90°

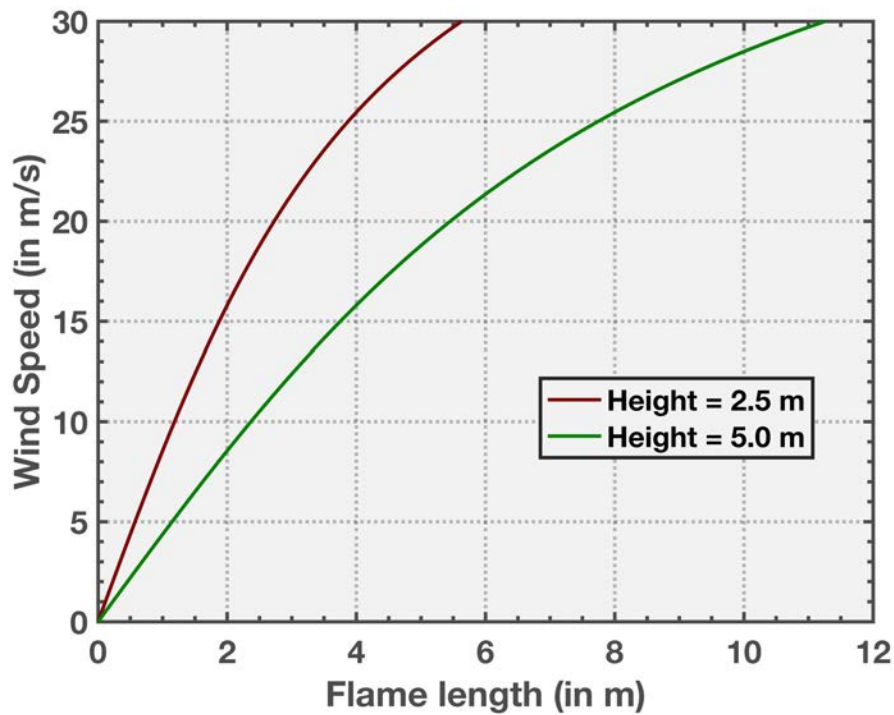


Figure 4.3: Variation of flame length (x-axis) with varying wind speeds (y-axis) for two cases of different node heights - (i) 2.5 m and (ii) 5 m

The convection model in this study does not account for all mechanisms involved in convective heat transfer, but this was done deliberately to minimize processing time. A sensitivity analysis on the effects of convection on community risk was conducted, which showed low sensitivity. Therefore, a simplified model for convection can be used to reduce processing time significantly without compromising accuracy. Other models can be used as substitution without altering the fundamental principles of the proposed graph framework. In context of future work, convection model can be substantially improved with the incorporation of wind field model to capture local changes in wind field. However, in order to make the graph framework compatible it would have to be modified into a dynamic framework from a static one. Since the scope of this study is limited to static graph model further discussion on the dynamic framework is not included.

4.2 Radiation Model

When an object burns, its surfaces tend to emit thermal radiation that can be transferred to other nearby objects resulting in increase in their temperature, and subsequently, ignition in some cases. Radiation is one of the fundamental mechanisms of heat transfer and plays a significant role in the spread of wildfires. Ignitable elements in a community, such as houses, are a major source of thermal radiation. When houses ignite, they emit thermal radiation that can be absorbed by neighboring vegetation and other houses to cause further ignitions. In the past, some studies have pointed out the importance of understanding the role of radiation in context of communities and wildfires. One of the prominent study was done by Cohen [36] that looked into the effect of stray vegetation around residential buildings for wildfire spread by means of radiation heat transfer.

To develop a theoretical understanding of the interactions between buildings and the vegetation around it the problem is formulated as a parallel plate heat transfer problem, wherein both the source (vegetation) and the sink (building) are represented as individual surfaces. The transfer of thermal radiation flux between the building and vegetations are studied to better understand the role of vegetation in wildfire ignition. The study showed that if the vegetation is within a particular threshold distance of buildings, they can have significant contribution in the building's ignition. The radiation flux transfer is evaluated using Stefan-Boltzmann law, which states that the total energy radiated per unit surface area of a black body per unit time is directly proportional to the fourth power of the black body's thermodynamic temperature, as shown in Eq. 4.8, where σ is the Boltzmann constant, ϵ is the emissivity, A is the surface area and T is the absolute temperature of surface. The net radiative heat transfer from surface 1 to surface 2 is given as the difference in heat flux emitted by surface 1 and the heat flux emitted by surface 2 (shown in Eq. 4.9), where $vf_{(1,2)}$ is the view factor when surface 1 is the source and surface 2 is the target and $vf_{(2,1)}$ is the view factor when the roles of surface 1 and 2 are reversed. View factors determine the percentage of thermal radiation received by the target surface considering the relative positioning and surface areas of the source and target surfaces. Using the reciprocity law for view factors, as given by Eq. 4.10, the

Eq. 4.9 can be reformulated as Eq. 4.11. The reciprocity law for view factors is discussed in detail in the subsequent sections.

$$E = \sigma \cdot \epsilon \cdot A \cdot T^4 \quad (4.8)$$

$$q_{(1,2)} = A_{(1)} \cdot E_{(1)} \cdot vf_{(1,2)} - A_{(2)} \cdot E_{(2)} \cdot vf_{(2,1)} \quad (4.9)$$

$$A_{(1)} \cdot vf_{(1,2)} = A_{(2)} \cdot vf_{(2,1)} \quad (4.10)$$

$$q_{(1,2)} = A_{(1)} \cdot vf_{(1,2)} \cdot \sigma \cdot (\epsilon_{(1)} \cdot T_{(1)}^4 - \epsilon_{(2)} \cdot T_{(2)}^4) \quad (4.11)$$

In the aforementioned study [36], it was assumed that all surfaces are parallel to each other when evaluating the radiation heat transfer between them. However, when considering heat transfer between different ignitable elements (buildings/areas) in a community the parallel plate assumption can be considered as an oversimplification. In reality, the presence of multiple surfaces on each building makes the heat transfer calculations between different buildings is complex. Depending on the structural boundaries of a building each one can have different number of surfaces and their varying inclinations with respect to each other have an impact on the amount of radiation flux transferred. In real life scenarios, each structure cannot be assumed a single homogeneous source of thermal radiation. Each surface of an ignited structure is a potential source of radiation with different properties, such as surface area and inclination. In this study, the effect of shape of each ignitable element on thermal radiation transfer is considered in detail by evaluating each source-target element pair interaction i.e. the radiation heat flux transfer between surfaces of different buildings are calculated individually.

To better understand the radiation heat transfer between different ignitable elements, the boundary of each element is first discretized into multiple surfaces, which generate independently dif-

ferent heat flux on individual surfaces of the target element. When considering the heat transfer interaction between two elements; one is considered as the source, which emits radiation, and the other is considered as the target, which receives the radiation. Radiation flux incident on a surface $l \in \mathcal{F}_{(n)} = \{1, \dots, l, \dots, N_l\}$ of element n due to a burning surface $k \in \mathcal{F}_{(m)} = \{1, \dots, k, \dots, N_k\}$ of element m is calculated using the Stefan-Boltzmann law, where the sets $\mathcal{F}_{(m)}$ and $\mathcal{F}_{(n)}$ represent the surfaces of elements m and n . N_k and N_l are the total number of surfaces of respective elements. The radiation flux ($q_{(k,l)}^{(m,n)}$) between different surfaces of elements is defined by rewriting Eq. 4.11, as shown in Eq. 4.12, where $A_{(k)}^{(m)}$ is area of k^{th} burning surface, $vf_{(k,l)}^{(m,n)}$ is the view factor from the source to target surface, $\epsilon_{(k)}^{(m)}$ is the emissivity of source surface, T_f is the flame temperature and T_a is the temperature of the surroundings.

The cumulative incident heat radiation for each target surface is function of the inclination of the source surface ($\Theta_{(k)}^{(m)}$), target surface ($\Theta_{(l)}^{(n)}$) and the distance between the surfaces ($d_{(k,l)}^{(m,n)}$). This is reflected by the view factors ($vf_{(k,l)}^{(m,n)}$) calculated between different surfaces of elements m and n . A part of incident heat radiation is absorbed by the surface and some part is reflected. The latter is not accounted for in the heat flux equation, since reflected radiation will have minimal impact on other surfaces of the same element or any other element for the given scenario.

$$q_{(k,l)}^{(m,n)} = (A_{(k)}^{(m)} \cdot vf_{(k,l)}^{(m,n)} \cdot \sigma \cdot \epsilon_{(k)}^{(m)} \cdot ((T_f)^4 - (T_a)^4))_{\{k \in \mathcal{F}_{(m)}, l \in \mathcal{F}_{(n)}\}} \quad (4.12)$$

4.2.1 View Factors Calculation

View factors describe the fraction of radiation flux transferred from one surface to another based on their relative positioning. View factors play a vital role when evaluating heat transfer between different surfaces as they are unique to each interaction, and thus, have to be calculated separately every time. The view factor for two differential areas $dA_{(1)}$ and $dA_{(2)}$ at a distance s is given by Eq. 4.13, where $\Theta_{(1)}$ and $\Theta_{(2)}$ are the angle between corresponding surface normals and the ray connecting the two surfaces. The generalized formulation for view factor from surface 1 to surface 2 can be written as Eq. 4.14. In context of ignitable elements, the view factor equa-

tion is rewritten as Eq. 4.15 to evaluate view factors of all surfaces between different elements individually.

$$dvf_{(1,2)} = \frac{\cos\Theta_{(1)} \cdot \cos\Theta_{(2)}}{\pi \cdot s^2} dA_{(2)} \quad (4.13)$$

$$vf_{(1,2)} = \frac{1}{A_{(1)}} \oint_{A_{(1)}} \oint_{A_{(2)}} \frac{\cos\Theta_{(1)} \cdot \cos\Theta_{(2)}}{\pi \cdot s^2} dA_{(2)} \cdot dA_{(1)} \quad (4.14)$$

$$vf_{(k,l)}^{(m,n)} = \frac{1}{A_{(k)}^{(m)}} \int_{A_{(k)}^{(m)}} \int_{A_{(l)}^{(n)}} \frac{\cos\Theta_{(k)}^{(m)} \cdot \cos\Theta_{(l)}^{(n)}}{\pi (d_{(k,l)}^{(m,n)})^2} dA_{(l)}^{(n)} \cdot dA_{(k)}^{(m)} \quad (4.15)$$

The double area integral for view factors can be reduced to a contour double integral formula (CDIF) [109] using Stokes' theorem, such that when the contours of the source surface k of element m and target surface l of element n are divided into segment vectors $\Gamma_{(k)}^{(m)} \in [\delta_1, \delta_2, \dots, \delta_{n(k)}]$ and $\Gamma_{(l)}^{(n)} \in [\delta_1, \delta_2, \dots, \delta_{n(l)}]$, the view factor can be approximated by the discretization expression [110] shown in Eq. 4.16.

$$vf_{(k,l)}^{(m,n)} = \frac{1}{2\pi A_{(k)}^{(m)}} \oint_{\Gamma_{(k)}^{(m)}} \oint_{\Gamma_{(l)}^{(n)}} \ln(S^{(m,n)}) ds_{(l)} \cdot ds_{(k)} \quad (4.16)$$

A_P is the area of surface P , Γ_P and Γ_Q are the contours bounding surfaces P and Q , ds_P and ds_Q are differential length vectors and S is the distance between differential elements of surface P and Q . The discretization equation is further simplified as shown in Eq. 4.17, where the discretization of surface Q is replaced by the mid-point of surface Q such that $S_m^{(l)}$ is given by the distance between l^{th} differential element of surface P and mid-point of surface Q . For the purpose of identifying pilot ignition, only a point on the surface needs to be ignited; therefore, discretization of the target surface is not required. The formulation is solved using a 10-point Gauss quadrature scheme for all calculations, as it provides sufficient accuracy [111].

$$vf_{(k,l)}^{(m,n)} = \frac{1}{2\pi A_{(k)}^{(m)}} \sum_{x=1}^{n(k)} \ln(S_{(k,l)}^{(m,n)}(x)) \cdot \Gamma_{(k)}^{(m)}(x) \quad (4.17)$$

4.2.2 Radiation Matrix

As described in the previous section, since each ignitable element is comprised of multiple surfaces the radiation transfer between two elements would require calculation of each surface interaction separately. To capture these interactions between multiple surfaces of each element a radiation matrix is developed between elements m and n , where m is the source and n is the destination element. All possible interactions between the different surfaces of both element are taken into account in this formulation.

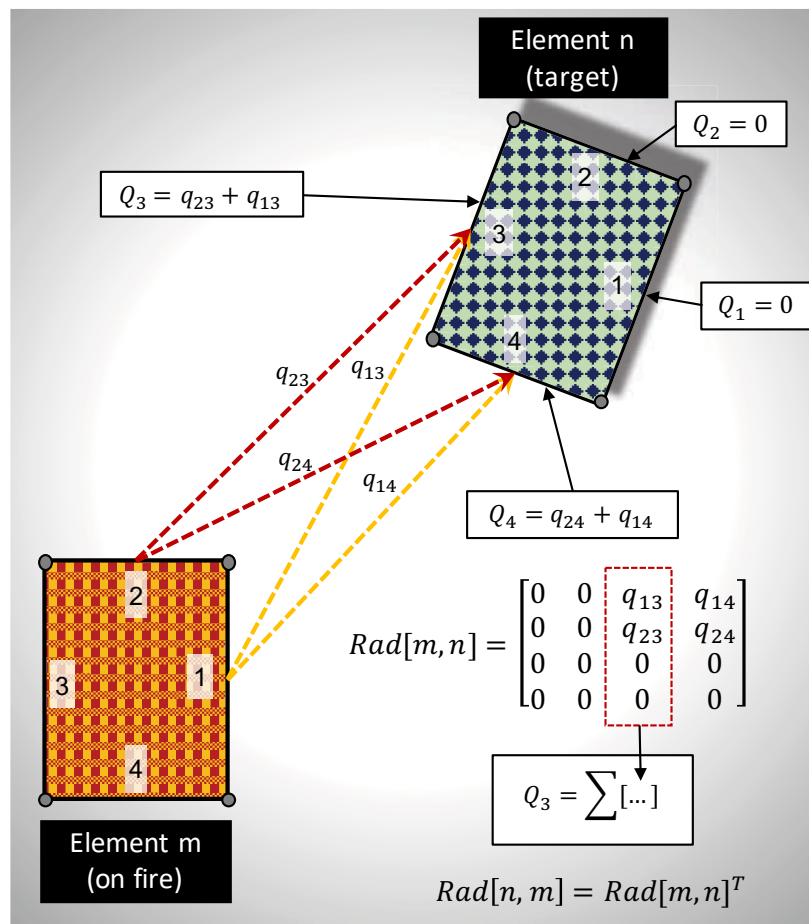


Figure 4.4: Procedure shown for calculating net radiative heat flux exchange between two ignitable elements such that element m is ignited.

Figure 4.4 shows the thermal radiation interaction between two ignitable elements, where element m is considered as the ignited source and element n as the target. The difference in view angles between the elements generate varied cumulative heat flux on each target element surface. To quantify the effects of radiation between two ignitable elements m and n , the local radiation matrix is defined as $Rad[m, n]$ of size $[k \times l]$ such that each entry represents the net thermal flux exchange between each possible source-target surface combination. The total radiation on the l^{th} surface of the target element is obtained as the summation along the rows of the l^{th} column of the radiation matrix. In case, the roles of ignitable elements m and n are reversed, the modified radiation matrix can be directly calculated as $Rad[2, 1] = Rad[1, 2]^T$.

Theorem 4.2.1 (Reciprocity theorem for view factors). *The theorem relates the view factor of the source surface with that of the incident surface in proportion to their respective surface areas, as given by equation: $A_{(k)}^{(m)} \cdot vf_{(k,l)}^{(m,n)} = A_{(l)}^{(n)} \cdot vf_{(l,k)}^{(n,m)}$*

Corollary 4.2.1.1. *If the roles of elements m and n are reversed such that element n is the source and element m is the incident element, the radiation matrix $Rad[n, m]$ can be evaluated as $Rad[m, n]^T$ if the elements m and n have the same material properties.*

Proof. Consider two ignitable elements, as shown in Fig. 4.4, such that m is the source element and n is the incident element. Each element is comprised of multiple surfaces, as shown in figure. The radiation matrix $Rad[m, n]$ is given by Eq. 4.12, which accounts for heat flux transfer between all surfaces of elements m and n . Based on the interaction of elements shown in Fig. 4.4 the radiation matrix can be established as shown in Eq. 4.18.

$$Rad[m, n] = \begin{bmatrix} 0 & 0 & q_{(1,3)}^{(1,2)} & q_{(1,4)}^{(1,2)} \\ 0 & 0 & q_{(2,3)}^{(1,2)} & q_{(2,4)}^{(1,2)} \\ 0 & 0 & 0 & 0 \\ 0 & 0 & 0 & 0 \end{bmatrix} \quad (4.18)$$

Assuming the flame temperature T_f and ambient temperature T_a to be a constant, Eq. 4.12 can be rewritten as Eq. 4.19

$$q_{(k,l)}^{(m,n)} = (A_{(k)}^{(m)} \cdot vf_{(k,l)}^{(m,n)} \cdot \kappa)_{\{k \in \mathcal{F}_{(m)}, l \in \mathcal{F}_{(n)}\}} \quad (4.19)$$

If the roles of ignitable elements m and n are reversed the radiation matrix $Rad[n, m]$ is given by Eq. 4.20.

$$Rad[n, m] = \begin{bmatrix} 0 & 0 & 0 & 0 \\ 0 & 0 & 0 & 0 \\ q_{(3,1)}^{(2,1)} & q_{(3,2)}^{(2,1)} & 0 & 0 \\ q_{(4,1)}^{(2,1)} & q_{(4,2)}^{(2,1)} & 0 & 0 \end{bmatrix} \quad (4.20)$$

Since elements m and n have similar material properties their flame temperatures would also be equal. Therefore, the heat flux $q_{(l,k)}^{(n,m)}$ can be written as given by Eq. 4.21.

$$q_{(l,k)}^{(n,m)} = (A_{(l)}^{(n)} \cdot vf_{(l,k)}^{(n,m)} \cdot \kappa)_{\{k \in \mathcal{F}_{(m)}, l \in \mathcal{F}_{(n)}\}} \quad (4.21)$$

By using the reciprocity theorem on Eq. 4.14, relation between $q_{(k,l)}^{(m,n)}$ and $q_{(l,k)}^{(n,m)}$ can be established.

$$q_{(k,l)}^{(m,n)} = A_{(k)}^{(m)} \cdot vf_{(k,l)}^{(m,n)} \cdot \kappa = A_{(l)}^{(n)} \cdot vf_{(l,k)}^{(n,m)} \cdot \kappa = q_{(l,k)}^{(n,m)} \quad (4.22)$$

The transpose of radiation matrix $Rad[m, n]$ is given by Eq. 4.23. Using Eq. 4.20 the radiation matrix $Rad[m, n]^T$ is observed to be equal to $Rad[n, m]$.

$$Rad[m, n]^T = \begin{bmatrix} 0 & 0 & 0 & 0 \\ 0 & 0 & 0 & 0 \\ q_{(1,3)}^{(1,2)} & q_{(2,3)}^{(1,2)} & 0 & 0 \\ q_{(1,4)}^{(1,2)} & q_{(2,4)}^{(1,2)} & 0 & 0 \end{bmatrix} \quad (4.23)$$

□

Depending on the configuration of source and target elements all surfaces of the source element do not transmit radiation to all surfaces of the target element. As seen from Fig. 4.4, only specific source-target surface combinations interact during radiation transfer. To assess which combinations result in successful transmissions a radiation interaction matrix is developed. Once the individual heat flux generated between different source-target surface combinations are calculated these values are updated using the interaction matrix. The general steps involved in formulating the radiation matrix are listed below.

- o Evaluate the order of numbering for each element to obtain the direction of numbering, as it plays an important role in subsequent calculations whether the numbering for an element are marked in a clockwise or anti-clockwise manner. Based on Eq. 4.24, if $A > 0$ it represents anti-Clockwise numbering and if $A < 0$ it represents clockwise numbering. $x_{(p)}^{(v)}$ and $y_{(p)}^{(v)}$ are the X and Y coordinates of the v^{th} node for the p^{th} element.

$$A = \sum_{v=1}^N (x_{(p)}^{(v+1)} - x_{(p)}^{(v)}) \cdot (y_{(p)}^{(v+1)} + y_{(p)}^{(v)}) \quad \forall \quad \{v \in [1, N_{element}], p \in \mathcal{W}_{(v)}\} \quad (4.24)$$

- o Find midpoint of all surfaces for both elements using the generalized X (Eq. 4.25) and Y (Eq. 4.26) coordinate equations. The midpoint is used as a reference point for all surfaces.

$$xm_{(p)}^{(v)} = \frac{1}{2}(x_{(p)}^{(v+1)} + x_{(p)}^{(v)}) \quad (4.25)$$

$$ym_{(p)}^{(v)} = \frac{1}{2}(y_{(p)}^{(v+1)} + y_{(p)}^{(v)}) \quad (4.26)$$

$$\hat{n}_{(p)}^{(v)} = [\hat{n}x_{(p)}^{(v)} \quad \hat{n}y_{(p)}^{(v)}] = A \cdot [-dy_{(p)}^{(v)} \quad dx_{(p)}^{(v)}] \quad (4.27)$$

- o Find normal vector for all surfaces at the corresponding midpoints calculated in previous step using Eq. 4.27, where $\hat{n}x_{(p)}^{(v)}$ and $\hat{n}y_{(p)}^{(v)}$ are the X and Y components of normal vector for v^{th} surface of p^{th} element.

$$dx_{(p)}^{(v)} = x_{(p)}^{(v+1)} - x_{(p)}^{(v)} \quad (4.28)$$

$$dy_{(p)}^{(v)} = y_{(p)}^{(v+1)} - y_{(p)}^{(v)} \quad (4.29)$$

- o Draw line segments joining the midpoints of all k surfaces of element m with all l surfaces of element n and obtain their respective vector equations individually using Eq 4.30 and Eq. 4.31, where $xm_{(k)}^{(m)}$ and $ym_{(k)}^{(m)}$ are the X and Y mid-point coordinates of k^{th} surface of source element m . Similarly, $xm_{(l)}^{(n)}$ and $ym_{(l)}^{(n)}$ are the coordinates of mid-points of l^{th} surface of target element n .

$$xr_{(k,l)}^{(m,n)} = xm_{(k)}^{(m)} - xm_{(l)}^{(n)} \quad (4.30)$$

$$yr_{(k,l)}^{(m,n)} = ym_{(k)}^{(m)} - ym_{(l)}^{(n)} \quad (4.31)$$

- o Check all line segments generated from the source element m for intersection with any of its other surfaces. For the thermal radiation, generated by any surface of the source element, the propagation path should not be obstructed by any of the other surfaces of the source element. The dot product of line segment with the normal vector of each surface is calculated, as shown in Eq. 4.32, where p is varied to consider each surface of source element.

$$tS_{(p,l)}^{(m,n)} = \frac{[xr_{(p,l)}^{(m,n)} \quad yr_{(p,l)}^{(m,n)}] \cdot [\hat{n}x_{(p)}^{(m)} \quad \hat{n}y_{(p)}^{(m)}]}{-[xr_{(k,l)}^{(m,n)} \quad yr_{(k,l)}^{(m,n)}] \cdot [\hat{n}x_{(k)}^{(m)} \quad \hat{n}y_{(k)}^{(m)}]} \quad \forall \quad p \in \mathcal{F}_{(m)} \quad (4.32)$$

A variable $M_s^{(m,n)}$ is defined to indicate if a line segment is obstructed. If $ts_{(p,l)}^{(m,n)}$ is not obstructed by any of the other surfaces of the source polygon $M_s^{(m,n)} = 1$, else 0.

- o Find the intersection point(s) for all line segments with each face of the destination element. The line segment generated from each surface can be hindered by surfaces of the target element. Similar to the previous step, the dot product of line segment with the normal vector of each surface is calculated, as shown in Eq. 4.33, where q is varied to consider each surface of target element.

$$td_{(k,q)}^{(n,m)} = \frac{[xr_{(k,q)}^{(n,m)} \quad yr_{(k,q)}^{(n,m)}] \cdot [\hat{n}x_{(q)}^{(n)} \quad \hat{n}y_{(q)}^{(n)}]}{-[xr_{(k,l)}^{(n,m)} \quad yr_{(k,l)}^{(n,m)}] \cdot [\hat{n}x_{(l)}^{(n)} \quad \hat{n}y_{(l)}^{(n)}]} \quad \forall \quad q \in \mathcal{F}_{(n)} \quad (4.33)$$

Another variable $M_d^{(m,n)}$ is defined to indicate whether the line segment is obstructed by any of surfaces of the target element n before the line segment reaches its target surface. If $td_{(k,q)}^{(n,m)}$ is not obstructed by any of the other surfaces of the target polygon $M_d^{(m,n)} = 1$, else 0.

- o A matrix is defined $Ac^{(m,n)}$ to assess whether the line segment generated from the source reaches its target surface. The matrix is given by Eq. 4.34, where 1 indicates successful transmission between a particular source-target combination and 0 indicates absence of transmission.

$$Ac^{(m,n)} = M_s^{(m,n)} \wedge M_d^{(m,n)} \quad (4.34)$$

- o The individual heat flux of each surface calculated using Eq. 4.35 is updated using the interaction matrix defined in previous step.

$$q_{(k,l)}^{(m,n)} = Ac^{(m,n)} \cdot q_{(k,l)}^{(m,n)} \quad (4.35)$$

4.2.3 Radiation Ignition

Once the total incident radiation flux for each target ignitable element surface $q_{(k,l)}^{(m,n)}$ is evaluated, the surfaces are checked for the possibility of ignition. The total flux of each surface is used to obtain the minimum residence time for flames $(t_{(l)}^{(m,n)})$ required for ignition. The residence time is defined as the time for which the flames continue to emit heat flux. Depending on the incident radiation flux, the flame is required to burn for a minimum residence time before it can cause ignition, and this time is given by Eq. 4.36 [36], where $FTP^{(n)}$ is the flux time product of the material of target element n , $Q_{(l)}^{(m,n)}$ is the total incident radiation on surface l calculated as the total sum of all incident radiation flux to a surface (as shown in Fig. 4.4), $Q_{cr}^{(n)}$ is the minimum critical flux required for ignition as a function of target element and $c^{(n)}$ is a constant derived based on material properties of the target element. The total incident flux is required to be higher than the critical flux for pilot ignition to occur.

$$t_{(l)}^{(m,n)} = \begin{cases} FTP^{(n)} \cdot (Q_{(l)}^{(m,n)} - Q_{cr}^{(n)})^c & \text{if } q_{(l)}^{(m,n)} > Q_{cr}^{(n)} \\ \infty & \text{otherwise} \end{cases} \quad (4.36)$$

Based on the minimum residence time, probability of ignition due to radiation for surface l ($p_{(l)}^{(m,n)}$) is calculated using Eq. 4.37, where $t_r^{(m)}$ is the residence time of each surface of source element m and $F(\cdot) : \mathbb{R} \mapsto \{0, 1\}$ represents a cumulative density function (CDF) of a normal distribution $\mathcal{N}(\mu, \sigma^2)$. The CDF is used to account for uncertainties associated with residence time of the source element. Eq. 4.38 gives the radiation ignition probability ($P_{rad}^{(m,n)}$) between elements m and n as the maximum of all surface probabilities of target element. The effects of radiation within a community are restricted to a specific distance, as seen from previous wildfire studies [36, 108, 112]. A threshold radiation distance (d_{th}) is introduced to ensure elements at a greater distance than the threshold distance are not affected by radiation. The distance $d_{min}^{(m,n)}$ is the minimum distance between all possible node combinations of elements m and n , as given by Eq. 4.39. The functions $\max(\cdot)$ and $\min(\cdot)$ correspond to the highest and lowest values in a set/matrix.

The mean residence time is calculated as $\mu = (t_{r,min} + t_{r,max})/2$. The parameter values used in the model are shown in Table 4.3.

$$p_{(l)}^{(m,n)} = \begin{cases} 1 - F(t_r^{(m)} - t_{(l)}^{(n)}) & \text{if } t_r^{(m)} \geq t_{(l)}^{(n)} \\ 0 & \text{otherwise} \end{cases} \quad (4.37)$$

$$P_{rad}^{(m,n)} = \begin{cases} \max(p_{(l)}^{(m,n)}) & \text{if } d_{min}^{(m,n)} < d_{th} \\ 0 & \text{otherwise} \end{cases} \quad (4.38)$$

$$d_{min}^{(m,n)} = \min(d_{(k,l)}^{(m,n)}) \quad (4.39)$$

Table 4.3: Radiation model parameter values

Parameter	Definition	Value	Reference
T_a	Ambient temperature of surroundings	300 K	[36]
T_f	Flame temperature	1000 K	[36]
$Q_{cr}^{(n)}$	Critical flux required for ignition (for wood)	13.1 kW/m ²	[36]
$FTP^{(n)}$	Flux time product (for wood)	13500 kW/m ² .s	[36]
c	Constant (obtained from experimental data)	-1.828	[36]
d_{th}	Radiation threshold distance	30 m	[36]
$t_{r,min}$	Lower bound on residence time	45 s	-
$t_{r,max}$	Upper bound on residence time	240 s	-
λ	Standard deviation	65 s	-
$\epsilon_{(k)}^{(m)}$	Emissivity (for wood)	0.84	-
σ	Stefan-Boltzmann constant	5.67x10 ⁻⁸ Wm ⁻² K ⁻⁴	-

4.3 Ember Spotting Model

One of the most prominent modes of propagation for wildfires is spotting due to the embers generated from fuels. The heat generated by ignited fuel heats up the air around it and creates an updraft, generally referred to as a Convection Column. These updrafts launch embers generated from the fuel into the atmosphere. Once the firebrands regain certain height based on their mass, since heavier embers rise to lower heights than lighter embers, the winds carry the embers forward. The embers follow a downward parabolic path, similar to projectile motion. A key difference in case of embers is that their mass decreases while falling due to continuous combustion. Based on the mass during landing, embers have a capacity to ignite fuel (if present) at the landing site. The embers provide significant amount of complexity to understanding wildfires, as they tend to travel farther downstream than the actual fire front, thereby resulting in multiple fire fronts. The unpredictability and capacity of embers for destruction is a major concern. The literature on theoretical ember models is quite scarce to begin with. Although, some researchers have developed stochastic models to capture distribution patterns of embers. Spotting has also been incorporated in well-known wildfire propagation frameworks such as PROMETHEUS and FARSITE. However, the limitation of these implementations lies in the fact that they are either entirely empirical in nature or entirely deterministic. In addition, almost all models are framed in context of wildlands and lack sufficient flexibility, making these models unsuitable in context of community propagation. In this study, stochastic formulation of ember spotting is required such that probability distribution of ember ignition can be obtained as a function of distance and direction from the fuel source.

Ember-driven fire ignitions are heavily influenced by a number of factors such as wind direction (θ), wind speed (v_w), ember size and shape, among others, which are difficult to account for deterministically. A separate probabilistic ember spotting model is formulated for the graph model, which incorporates the effect of embers in regards to possible ignition as a combination of these factors. The probability of ignition due to ember spotting $P_{ember}^{(i,j)}$ is given by Eq. 4.40, where $P_{acc}^{(i,j)}$ is the relative probability of access for embers and $g^{(i,j)}(.) : \mathbb{R} \mapsto [0, 1]$ is the probability distribution function between nodes i and j , given by a distribution function $S(i, d^{(i,j)}, v_w)$ (Eq. 4.41).

The distribution is uniquely defined for each (i, j) node pair interaction as a function of volume of source node i ($V_n^{(i)}$), the distance between nodes i and j ($d^{(i,j)}$), and wind speed (v_w).

$$P_{ember}^{(i,j)} = P_{acc}^{(i,j)} \cdot F_{cc}^{(i,j)} \cdot g^{(i,j)} \quad (4.40)$$

$$g^{(i,j)} = S(V_n^{(i)}, d^{(i,j)}, v_w); \quad (4.41)$$

The probability of access ($P_{acc}^{(i,j)}$) is an indication of the ease with which an ember can ignite an element based on its design, which may include material properties [32], layout design [33] and other factors. In the proposed model, different type of elements are considered based on their functions, for instance - commercial, residential, natural areas and others. Relative probabilities are assigned to elements based on their functional classification (Table 4.4). The idea behind the accessibility factor is that the same amount of embers would not have the same probability of causing ignition to different type of areas. For instance, consider an area with vegetation and a wooden house. If the same number of embers accumulate in both areas the chances of vegetative area catching fire would be higher than the house. Similarly, a wooden house would have a higher chance of ignition than a steel warehouse. In light of no literature on this concept, relative probabilities were assigned in this study, but in the future it is hoped that these can be calibrated using experimental studies.

The ember model developed by Martin and Hillen [113] is utilized to obtain the nodal ember probability distribution ($S(V_n^{(i)}, d^{(i,j)}, v_w)$). The authors utilized general concepts of birth-jump processes [114] to formulate distribution functions for different ember spotting conditions. The concept of birth-jump is used to describe processes in which growth and spatial spread cannot be decoupled, as in the case of embers generated during wildfires. Other examples of birth jump

Table 4.4: Relative access probabilities for different type of ignitable elements

Landuse	Building	Natural area	Leisure	Shop	Office
1.0	0.90	1.0	0.80	0.85	0.70

processes include - distribution of pollen generated by flowers and scatter of confetti thrown in air. The ember spotting can be theoretically categorized into four key phases - (1) Launching phase (2) Transport and Combustion phase (3) Landing phase (4) Ignition phase. As described earlier, launching phase involves embers being uplifted into the atmosphere, followed by transport by winds during which combustion of embers also occurs. Finally, based on landing distribution of embers the fuel is ignited. For this study, it is assumed that embers cause ignition of fuel at landing site on contact; hence, micro level factors affecting ember ignition are not taken into account and the ignition phase is considered equivalent to the landing phase. Within the three phases mentioned different mechanisms were individually modeled by the authors and combined together to obtain the ember probability distribution.

The launch phase of embers is described by launching distribution $\phi(z, m)$ such that it gives the number of embers generated of mass m (in kg) at the height z (in m). It is assumed that the height attained by embers is independent of their mass, thus, the distribution is given by Eq. 4.42. The height distribution is assumed, as given by Eq. 4.43, since this kernel has been observed to be a good fit for fire propagation [113].

$$\phi(z, m) = Z(z)\mu(m) \quad (4.42)$$

$$Z(z) = \lambda e^{-\lambda z} \quad (4.43)$$

The mass distribution is assumed as shown in Eq. 4.44 such that $0 \leq m \leq m_{max}$ holds true. The mass distribution was selected to fit the ember experiments conducted at NIST [87–91]. The rate change of mass with time is assumed at a constant rate, as shown in Eq. 4.45.

$$\mu(m) = am^{-0.5} \quad (4.44)$$

$$\frac{dm}{dt} = -\kappa \quad (4.45)$$

A Combustion operator $C(m, t)$ was introduced to determine extent of combustion by tracking the mass of embers with respect to time. The combustion operator $C(m, t)$ gives the mass remaining while the inverse operator $C^{-1}(m, t)$ gives the burnt out mass, such that relation Eq. 4.46 holds true, which results in Eq. 4.47.

$$C^{-1}(C(m, t), t) = m \quad (4.46)$$

$$C^{-1}\left(m, \frac{x}{w}\right) = m + \kappa\left(\frac{x}{w}\right) \quad (4.47)$$

The landing distribution $L(x, m)$ determines the number of embers of mass m (in kg) at a distance x (in m) at time t (in s) and can be approximated as the asymptotic landing distribution, as given by Eq. 4.48. Based on the principle of birth jump processes, the launching distribution ($\phi(z, m)$) of embers can be correlated to the landing distribution. The derivation of correlation between the two distributions has been described in detail in [113] and is given by Eq. 4.49, where v_t is the terminal velocity of embers and v_w is the horizontal wind speed.

$$\mathbb{L} = \lim_{t \rightarrow \infty} L(x, m, t) \quad (4.48)$$

$$\mathbb{L} = N\phi\left(\left|v_t\right|\frac{x}{v_w}, C^{-1}\left(m, \frac{x}{v_w}\right)\right) \quad (4.49)$$

The probability of an ember to cause ignition at the landing site is strictly correlated to the amount of mass present in an ember during the landing phase. If m represents the mass of embers the total landing mass of embers (M) can be calculated as given by the general Eq. 4.50, which is solved to obtain Eq. 4.51, wherein the index i is added since number of embers generated can vary for different nodes in a graph. Using the landing mass the probability of ignition S is obtained by formulating an ignition function E , which can be defined in a number of ways, specifically based on experimental studies conducted on embers. A viable choice for an ignition function can

be defined as a piecewise linear function to obtain the ember probability function S , as shown in Eq. 4.52. The ember probability function can be written as $S(V_n^{(i)}, d^{(i,j)}, v_w)$ since the number of embers generated is a function of volume of a node.

$$M(x) = \int_0^{m_{max}} m \mathbb{L}(x, m) dm \quad (4.50)$$

$$M(i, x, v_w) = N_e^{(i)} \lambda a \left(\exp^{-\lambda |v_t| \frac{x}{v_w}} \right) \left(\frac{2}{3} m_{max}^{\frac{3}{2}} - \frac{2\kappa x m_{max}^{0.5}}{v_w} + \left(\frac{4}{3} \frac{\kappa x}{v_w} \right)^{1.5} \right) \quad (4.51)$$

$$S(i, x, v_w) = E(M(i, x, v_w)) = \begin{cases} \frac{M(i, x)}{m_{min}} & \text{if } M(i, x) \leq m_{min} \\ 1 & \text{if } M(i, x) > m_{min} \end{cases} \quad (4.52)$$

$N_e^{(i)}$ is the number of embers generated by node i and given by Eq. 4.53 as a function of its fuel volume ($V^{(i)}$). N_e^* and V^* are scaling parameters. The fuel volume of a node ($V_n^{(i)}$) is the amount of ignitable fuel present at a node and it is calculated assuming equal distribution between all nodes of an ignitable element. It is given by Eq. 4.54, where $V_w^{(m)}$ is the total fuel volume of element m (ignited or source element), $W_{(m)}$ is the node set of element m and $N_{(m)}$ is the total number of nodes. In this study, stray vegetation around the elements is not marked explicitly in the community layout; therefore, the entire volume of elements is considered as fuel volume to offset the absence of vegetation and to keep the analysis on the conservative side. For best practice, the fuel volume at each node would have to be considered explicitly based on nature of the element.

$$N_e(i) = V_n^{(i)} \left(\frac{N_e^*}{V^*} \right) \quad (4.53)$$

$$V_n^{(i)} = \left(\frac{V_w^{(m)}}{N_{(m)}} \right)_{i \in W_{(m)}} \quad (4.54)$$

To calibrate the ember distribution model, previous experimental investigations on ember spotting are used [87, 90, 115]. The experiments comprised of burning individual tree samples under constant wind and collecting generated embers to determine their respective mass distribution. N^* is the number of embers collected and V^* is the volume of tree used in the experiment (Eq. 4.55), which is calculated assuming a cylindrical configuration. r^* and h^* are the radius and height of tree used. The values of all parameters are shown in Table 4.5.

$$V^* = \pi(r^*)^2 h^* \quad (4.55)$$

Table 4.5: Ember model parameter values

Parameter	Definition	Value	Reference
m_{min}	Minimum ember mass observed	0.001 kg	[87]
m_{max}	Maximum ember mass observed	0.004 kg	[87]
a	Mass distribution parameter	7.91	[87]
v_t	Ember terminal velocity	-4.3 m/s	[116]
κ	Ember combustion rate	0.00005 m/s ²	[113]
λ	Ember decay rate	0.01 m/s ²	[113]
N^*	Reference number of embers	100	[87]
r^*	Reference radius	2 m	[87]
h^*	Reference height	5.2 m	[87]

Figure 4.5 shows the effect of three key parameters - Fuel volume of node, distance between nodes and wind speed, on the ember distribution obtained from the discussed formulation. The ember distribution model discussed is only one such model. There exist several other variations based on the underlying assumptions considered in formulating the model. These include consideration of (1) change in shape of embers (2) variation in wind speed with height (3) change in ember paths midflight and several others. Hence, the ember model can be further modified to include other factors.

One of the biggest limitations of the discussed ember model is that it is highly sensitive to changes in wind speed. In actual wildfires, severe fluctuations in the local wind field occurs due to

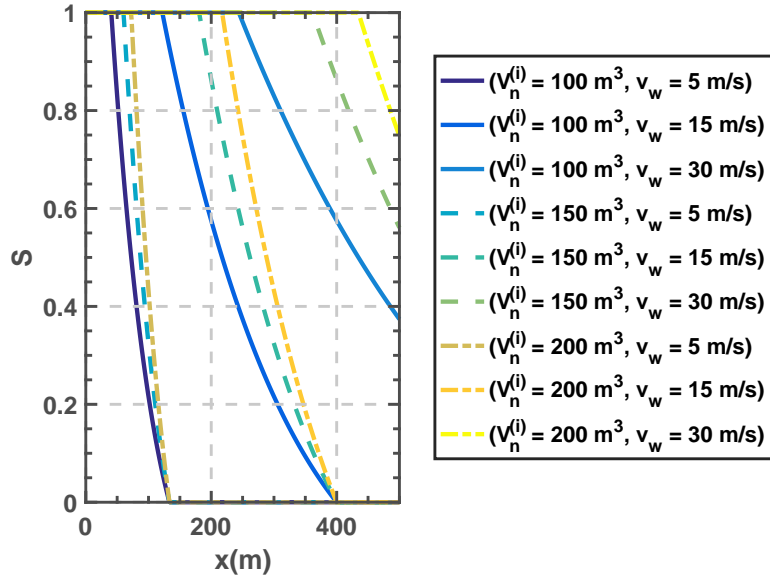


Figure 4.5: Ember ignition probabilities as a function of distance x for different values of volume $V_n^{(i)}$ and wind speed v_w

change in temperature gradient with time. As a result, embers in most cases are observed to fly in different directions than the dominant wind direction. A prominent example of this phenomena is the generation of fire vortices, which are observed in high intensity wildfires. These vortices tend to distribute embers in all directions irrespective of the dominant wind direction over the area. The graph model in this study has been formulated in a way that any changes to the wind field can be incorporated seamlessly and phenomena such as fire vortices can be modeled as well. In order to utilize the full potential of the formulated graph model the ember model would have to be coupled with a computational fluid dynamics model to keep track of the local changes in wind, which would update the ember model at each time step. Since the scope of this study is kept restricted to static version of the graph model this aspect is not discussed in this study.

4.4 Community Model Validation

The proposed graph model and its sub-models would require validation before the study can be considered complete. All the three sub-models for different heat transfer modes were formulated using existing validated theories and models from wildfire literature. The basis for each model is

described in their subsequent sections. The graph model as a whole was tested on the community of Oakland (California, USA) to simulate conditions similar to the infamous 1991 Oakland wildfire, as discussed in Section 5.4 of Chapter 5. The case study is conducted to draw out meaningful results that may confirm the applicability of the proposed model. The observations from the analysis conducted reaffirmed some of the long-stated findings from previous studies. The results provided a better understanding of the effects of intrinsic factors, which relate to factors that are naturally present in a community, and mitigation factors, which can be altered to regulate vulnerability of the community, on communities. There still exist certain aspects of the graph model that still need to be validated, which primarily require a dynamic version of the graph model.

Chapter 5

Community Vulnerability and General Observations

5.1 Introduction

The problem of wildfire propagation constitutes a parallel replication flow problem, similar to the principle involved in disease transmission. In case of disease spread, viruses can spread through short-range, as well as, long range modes by means of either physical contact or through airborne vectors. Similarly, depending on wind conditions, wildfires also propagate both short- and long-range distances at the same time using radiation, convection and embers modes of heat transfer. As described in the previous chapter, considering different modes of heat propagation between nodes of different ignitable elements the probability of ignition can be calculated between them. By combining the individual probabilities calculated between individual elements the total probability of ignition from a particular source to a target element can be calculated, since the probability of ignition due to any of the modes is mutually exclusive to one another. Thus, vulnerability of a element can be defined as the probability of wildfire reaching it once a fire has been initiated from single or multiple sources. In this chapter, description on the theoretical formulation and the algorithms used to evaluate community vulnerability have been detailed. Followed by application of the vulnerability framework on Oakland, CA, to better understand the mechanisms of wildfire propagation inside communities.

5.2 Vulnerability Evaluation

Based on the above discussion, in order to evaluate vulnerability of a target element high probability paths need to be identified between source and target elements as the fire would travel the paths of least resistance. These paths would entail the highest likelihood of wildfire propagation and are referred to as Most Probable Paths (MPP) in the study. The first step to evaluating vulnerability is to assess the total probability of propagation along an MPP, which is calculated as

the product of the edge weights (Eq. 5.1), such that $\mathcal{M}_{(x)}$ is the adjacency list of x^{th} MPP given by $\mathcal{M}_{(x)} = \{(n_{(1)} \rightarrow n_{(2)}), \dots, (n_{(N_{\mathcal{M}_{(x)}}-1)} \rightarrow n_{(N_{\mathcal{M}_{(x)}})})\}$, where $N_{\mathcal{M}_{(x)}}$ is the total members in adjacency list $\mathcal{M}_{(x)}$ and n_i are the individual nodes in the corresponding MPP.

$$P_{MPP}^{(x)} = \prod_{(i \rightarrow j) \in \mathcal{M}_{(x)}} P_{tr}^{(i,j)} \quad (5.1)$$

Once the fire is initiated from a single or multiple sources, the wildfire is not restrained to a single path, instead, multiple surrogate paths are expected to reach a target ignitable element; hence, the total probability of fire reaching a particular element is defined as the mean probability of K MPPs $P_m^{(s)}$ (Eq. 5.2). K is a user defined number that determines the different number of paths considered from single or multiple sources to a target element. Due to computational limitations, $K = 10$ is used for all analysis in this study. By increasing the number of parallel paths, accuracy of the model can be improved at the cost of increased computation time. A community layout with high density would require a low K value, and vice-versa. It would be the users' decision to balance this trade-off.

$$P_m^{(s)} = \frac{1}{K} \sum_{x=1}^K P_{MPP}^{(x)} \quad (5.2)$$

A wildfire entering a community has multiple source nodes (initial point of fire origin in the community) at the wildland-urban interface, or some even inside the community, due to ember spotting from wildlands [92, 108, 112]. The final step in evaluating vulnerability of a particular element is to account for the presence of multiple sources. Eq. 5.3 is used to calculate the total vulnerability ($V^{(z)}$) of destination node $z \in \mathcal{W}_{(m)}$, where $\mathcal{W}_{(m)}$ is the node set for element m , $P_i^{(s)}$ is the ignition probability of source node s and \mathcal{S} is the node set of all sources. The term ignition probability $P_i^{(s)}$ for a particular source node is introduced to take into account the spatial characteristics of each source. Since probability of ignition for each source is correlated to wind conditions and wildland vegetation in the vicinity of the community (Fig. 5.1), these conditions need to be considered while evaluating ignition probability for each source. The wildfire is required

to reach the target from only one of the sources for pilot ignition; the vulnerability is defined as the maximum probability from all source nodes. The total vulnerability of a community is further defined using the individual element vulnerabilities using Eq. 5.4, where $N_{W(m)}$ is the total number of nodes in element m . Vulnerability of community and its components (elements) can be defined in several forms and the approach discussed in this study is one such possibility.

$$V^{(z)} = \max_{\{s \in \mathcal{S}\}} \left(P_i^{(s)} \cdot P_m^{(s)} \right) \quad (5.3)$$

$$V_{avg} = \frac{1}{N_W N_{W(m)}} \sum_{m=1}^{N_W} \left(\sum_{z=1}^{N_{W(m)}} V^{(z)} \right) \quad (5.4)$$

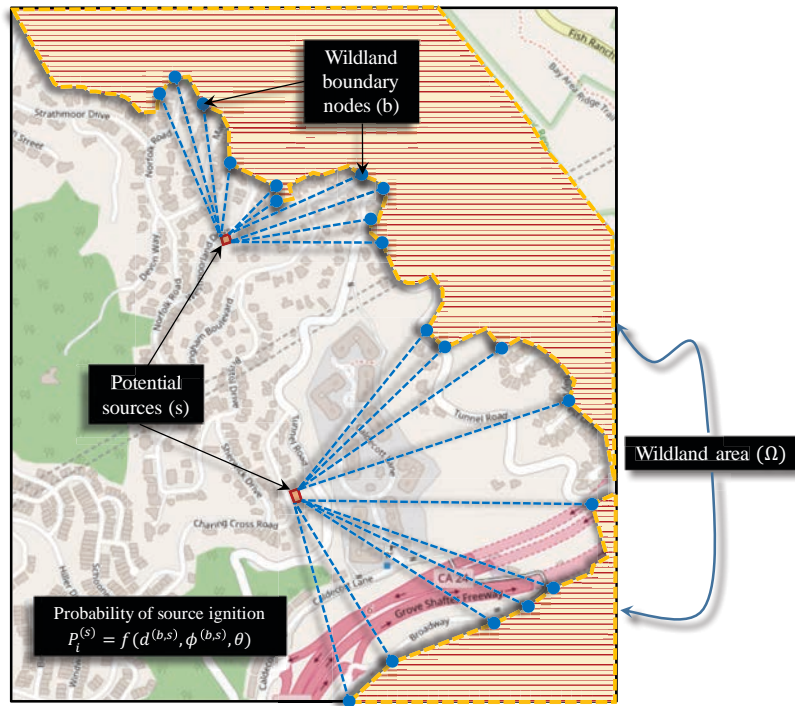


Figure 5.1: Procedure for evaluating probability of ignition for any source node s inside the community due to the wildlands Ω (©OpenStreetMap contributors [107])

5.2.1 Shortest Path Algorithm

The theoretical formulation of vulnerability discussed above is strictly contingent on finding the most probable paths (MPP) within a given community layout. The MPPs are obtained by solving the maximization problem shown in Eq. 5.5, where the main objective is to maximize P the cumulative product of edge weights $a^{(i,j)}$ within individual propagation paths $\mathcal{M}_{(x)}$ to determine path x with maximum value for P . In context of graph theory, there has been significant research on algorithms to determine shortest path for both directed and undirected graphs. The Shortest Path problem is an optimization problem that has been studied extensively over the years. The Shortest Path problem has applications in many different areas including operations research, robotics, transportation and communications. In graph theory, the shortest path problem is defined as the problem of finding a path between two vertices in a graph between ignitable elements such that the sum of the weights (costs) of edges comprising the path is minimized and can be summarized as shown in Eq. 5.6, where D is the cumulative sum of edge weights to be minimized. Weights can be distance, time, cost or any other measuring criterion depending on the nature of the problem involved. By introducing a modification, the shortest path algorithms can be used to evaluate most probable paths as well. If the weights of a graph are modified by taking the modulus natural logarithm the shortest path problem can be rewritten as Eq. 5.7, which is converted to a maximization problem since logarithm functions are monotonically decreasing. Using the product property of logarithms the edge weight summation is converted to a product (Eq. 5.8). Using Eq. 5.5 and Eq. 5.8 a correlation can be established between P and D^* , as shown in Eq. 5.9. Thus, by modifying the edge weights $P_{tr}^{(i,j)}$ in the formulated wildfire graph \mathcal{G} shortest path algorithms can be applied to obtain the most probable paths.

$$\max_x \left\{ P = \prod_{(i \rightarrow j) \in \mathcal{M}_{(x)}} a^{(i,j)} \right\} \quad (5.5)$$

$$\min_x \left\{ D = \sum_{(i \rightarrow j) \in \mathcal{M}_{(x)}} a^{(i,j)} \right\} \quad (5.6)$$

$$\max_x \left\{ D^* = \sum_{(i \rightarrow j) \in \mathcal{M}(x)} |\log(a^{(i,j)})| \right\} \quad (5.7)$$

$$\max_x \left\{ D^* = \left| \log \left(\prod_{(i \rightarrow j) \in \mathcal{M}(x)} a^{(i,j)} \right) \right| \right\} \quad (5.8)$$

$$P = e^{|D^*|} \quad (5.9)$$

To identify most probable path Dijkstra's shortest path algorithm [117] is used. In 1956, Dutch computer scientist, Edsger Dijkstra, introduced Dijkstra's Algorithm, a graph search algorithm that solves the single-source shortest path problem for a graph with non-negative edge weights. The single-source shortest path is a variation of the shortest path problem in which finding the shortest path from the source vertex (node) to all other vertices in the graph is considered. For a directed graph $G \in \mathcal{V}, \mathcal{E}$ such that \mathcal{V} are the vertices and \mathcal{E} are the edges with A as the adjacency matrix. The Dijkstra's algorithm is used to create a spanning tree T from a vertex, such that the total distance between the vertex and any other node in T is the minimum distance. To create the spanning tree T the following steps are considered according to Dijkstra's algorithm:

1. Dijkstra's algorithm starts from the initial node selected as the source node (v_0). All nodes are initially marked as unvisited and assigned to set U .
2. The Initial node is set as the current node and assigned a distance value of zero. For all other nodes a value of infinity is assigned.
3. For the current node, distances are calculated to all of its unvisited neighbors, which is defined as the sum of distance to the current node and the distance from it to the neighboring node. If the distance is lower than previously set distance value for the node then it is updated by the recent value.
4. Once distances to all unvisited neighbors of the current node have been calculated the current node is set to be visited and removed from set U .

5. The algorithm is stopped when the destination node has been removed from the unvisited set (U) or when no possible path can be found between the initial and destination node, i.e. smallest distance between them is infinity.
6. If termination does not occur, the node in set U with the shortest total distance is marked as current node and the process repeated from step 3.

Dijkstra's algorithm is used to evaluate the shortest path between the source and sink. To determine K-shortest paths Yen's algorithm [118] is used. In case of the proposed wildfire graph framework, certain modifications are made to increase the accuracy of the algorithm. Since each element in the community is a collection of nodes of similar properties (ignition likelihood primarily), a element can be essentially represented as a complete graph. Due to similar properties within a element internal edge weights are always unity (as shown in Eq. 4.1), Yen's algorithm could provide superfluous paths. Thus, the algorithm is modified such that multiple paths through different nodes of the same element are removed from the K-shortest path list. The wildfire graph \mathcal{G} is formulated from the nodes of ignitable elements present in a community. Each element is represented by a set of nodes ($\mathcal{W}_{(k)}$). Once a path is found to the destination node, any paths found after it that comprises of any nodes belonging to same elements are removed from the shortest path list. Since the nodes of each element form a complete graph there would be no point in keeping multiple paths with different nodes of the same element, as they would result in the same vulnerability and thus introduce bias. An algorithm flowchart of Yen's algorithm is shown below.

Result: Determine K shortest paths

// Shortest path from source to target

A[0] = Dijkstra(Graph, source, sink) ;

// Initialize variable to store K^{th} shortest path

for $k = 1$ **to** K **do**

 // Loop to control node range from first to last node in the previous k-shortest path

for $i = 0$ **to** $size(A[k - 1]) - 2$ **do**

 // Spur node obtained from previous k shortest path (k-1)

 spurNode = A[k-1].node(i) ;

 // The sequence of nodes from the source to the spur node of the previous k-shortest path

 rootPath = A[k-1].nodes(0, i) ;

for each path p in A **do**

if $rootPath == p.nodes(0, i)$ **then**

 // Remove links that are part of the previous shortest paths sharing same root path

 remove $p.edge(i, i + 1)$ from Graph ;

end

end

for each node $rootPathNode$ in $rootPath$ except $spurNode$ **do**

 remove $rootPathNode$ from Graph ;

end

 // Calculate the spur path from the spur node to the sink

 spurPath = Dijkstra(Graph, spurNode, sink) ;

 // Entire path is made up of the root path and spur path

 totalPath = rootPath + spurPath; // Add the potential k-shortest path to the heap

 B.append(totalPath) ;

 // Add back the edges and nodes that were removed from the graph

 restore edges to Graph ;

 restore nodes in $rootPath$ to Graph ;

if B is empty **then**

 break ;

end

 // Sort the potential k-shortest paths by cost

 B.sort() ;

 // Add the lowest cost path becomes the k-shortest path

 A[k] = B[0] ;

 B.pop() ;

 return A ;

end

end

Algorithm 1: Yen's Algorithm

5.2.2 Polar Fragility

Wind conditions have a significant impact on wildfire intensity and behavior, as observed from different wildfire cases seen in the past. Wind speed, on one hand, has a directly proportional effect on the intensity. Higher the wind speed higher the rate of spread will be. On the other hand, the effect of wind direction has a significant impact on the direction of propagation, however, the effect is not so straight forward as it depends on the community layout. There might be multiple favorable directions of wind that might accentuate wildfire spread for a particular community layout and these directions would vary depending on the characteristics of each layout. To understand wildfire behavior, considering the effects of wind conditions is vital. To represent vulnerability as a function of wind speed and direction a unique fragility curve is introduced, referred to as Polar fragility in the study. The individual data points in the polar fragilities represent the mean probability of fire reaching a house in the community from the wildland urban interface for a particular wind direction. These fragilities are formulated by varying the wind direction at specific intervals, which in this case is selected to be 30° , and calculating the mean vulnerability of community, as described in the previous section. For each wind direction a new graph is formulated by updating the nodal probabilities. Based on the framework discussed in Chapter 4, wind direction has an effect on Convection and Ember modes of heat transfer. Therefore, for each wind direction selected, the convection and ember probabilities have to be updated between each ignitable element in the community layout. Once all probabilities are updated and a new graph has been formulated, the shortest path algorithms are applied again to obtain the new vulnerability of each element, and thereafter, the new mean vulnerability of the community for the wind direction chosen.

A part of Hacienda Heights (HH) in Los Angeles (California) is used as a test case to demonstrate the importance of the concept. The layout is chosen to represent a typical medium density community. Fire pathways are identified for a target element from a source element for different wind directions (Fig. 5.2). For wind direction parallel to the line segment joining source and target elements, a high vulnerability is to be expected ($V = 0.90$ for $\theta = 300^\circ$ and $v_w = 15m/s$). However, a relatively high vulnerability is observed for other wind directions as well (Fig. 5.2(c)).

Wind direction is measured anti-clockwise from the positive x-axis, such that a N-S wind would be represented by $\theta = 270^\circ$ and S-N wind by $\theta = 90^\circ$. The fire utilized inherent path redundancy present in the community layout to its advantage. The effect of wind direction on vulnerability is seen to be negligible for wind speeds 15 m/s and 5 m/s. In these cases, ember and radiation modes, both, played a dominant role, thereby providing sufficient buffer to each other. A strong dependency of wildfire propagation on community layout is known to exist [92, 112]. For low wind speed ($v_w = 2\text{m/s}$), wind direction governs vulnerability to a great extent, since the effect of ember and convection modes are reduced. As a result, for wind directions not parallel to line segment connecting the source and target elements, the fire has to rely only on radiation mode. Discontinuities in the community layout inversely affects radiative propagation [112, 119], thereby reducing the vulnerability. Based on the polar fragilities, the net vulnerability of a community can be evaluated as given by Eq. 5.10, for a particular range of wind directions.

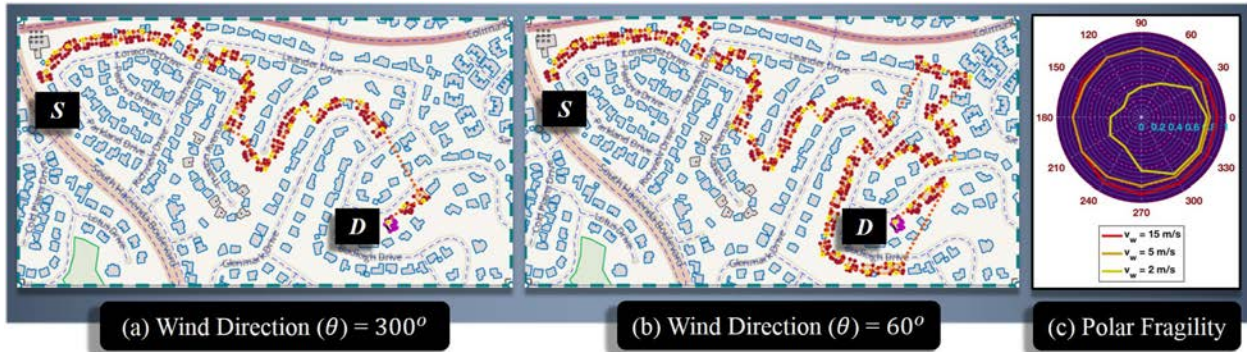


Figure 5.2: Calculation of vulnerability of destination element (D) due to source element S for a part of an actual community Hacienda Heights, Los Angeles, CA. (a) Fire pathways shown for wind direction $\theta = 300^\circ$ (b) Fire pathway shown for wind direction $\theta = 60^\circ$ (c) Fragility curve to represent variation in vulnerability of element D for different wind directions (θ) and wind speed v_w (©OpenStreetMap contributors [107])

$$V_{total} = \frac{1}{\pi} \int_0^{360^\circ} V_{avg}(\theta) d\theta \quad (5.10)$$

5.3 Intervention Framework

Community vulnerability is a function of the topographic features and the meteorological conditions, but it is also affected by the response of community to the wildfire. Fire mitigation efforts are an integral part of evaluating community vulnerability. To get an accurate account of it some form of fire mitigation needs to be modeled with the wildfire propagation model. Intervention measures can be primarily classified into two types - (1) Passive and (2) Active strategies. The former includes, but not limited to, measures like cleaning ignition zone around houses of mulch and unnecessary vegetation, implementing fire-proof roofing and others. Passive intervention primarily deals with fire mitigation measures that are effective pre-ignition i.e. before a house catches fire. On the other hand, Active strategies refer to measures that are activated/effective post-ignition i.e. once a house catches fire, such as automatic sprinkler systems. Both strategies are essential to mitigate wildfire risk, however, in this study the intervention framework developed pertains to primarily the effect of passive strategies. In order to implement active strategies, the exact time frame for ignition is required. Since the proposed graph model is formulated in a way so as to make it static i.e. time independent, active strategies cannot be yet implemented. A dynamic variant of the proposed graph model would be required to implement the effect of active strategies, and as mentioned in earlier sections, the scope of this study is restricted to static formulation.

In this study, a passive intervention framework is implemented to account for different fire mitigation efforts adopted by communities. The general steps involved in modeling the effect of passive strategies in context of the graph model are listed below:

- o The graph model is implemented to obtain a directed cyclic graph (\mathcal{G}) for the community layout.
- o A term μ is defined to represent intervention strength possessed by a community. An appropriate value for μ is defined for the given community to reflect fire mitigation capacity in terms of percentage of ignitable elements. In other words, intervention strength is defined as

the percentage of houses in a community on which some form of intervention has been applied. Therefore, higher the value higher the number of elements protected in a community.

- o Based on the strength of fire mitigation chosen (μ), a percentage of the total ignitable elements present in the community $\mu \cdot N_{\mathcal{W}}$ are chosen at random, assuming a uniform distribution such that each element has an equal likelihood of being selected, to create the set $\{\mathcal{W}_M | \mathcal{S} \notin \mathcal{W}_M\}$, where \mathcal{S} is the set of source nodes. The elements incorporated into the newly formed set are the houses on which intervention is applied. In a particular community, for $\mu < 100\%$ there can be several possibilities of intervention strategies based on which elements are selected.
- o When an ignitable element is protected by some form of intervention measure its capacity for ignition and its capacity for transmission of fire should reduce. The inflow and outflow for each node of the elements in the formulated set \mathcal{W}_M , which represent the elements selected for intervention, are altered to modify the original graph (G), as shown in Fig. 5.3. Equation 5.11 represent the change in indegree and outdegree of each node for the selected elements. n is the total number of nodes in graph \mathcal{G} .

$$a_{(v,j)} = \alpha \cdot a_{(v,j)} \quad a_{(j,v)} = \beta \cdot a_{(j,v)} \quad \forall \quad \{v \in \mathcal{W}_M^{(l)} | l = 1 : N_{\mathcal{W}_M}, j = 1 : n\} \quad (5.11)$$

- o α represents the scaling factor for outflow from node v to other nodes j , which would be affected by factors such as sprinkler systems and others. β represents the scaling factor for inflow to node v from other nodes j , which would include effect of fire-proof paint and barriers and others. α and β are mitigation scaling factors that are assumed to be 0.10 and 0.75. The former value is assumed based on the fire mitigation capacity of sprinklers [120]. Ideally, both the mitigation factors should have been assumed as 0, however in reality such is not the case. No matter how much protection is given to a structure if there are significant sources present in the vicinity the target structure will most likely get ignited. On the other

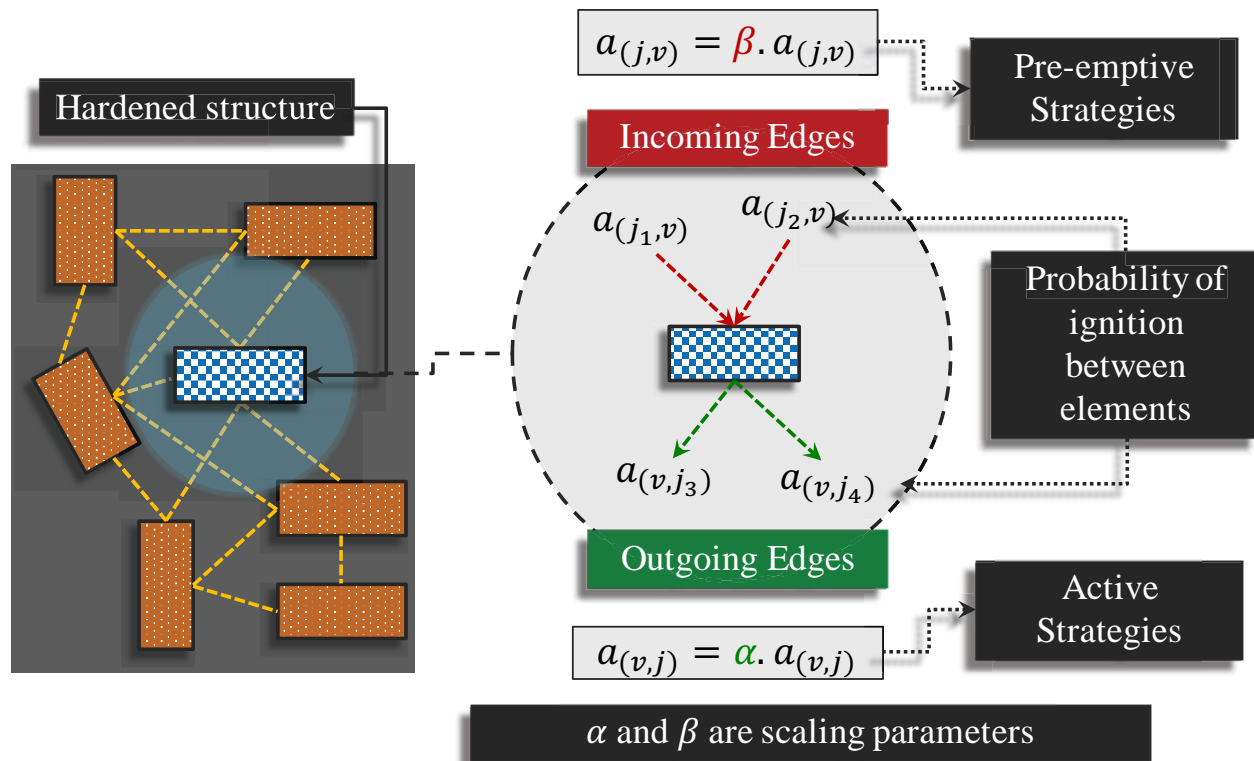


Figure 5.3: Active and Passive intervention formulations applied to the graph theory model

hand, the transmission capacity of a structure to spread the fire onwards can be significantly reduced, therefore $\beta \gg \alpha$.

- o Once the graph G is modified, the vulnerability framework, discussed in previous section, is applied to obtain the new vulnerabilities of each individual ignitable element and the mean vulnerability of the community.

5.4 Community Analysis Results

To identify and understand the underlying sources of community vulnerabilities for wildfire, the 1991 Oakland Hills wildfire is considered as a case study. The infamous wildfire, also known as the 'Tunnel Fire', resulted in 25 fatalities, 150 casualties and approximately US\$ 1.5 billion in economic losses, making it one of the most destructive wildfires in history [121]. Figure 5.4 shows the affected region and the origin of the wildfire. The fire started as an incompletely extinguished grass fire. However, it quickly escalated to a firestorm when seasonal northerly winds, commonly

referred to as 'Diablo' winds, entered Oakland hills (at a speed $> 100\text{km/hr}$) and reignited the brush fire. The winds propelled the wildfire rapidly in the south-west direction. By noon, the wildfire had crossed two highways and reached Piedmont (South of Oakland hills), after which the winds shifted towards south-east [122, 123]. The graph model is tested on Oakland to understand the level of vulnerability posed to the community in case of a similar event. Second, the model is utilized to identify vulnerability factors of communities to WUI fires. For the tests, conditions similar to that of the 1991 wildfire are simulated. The analysis is performed in two steps by dividing the regions into - (a) O_I and (b) O_{II} (Fig. 5.4), for which the wind directions are chosen to be $\theta = 225^\circ$ and $\theta = 300^\circ$, and the wind speed to be $v_w = 29.058\text{ m/s}$ (104.42 km/h) [122, 123].

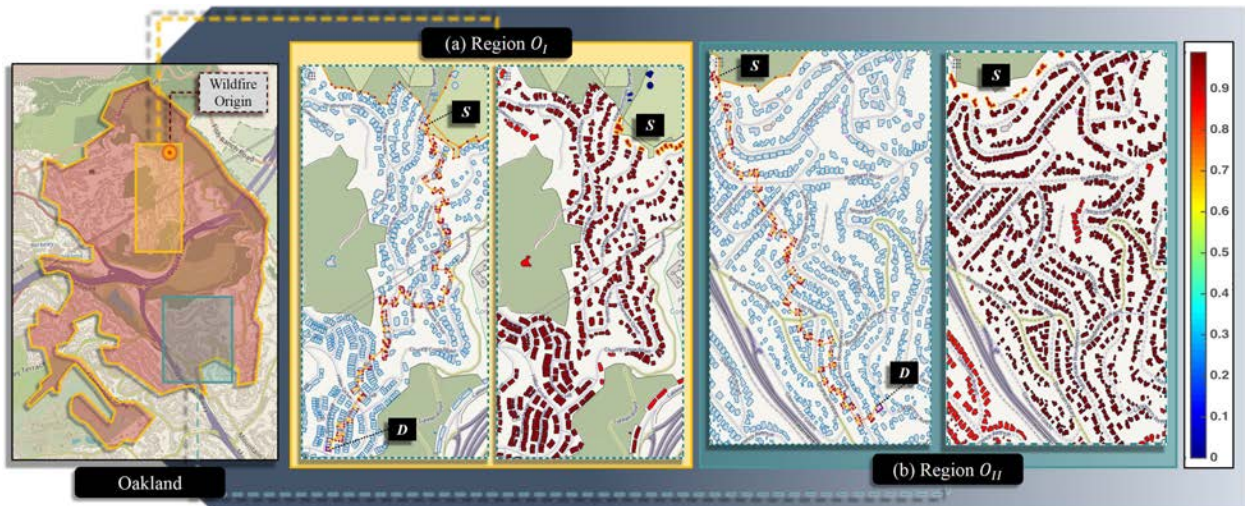


Figure 5.4: Region of Oakland affected by the 1991 wildfire along with the point of origin. Two regions are selected for analysis (a) Region O_I with wind direction $\theta = 225^\circ$ and (b) Region O_{II} with wind direction $\theta = 300^\circ$. For both regions vulnerability for each element is calculated from the source in their respective layouts. Significantly high vulnerability of all elements observed in both layouts in absence of any fire mitigation (©OpenStreetMap contributors [107])

5.4.1 Community inherent vulnerability

The respective vulnerability maps obtained for both regions of Oakland are shown in Fig. 5.4. The total vulnerability, which is calculated as the mean vulnerability of all ignitable elements in the community, for region O_I is observed to be $V = 0.9772$ and for region O_{II} to be $V = 0.9815$.

Without any form of fire mitigation, internal or external, the vulnerability of wildfire propagation is found to be sufficiently high for both regions of Oakland. This can be attributed to high path redundancy present in the communities due to significant clustering of elements and absence of discontinuities. The vulnerability of Hacienda Heights (HH) (from Section 5.2.2) for $\theta = 300^\circ$ (maximum effect seen for this direction) and $v_w = 29.058m/s$ is calculated to be $V = 0.9326$. Even though the fuel density I of region O_I is lower than HH (Table 5.1), the vulnerability for O_I is relatively the highest. The fuel content percentage I of each community is measured as the ratio of the total ignitable area to the total analysis area (Eq. 5.12). N_W is the total number of elements, $A_w^{(m)}$ is the area of element m and A^* is the total area of the region used for analysis. This shows that the layout structure of communities, indeed, plays a role in determining the level of vulnerability for communities [124], in addition to wind speed and wind direction (from Section 5.2.2).

$$I = \frac{\sum_{m=1}^{N_W} A_w^{(m)}}{A^*} \quad (5.12)$$

Table 5.1: Details for each community layout

Location	Total Nodes	Total Ignitable Elements	Fuel Density
Hacienda heights	1304	156	16.37%
Oakland (O_I)	7445	636	12.82%
Oakland (O_{II})	9326	845	18.03%

5.4.2 Effect of Individual Ignitable Elements

Eigenvector and Bonacich Centrality

To better understand the effect of layout characteristics of a community on fire propagation, the importance of individual elements is classified using specific Centrality measures, as defined in traditional graph theory. Primarily, elements which assert global influence on the wildfire network are identified using Eigenvector centrality. The eigenvector centrality ($C_w^e(m)$) is calculated as the

mean of nodal eigenvector centralities ($C_n^e(v)$) of all nodes z that belong to nodal set $\mathcal{W}_{(m)}$ (Eq. 5.13).

$$C_e^w(m) = \frac{\sum_{z \in \mathcal{W}_{(m)}} C_n^e(z)}{N_{\mathcal{W}_{(m)}}} \quad (5.13)$$

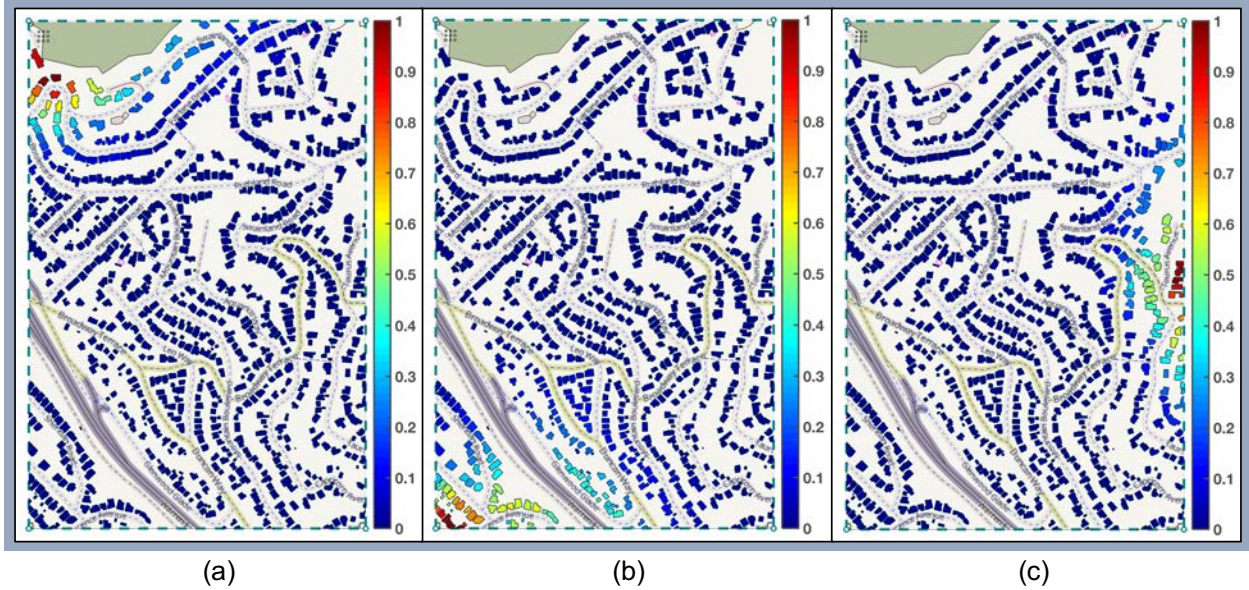


Figure 5.5: Eigenvector centrality of region O_{II} for wind directions (a) $\theta = 300^\circ$ (b) $v_w = 60^\circ$ (c) $v_w = 180^\circ$ (©OpenStreetMap contributors [107])

The most influential elements are observed at the wildland-urban interface (Fig. 5.5(a)) and the position of these elements changed in correlation to the wind direction (Fig. 5.5(b) and Fig. 5.5(c)). This can be explained by high wind speed conditions that allow the elements at the interface to connect to maximum elements by dispersing embers in the direction of wind. Due to high directionality in the graph, the edge nodes have the highest contribution to the network. For the 1991 Oakland wildfire, the location of origin of fire (Fig. 5.4) coincided with the highest centrality elements (Fig. 5.5(a)) that probably maximized the spread capacity of the wildfire. The global elements ignite other elements, which further distribute the fire throughout the community. This transition is observed by evaluating Bonacich centrality [125] (Fig. 5.6) for different values of attenuation factor $\beta \in [0, 1]$, such that $\beta = 1$ corresponds to eigenvector centrality and $\beta = 0$

corresponds to degree centrality. The Bonacich centrality is calculated in the same element as well. A uniform spread pattern is seen for O_{II} , which is to be expected due to high ember dispersal capacity of all elements under high speed winds and homogeneous density of the community.

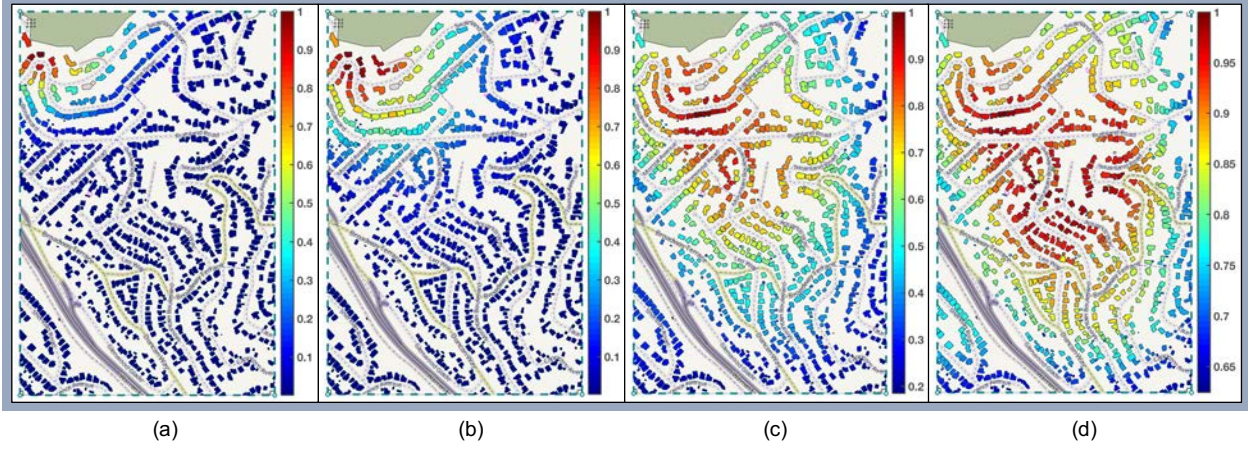


Figure 5.6: Bonacich centrality of region O_{II} for (a) $\beta = 0.75$ (b) $\beta = 0.50$ (c) $\beta = 0.25$ (d) $\beta = 0.10$ (©OpenStreetMap contributors [107])

Degree Centrality

To better realize the participation role of each ignitable element, total degree centrality [126] is utilized. For a directed graph, the indegree ($C_{d,i}^n(v)$) of each node v is calculated as the sum of all edge weights incident on the node, and outdegree ($C_{d,o}^n(v)$) as the sum of all edge weights originating from node v . The total degree ($C_d^n(v)$) is calculated as the sum of indegree and outdegree. To calculate degree centralities for element m the nodal degree centralities is readjusted first, as shown in Eqs. 5.14 and 5.15. When calculating element degree centralities, the edges corresponding to internal propagation are removed as they provide no relevant information. The element centralities are then calculated as the sum of adjusted nodal degree centralities (Eq. 5.16) for all z nodes that belong to the nodal set of element m , as given by Eq. 5.17.

$$C_{d,i}^{n*}(v) = (C_{d,i}^n(v) - N_{\mathcal{W}(m)})_{\{v \in \mathcal{W}(m)\}} \quad (5.14)$$

$$C_{d,o}^{m*}(v) = (C_{d,o}^m(v) - N_{\mathcal{W}(m)})_{\{v \in \mathcal{W}(m)\}} \quad (5.15)$$

$$C_d^{m*}(v) = C_{d,i}^{m*}(v) + C_{d,o}^{m*}(v) \quad (5.16)$$

$$C_d^w(m) = \sum_{z \in \mathcal{W}(m)} C_d^{m*}(z) \quad (5.17)$$

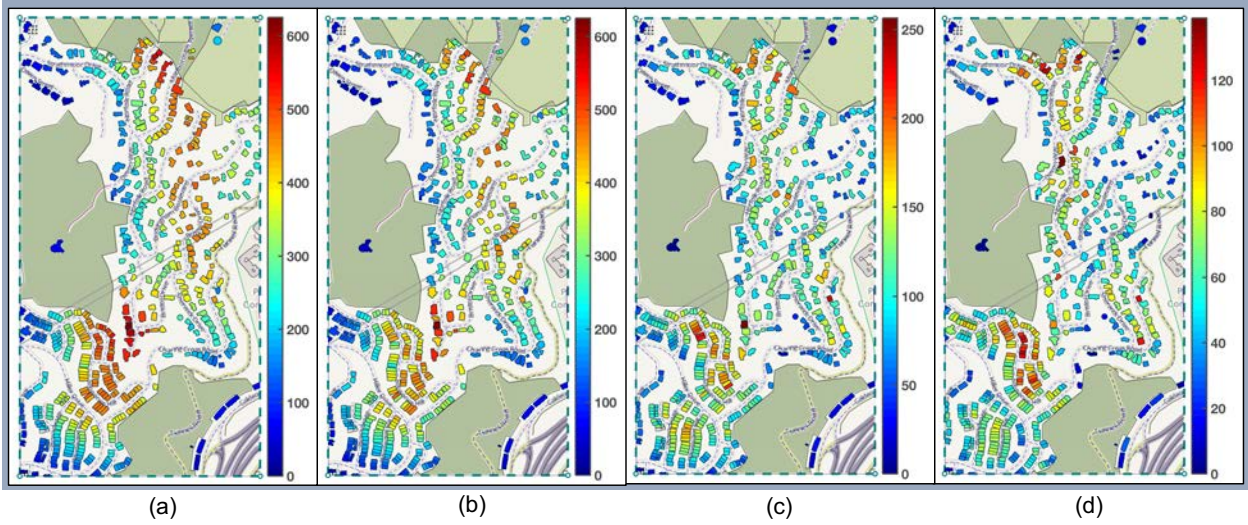


Figure 5.7: Degree centrality of region O_I for wind speeds (a) $v_w = 29.058$ m/s (b) $v_w = 10$ m/s (c) $v_w = 5$ m/s (d) $v_w = 1$ m/s (©OpenStreetMap contributors [107])

The effect of ember mode dominates over the short-range modes (convection and radiation) due to high wind speed and a large number of elements contributes equally to ember dispersion (Fig. 5.7(a) and Fig. 5.8(a)). Most houses in Oakland during the 1991 fire comprised of wooden shingle roof, which were identified as the main factor that led to significant increase in ember generation [127]. As a result, the embers completely overwhelmed all suppressive actions and spread rapidly. Therefore, degree centrality is clearly related to wind speed. The total degree centrality is observed to decline with decrease in wind speed and the centrality of elements also shifts (Fig. 5.7 and Fig. 5.8). The correlation (Kendall rank) of degree centrality is observed to

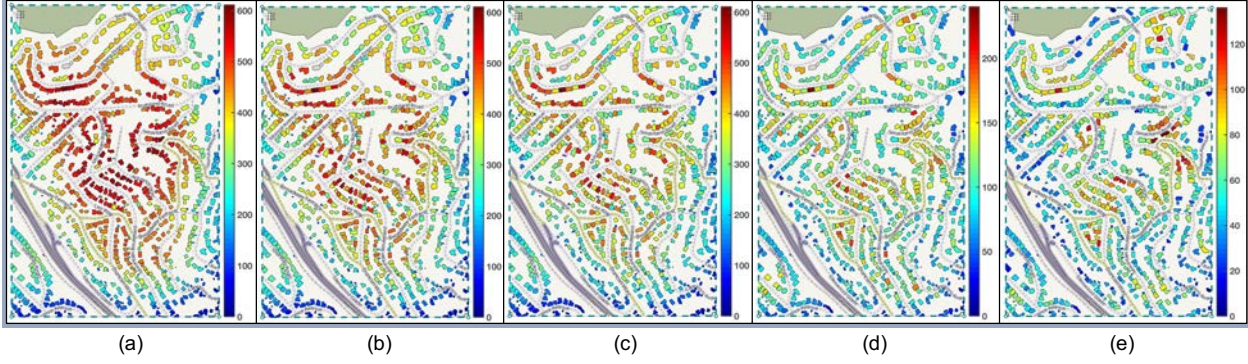


Figure 5.8: Degree centrality of region O_{II} for wind speeds (a) $v_w = 29.058$ m/s (b) $v_w = 12.5$ m/s (c) $v_w = 10$ m/s (d) $v_w = 5$ m/s (e) $v_w = 1$ m/s (©OpenStreetMap contributors [107])

reduce for region O_I (Table 5.2) and O_{II} (Table 5.3) as the difference in wind speed increases. This highlights the fact that elements which contribute more for a particular mode might not be significant contributors with respect to other modes. To develop effective fire mitigation strategies, the elements would need to be classified for each mode separately.

Table 5.2: Kendall rank correlation (τ) for degree centrality of region O_I at different wind speeds

Wind Speed	29.058 m/s	10 m/s	5 m/s	1 m/s
29.058 m/s	1.0	0.045	0.035	0.035
10 m/s	0.045	1.0	0.04	0.010
5 m/s	0.035	0.04	1.0	0.067
1 m/s	0.035	0.010	0.067	1.0

Table 5.3: Kendall rank correlation (τ) for degree centrality of region O_{II} at different wind speeds

Wind Speed	29.058 m/s	10 m/s	5 m/s	1 m/s
29.058 m/s	1.0	0.75	0.543	0.381
10 m/s	0.75	1.0	0.697	0.464
5 m/s	0.543	0.697	1.0	0.707
1 m/s	0.381	0.464	0.707	1.0

Transitivity

The transitivity, also commonly known as clustering coefficient, is a measure of the ability of the nodes to form triplets. When transitivity is applied to both regions of Oakland no clear pattern is observed (Fig. 5.9(a) and Fig. 5.10(a)). At high wind speeds, since the ember mode is dominant, each element is able to form triplets easily. As a result, a uniform distribution of centrality is observed. When transitivity is applied to both regions without the effect of wind (Fig. 5.9(b) and Fig. 5.10(b)), an interesting pattern is observed. That is, elements with high volume and situated in high density regions exhibited high transitivity, which is to be expected as they have higher capacity to spread fire. However, in region O_{II} , elements with significantly low area situated close to other larger elements also showed high transitivity (Fig. 5.10(b)). It has already been well established that low intensity exposure from easily ignitable objects, such as garbage, mulch and vegetation, in the vicinity of households tend to maximize the probability of ignition [12, 18, 32, 92]. The ordered set of elements with area smaller than 10th percentile yields mean transitivity of 0.3620 for region O_I and 0.3928 for region O_{II} , which corresponds to 86th and 90th percentile of the transitivity distributions observed, indicating high transmission capacity of low area elements.

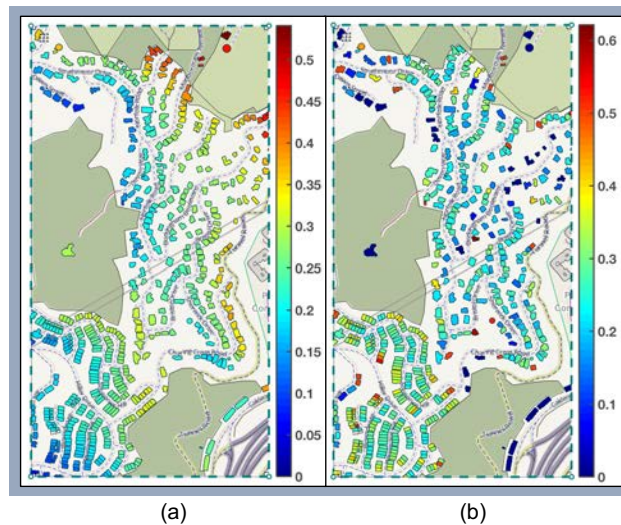


Figure 5.9: Transitivity of region O_I for (a) $v_w = 29.058$ m/s and (b) $v_w = 0$ m/s (©OpenStreetMap contributors [107])

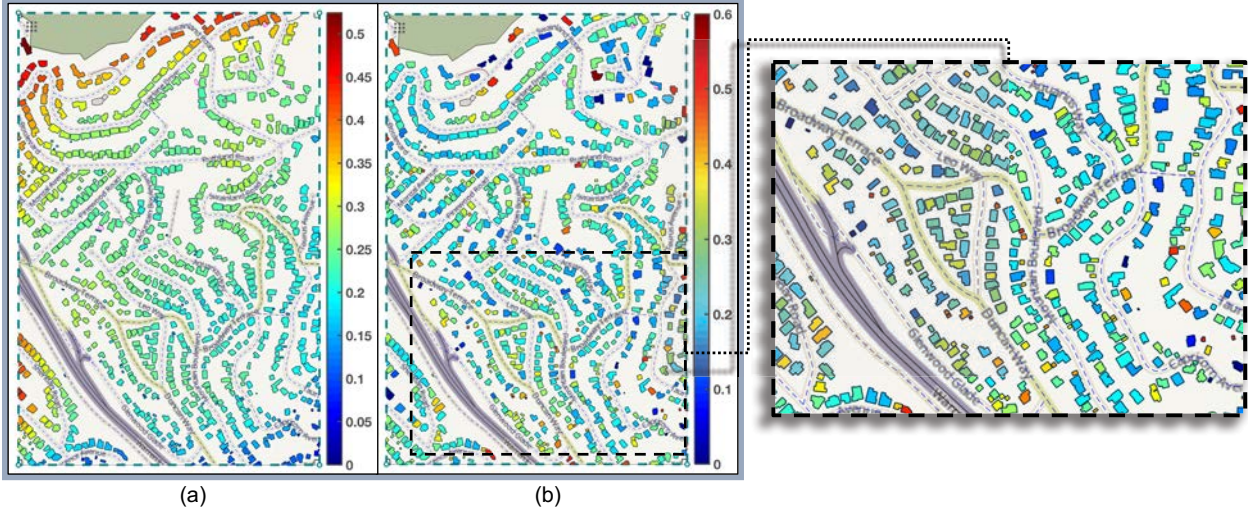


Figure 5.10: Transitivity of region O_{II} for (a) $v_w = 29.085$ m/s and (b) $v_w = 0$ m/s. The magnified snapshot shows certain ignitable elements with low area to exhibit high transitivity values (©OpenStreetMap contributors [107])

5.4.3 Effect of Fire Intervention

Fire intervention (mitigation) is characterized by two components - (1) Intervention strength (μ), which is related to number of ignitable elements under the effect of some form of fire mitigation, and (2) Strategy efficiency (η), which is related to the change in vulnerability as the location of elements under fire mitigation are altered. To observe the effect of these factors the framework discussed in Section 5.1 is implemented on both regions of Oakland O_I and O_{II} for $N = 100$ iterations and $\mu \in [0, 100\%]$ under original wind conditions ($v_w = 29.058$ m/s), to obtain respective vulnerability distributions (Fig. 5.11(a) and Fig. 5.11(b)). Intervention strength has a direct impact on vulnerability, which reaffirms the theory that management of WUI fires is only possible by regulating fire management at the individual structural level [7, 12, 112, 124, 128]. The mean vulnerability for different μ values is observed to be in range $[0.089, 0.977]$ for region O_I and $[0.049, 0.982]$ for region O_{II} . Fire intervention is observed to be more effective for region O_I than region O_{II} , which can be attributed to the difference in topographic features of the region layouts. Region O_I has a relatively constricted layout (less redundant paths), whereas, the layout of region O_{II} is more spread out (more redundant paths). For each intervention strength μ , some strategies (iterations) provides better resistance from wildfire than others, suggesting the importance of

strategy efficiency. Depending on the location of elements chosen for intervention, a spread in vulnerability (η) is observed. Therefore, given a particular community layout, optimal fire intervention configurations can be evaluated to minimize the effect of wildfires on communities.

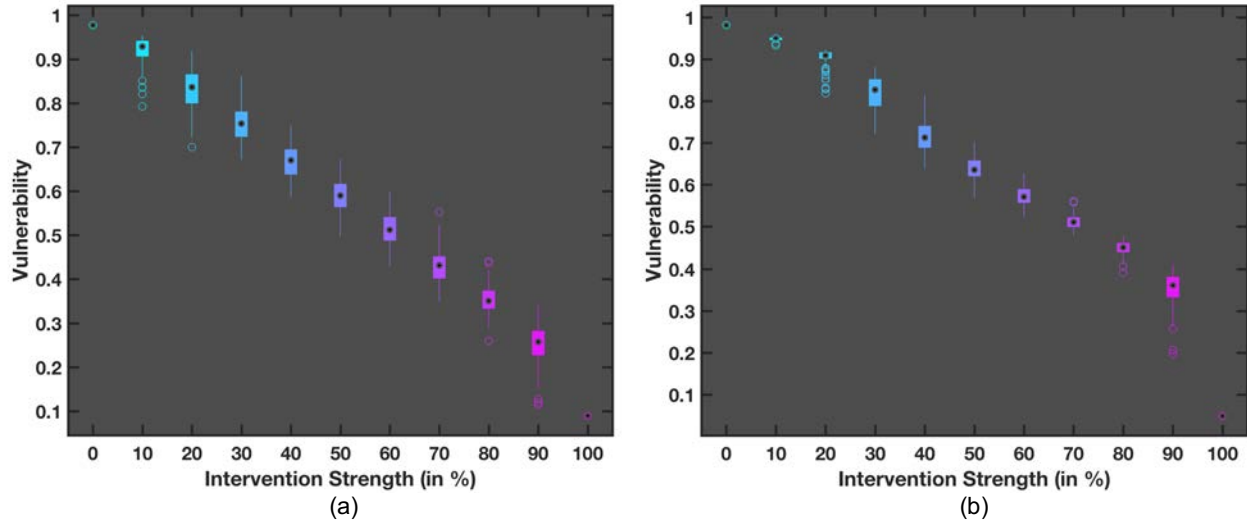


Figure 5.11: Vulnerability distributions obtained for $N = 100$ iterations at different intervention strengths (μ) for (a) region O_I (b) region O_{II} . The lower and upper edges of the box correspond to the 25th and 75th percentile, the center dot represents the median and circular markers represent the outliers

During the Oakland fire, all suppressive actions taken by firefighters proved ineffective throughout the day. It was not until the evening when wind speed gradually reduced and at some point stopped completely, firefighters were able to stop the fire [122, 123]. The intervention framework is applied to both regions at different wind speeds for $\mu = 50\%$ (Fig. 5.12). At high wind speeds ($v_w = [30, 15]$ m/s), the effect of intervention is nearly constant for both regions, followed by improvement for medium wind speeds. For low wind speeds, the effect is quite significant to the point that some of the configurations result in near zero vulnerabilities. This explains how firefighters were ultimately able to control the 1991 Oakland fire. Strong correlation between wind speed and intervention strength (Fig. 5.11(a) and Fig. 5.11(b)) is to be expected. Interestingly, the effect of strategy, which is measured as standard deviation of vulnerability distribution (η), is observed to be maximum for specific range of wind speeds (Fig. 5.12).

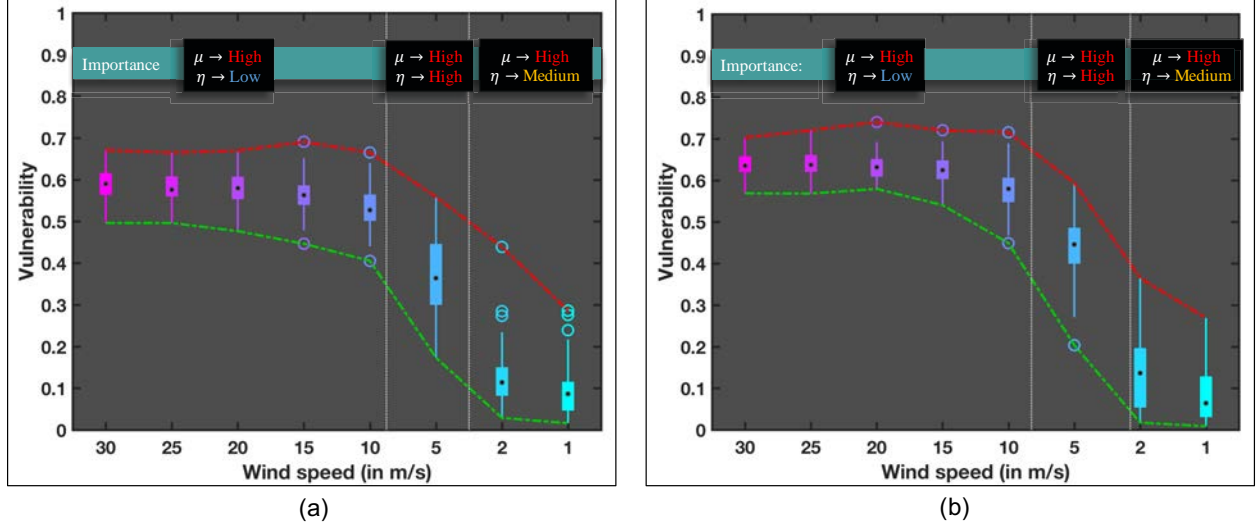


Figure 5.12: Effect of fire intervention (mitigation) showed for (a) region O_I and (b) region O_{II} of Oakland at intervention strength $\mu = 50\%$ for different wind speeds to highlight significance of intervention strategy. Vulnerability distributions are calculated for $N = 100$ iterations at each wind speed and the efficiency of strategy η is measured as the standard deviation for each distribution

5.4.4 Effect of Wildlands

All analysis conducted to this point only considered sources at the wildland urban interface (Fig. 5.4). During the 1991 fire, high speed winds resulted in ignition of several structures in the community by embers generated from the wildlands, which is a familiar observation in high intensity WUI fires [92, 127]. To observe the effects of these internal sources, a source selection framework is developed and implemented. The steps involved in the framework are listed below:

- o Initial source location is selected.
- o A temporary second source is placed at a randomly selected ignitable element $\{m \in N_W\}$.
- o Probability of ignition due to wildland nodes for every element (Eq. 5.18) is calculated, as shown in Fig. 5.1. For each node of an element the probability of ignition is calculated as the maximum of ignition probabilities from all boundary nodes of wildland (Ω). $g^{(b,s)}$ is the ember ignition probability function, as discussed in Section 4.3.

$$P_i^{(s)} = \max_{\{b \in \Omega, s \in n\}} \left(F_{cc}^{(b,s)} \cdot g^{(b,s)} \right) \quad (5.18)$$

- o The ignition probability for the selected source is utilized with Eq. 5.3 to determine the vulnerability of each node in the graph, followed by the mean vulnerability of the community using Eq. 5.4.
- o The element that results in the maximum vulnerability of the community is added as the next source location.
- o The above process is repeated for l number of iterations to obtain l source locations.
- o The process is stopped when increment in total vulnerability is reduced below a threshold percentage ($< 1\%$).

For both regions of Oakland, the framework is applied for different iterations, such that the increase in vulnerability is reduced to less than 1% for further iterations. Specific configurations for fire intervention strength $\mu = 50\%$ are selected for both regions, such that the initial corresponding vulnerabilities (before applying the framework) are calculated to be $V = 0.541$ for region O_I and $V = 0.610$ for region O_{II} . The maximum vulnerability (after 5 iterations) is evaluated to be $V = 0.774$ for region O_I and $V = 0.733$ for region O_{II} . Even though the effect of fire intervention is evaluated to be higher for region O_I than region O_{II} , the effect of additional sources result in higher vulnerability for the former region. Region O_I has a higher percentage of wildland vegetation surrounding it than region O_{II} , as a result, the wildlands are able to generate internal sources further deep into the community. During the first hour of the Oakland fire, a similar pattern of internal sources was observed (Fig. 5.13) and the vulnerability for this configuration is calculated to be $V = 0.7933$. Two of the actual observed internal source locations coincide with the optimal internal source locations calculated from the framework (Fig. 5.14(e)). The internal source framework shows that just by igniting five critical elements in the community, the vulnerability can be increased significantly even after considering 50% intervention strength. Wildlands surrounding communities worsen the problem by creating additional internal sources and these need to be accounted for proper community risk assessment [124]. Furthermore, by determining the most effective source locations, the number of sources to be considered while

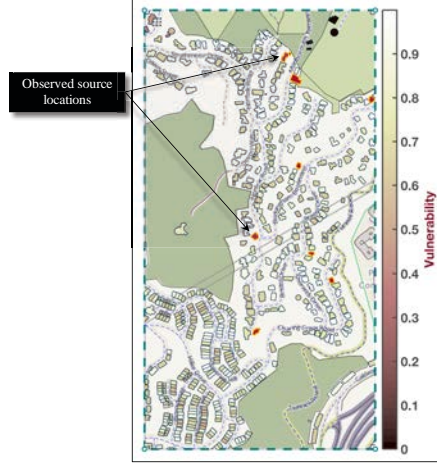


Figure 5.13: Vulnerability distribution of region O_I for source locations observed during 1991 Oakland fire (Reconstructed from [129]) (©OpenStreetMap contributors [107])

calculating the vulnerability are significantly reduced without compromising on accuracy. This results in significant reduction in computation time.

5.4.5 Identifying Flow Paths

The flow paths of radiation and convection modes are strictly dependent on community layout, unlike ember paths, which are more or less independent of community layout at high wind speeds. Instead, they are function of individual element properties. Betweenness centrality is used to identify most probable paths (MPP) within the communities for short-range propagation modes (radiation and convection). Betweenness centrality is a measure based on the shortest path between nodes (69). The application of betweenness to wildfire graphs, can determine the pattern of maximum flow paths within a community. However, the traditional definition of betweenness does not suffice in this case. Betweenness centrality measures the connectivity of a graph assuming an unbiased directionality in flow. There are only specific nodes in wildfire network that generate flow. By including other non-source nodes the centrality measure is diluted. The betweenness centrality measure for wildfire propagation in a community can be considered a sub-case of betweenness in a typical graph. To identify the maximum flow paths the normalized centrality (C_n) is defined as shown in Eq. 5.19, where $\sigma^{(i,j)}$ is the shortest number of paths between nodes i and j , $\sigma^{(i,j)}(z)$ is number of those paths passing through node z , \mathcal{S} is the source node set, $N_{\mathcal{S}}$ is the total number

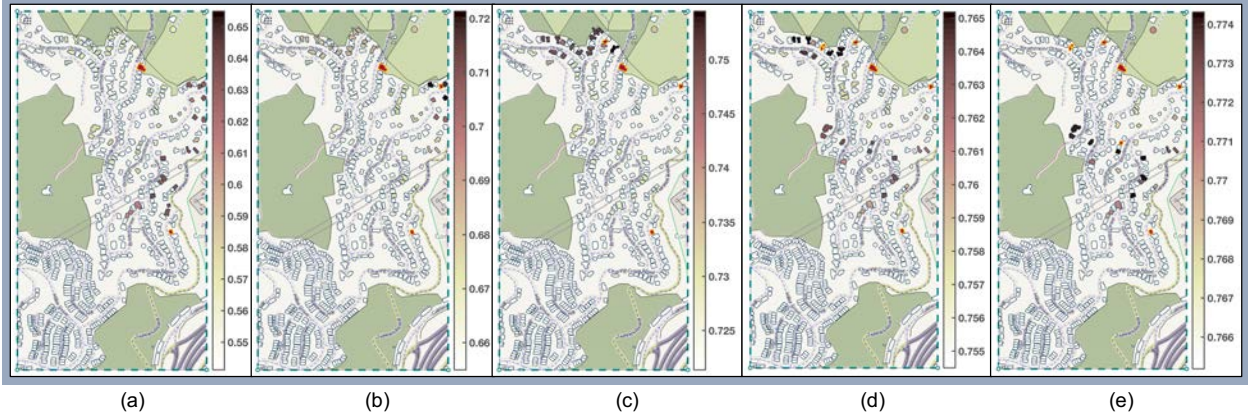


Figure 5.14: Total community vulnerability shown at each element when that specific element is considered as a source. With each iteration the element which results in maximum community vulnerability is added to the list of sources. The figures show the change in community vulnerability for region O_I as sources are added for iteration (a) $i = 1$ (b) $i = 2$ (c) $i = 3$ (d) $i = 4$ (e) $i = 5$ (©OpenStreetMap contributors [107])

of sources considered for analysis and N^* is the normalization constant (Eq. 5.20). Since each ignitable element is a complete directed graph, ignition of any node would cause ignition of its respective element, therefore, the betweenness of an element ($C_{b^*}^w(m)$) is calculated by Eq. 5.21.

$$C_{b^*}^m(z) = \frac{1}{N^*} \sum_{s=1}^{N_S} \left(\frac{\sum_{i \neq z \neq j} \sigma^{(s,j)}(z)}{\sigma^{(s,j)}} \right)_{\{s \in S, (z,j) \in \mathcal{V}\}} \quad (5.19)$$

$$N^* = \frac{(N_S)(n - N_S - 1)}{2} \quad (5.20)$$

$$C_{b^*}^w(m) = \sum_{z \in \mathcal{W}(m)} C_{b^*}^n(z) \quad (5.21)$$

The identified paths for both regions of Oakland and region of Hacienda Heights (for $\theta = 300^\circ$) are shown in Fig. 5.15. These are identified by selecting ignitable elements with centrality above a certain threshold ($C_b^w > 0.075$). The betweenness values are highest for HH, followed by region O_I , and finally region O_{II} . High centrality values for HH ($C_b^w \in [0, 0.84]$) suggest higher use of flow paths, which coincide with the fact that the intervention framework has the most impact on HH ($V(\mu = 50\%) = 0.403$ for $\theta = 300^\circ$) among the 3 test regions. On the other hand, region O_{II} shows lowest centrality values ($C_b^w \in [0, 0.73]$), which implies that the wildfire spread

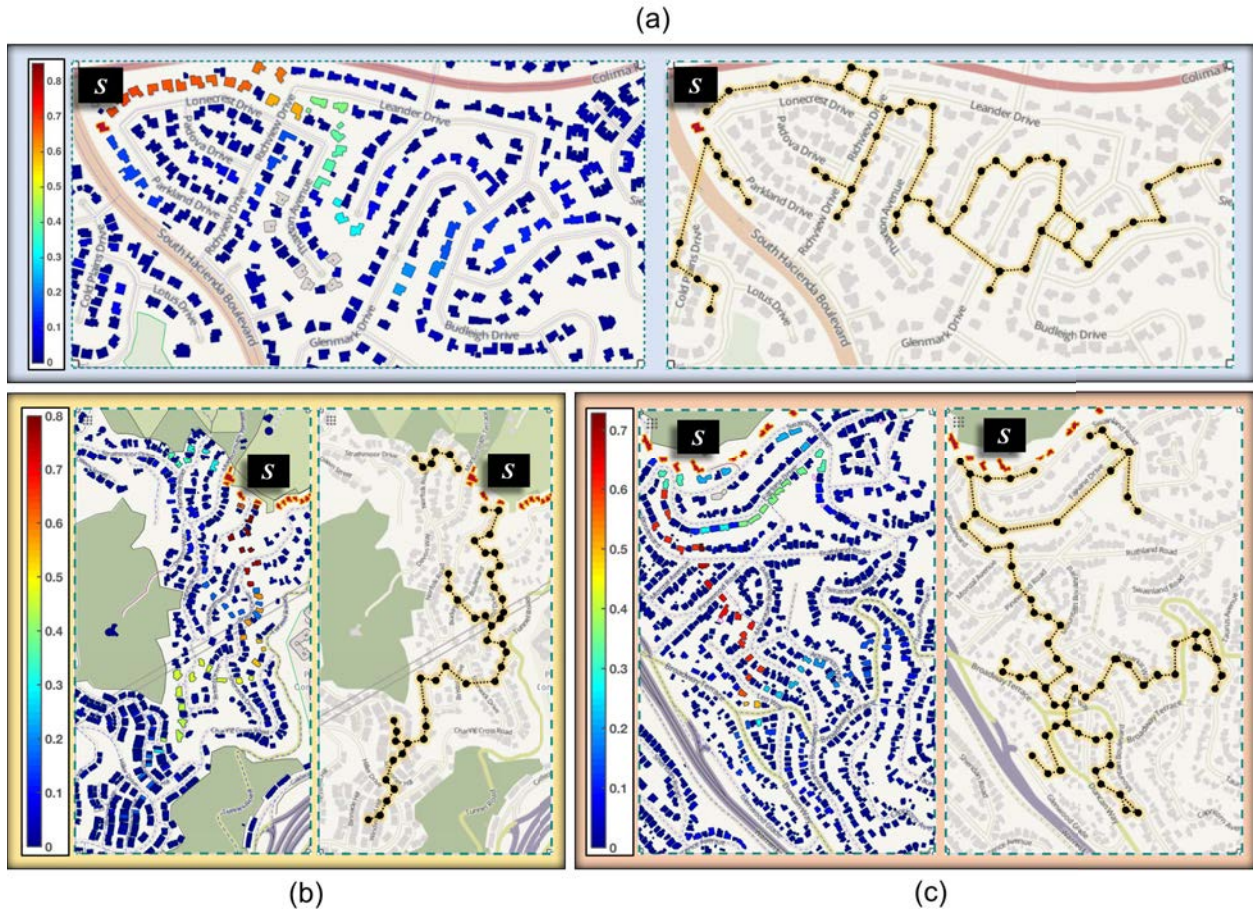


Figure 5.15: Maximum probability flow paths at wind speed $v_w = 29.058$ m/s, considering only short-range propagation modes - radiation and convection, for regions (a) Hacienda Heights ($v_w = 300^\circ$) (b) Oakland region O_I (c) Oakland region O_{II} (©OpenStreetMap contributors [107])

throughout the community via multiple paths in the region. This indicates a closeness among path probabilities; hence, intervention had the least effect, as the fire is able to find surrogate paths much easily. Identification of high probability paths can aid in improving the efficiency of fire mitigation strategies.

5.4.6 Computational resources and observations

All analysis in this study are performed on an Intel Xeon E5-2620 v3 12-core processor. The primary computation, which pertains to calculation of vulnerability, either of a single element or all elements in a community, is divided into two phases - (a) Graph formulation of community by identifying ignitable elements (phase-I) (2) Calculation of vulnerability for each element using

shortest path algorithms (phase-II). The first phase is conducted by CPU parallel computing, while the latter without. Due to high information overhead, GPU parallel computing cannot be utilized for this step. Information overhead relates to the latency introduced in processing time due to large amount of information transfer to the processing unit. Since the CPU is located closer to the GPU the information overhead is relatively low, and as expected, the overhead increases exponentially as the amount of information transfer increases. For the proposed graph algorithm significant amount of information needs to be transferred first in order to develop the graphs for communities.

The run times for the different community layouts are shown below in Table 5.4. These were found to be reasonable from a practical application point of view, given the size of communities shown. An important point to note is that the run times shown below are only for calculating vulnerability of all elements of a community for a particular configuration. For certain steps, such as evaluation of fire intervention efficiency, multiple configurations have to be considered, which requires multiple runs of phase-II, and thus, increased computation time.

Table 5.4: Computational details for the test cases

Location	Total Nodes	Total Ignitable Elements	Phase-I	Phase-II
Hacienda heights	1304	156	300 ± 20 secs	15 ± 5 secs
Oakland (O_I)	7445	636	720 ± 20 secs	65 ± 5 secs
Oakland (O_{II})	9326	845	660 ± 20 secs	95 ± 5 secs

The observed processing time can be considered practical for small-medium communities, however, for communities with households in the order of 100,000 might be a problem. For significantly large communities, the graph formulation step would require significant computational resources. To make the proposed model applicable for such situations a few modifications can be made. If Parallel computing can be utilized in this step the processing time can be brought within practical range. Consider a graph \mathcal{G} for a community such that $\mathcal{V} = \{v_1, \dots, v_n\}$ is the node set and $\mathcal{E} \subseteq \mathcal{V} \times \mathcal{V}$ is the edge set. If the community is divided into a $M \times N$ grid, such that each cell is represented by subgraph $\mathcal{G}_{(m,n)}$ with $\mathcal{V}_{(m,n)}$ as the node set and $\mathcal{E}_{(m,n)}$ as the edge set, such that Eq.

5.22 and Eq. 5.23 are satisfied. For each subgraph the nodes can be classified into - (1) Boundary nodes and (2) Intermediary nodes. The former refers to nodes closest to the local cell boundaries and the latter to the remaining nodes (Fig. 5.16). An Adjacency matrix $A_{(m,n)} \in N_{\mathcal{V}_{(m,n)}^b} \times N_{\mathcal{V}_{(m,n)}^b}$ be formulated for each subgraph, where $N_{\mathcal{V}_{(m,n)}^b}$ is the total number of boundary nodes within a cell and $a_{(m,n)}^{(k,l)}$ is the maximum probability of fire reaching from the k^{th} boundary node to l^{th} boundary node of cell (m, n) .

$$\mathcal{G} = \cup_{m=1}^M \left(\cup_{n=1}^N \mathcal{G}_{(m,n)} \right) \quad (5.22)$$

$$\mathcal{V}_r = \cup_{m=1}^M \left(\cup_{n=1}^N \mathcal{V}_{(m,n)}^b \right) \quad (5.23)$$

Using the Adjacency matrices of each cell and the Adjacency matrix of \mathcal{G} a new graph \mathcal{G}_r can be formulated, which satisfies $\mathcal{G}_r \subset \mathcal{G}$, such that the node set is given by \mathcal{V}_r (Eq. 5.7) and the edge set by \mathcal{E}_r . The corresponding Adjacency matrix for graph \mathcal{G}_r is defined by Eq. 5.24, where $a_{(m,n)}^{(i,j)}$ is the maximum probability of fire reaching node j if the fire started at node i for the subgraph in cell (m, n) and $a^{(i,j)}$ is the probability of fire reaching node j from node i based on the original (unreduced) graph. The reformulated graph is a a simpler representation of the original graph. In case of significantly large communities, this reformulation of the community graph will aid in reducing the processing time significantly. The separate subgraphs can be run all at once using parallel computation, which was not possible before, to formulate the adjacency matrix of each sub graph. The developed subgraphs are used to obtain the reduced graph \mathcal{G}_r , which is used to obtain the individual vulnerabilities of each node. Due to substantially lesser number of nodes in the reduced graph the processing time for vulnerability calculation will be much more manageable.

$$a_s^{(i,j)} = \begin{cases} a_{(m,n)}^{(i,j)} & \text{if } \{v_{(r)}^{(i)} \in \mathcal{V}_{(m,n)}^b : v_{(r)}^{(j)} \in \mathcal{V}_{(m,n)}^b\} \\ a^{(i,j)} & \text{if } \{v_{(r)}^{(i)} \notin \mathcal{V}_{(m,n)}^b : v_{(r)}^{(j)} \in \mathcal{V}_{(m,n)}^b\} \end{cases} \quad (5.24)$$

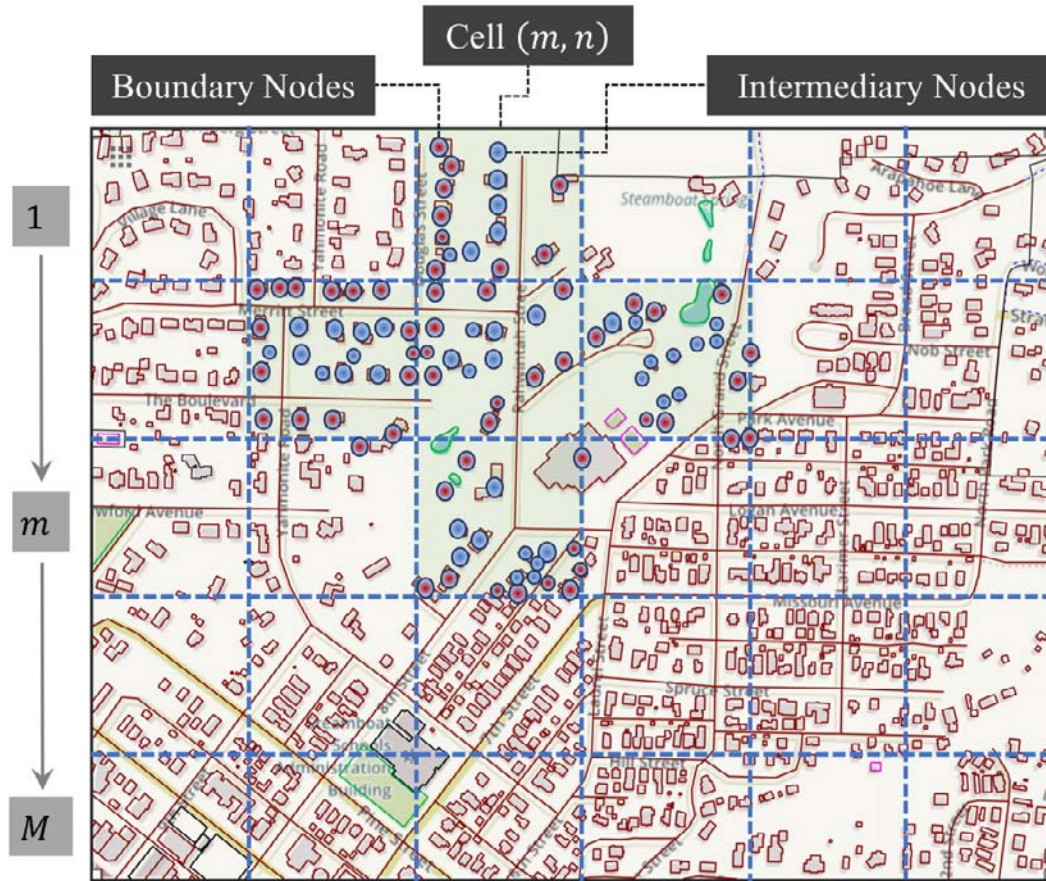


Figure 5.16: Community layout showing spatial discretization (Map data ©OpenStreetMap contributors [107])

There can be other elements for reducing the computation time. Phase-I includes formulation of the graph by calculating the weights of each edge. The weights are calculated by combining the results from the heat transfer models of Conduction, Convection, Radiation and Embers. About 95% of the computation time for phase-I is attributed to the radiation model. Based on the framework discussed in Section 4.2, the view factor calculation between surfaces of incident and target elements require substantial computational resources. Therefore, replacing the model by a suitable approximation can result in significant reduction in overall computation.

Chapter 6

Risk Assessment and Intervention Strategy

Optimization

6.1 Risk Framework

Every natural hazard has certain characteristics, based on which their risk is quantified and communicated. For earthquakes, risk is communicated through magnitude of the shaking, hurricanes by wind velocity and storm surge, floods by measured depth of water, and so on. For wildfires, researchers have developed detailed frameworks to quantify the potential of fire spread in wildlands; however, there is currently no standardized method of risk assessment or communication that can be applied nationwide to WUI communities [94]. Several researchers have looked into application of risk analysis for quantifying risk of communities to wildfires [130–133], but comprehensive theoretical frameworks are yet to exist. Available frameworks only account for risk from the perspective of wildlands and do not take into consideration the susceptibility of the community based on its own characteristics. A comprehensive definition of wildfire risk entails assessment of two key components - (1) probability of a wildfire event and (2) susceptible assets to wildfire [12].

Under the framework implemented in this study, the community risk is reclassified into three stages of wildfire - (1) Probability of wildland ignition ($P(Z(t))$) (2) Probability of wildfire that started in wildland to reach a specific wildland-urban interface ($P(Y(t)|Z(t))$) (3) Susceptibility of community provided that a wildfire reached the wildland-urban interface ($P(X(t)|Y(t))$). Using these three stages the net risk of a community ($R(t)$) for a particular day t can be defined as given by Eq. 6.1. Since susceptibility of a community can be defined as the mean probability of fire reaching a house and causing ignition from the boundary of surrounding wildland urban interface,

the risk can be defined as the mean probability of fire reaching a house from the initial ignition point in the wildlands.

$$R(t) = P(Z(t) \cap Y(t) \cap X(t)) = P(Z(t)).P(Y(t)|Z(t)).P(X(t)|Y(t)) \quad (6.1)$$

The general definition of risk for any hazard is characterized by 3 components - (1) Hazard, which is defined as the temporal probability of occurrence for a hazard of a particular intensity, (2) Vulnerability, which is defined as the degree of exposure, and (3) Amount of elements-at-risk, which is also known as exposure. In this study, the daily probability of ignition from the National Fire Danger Rating System (NFDRS) is used as the probability of occurrence. The terms Vulnerability and Elements at risk are coupled to form the vulnerability term. This is because for other hazards a typical prototype structure has a distinct value for vulnerability (probability of failure, obtained from fragility functions). This is because for other hazards a typical prototype structure has a distinct value for vulnerability (probability of failure, obtained from fragility functions). For example, a moment frame on soil type D subjected to specific earthquake excitation will perform the same way regardless of its location (i.e. as long as the building is the same and the load is the same, it does not matter where the building is placed). For wildfire, the vulnerability of a specific type of building will vary depending on its location and orientation within the community. Based on the framework discussed, the three input components shown in Eq. 6.1 have to be determined to evaluate wildfire risk for a community. The derivation of each component is described in the subsequent sections.

6.1.1 Background and modeling details

Parts of four different communities - (1) Oakland (California), (2) Jackson (Wyoming), (3) Steamboat Springs (Colorado), and (4) Austin (Texas), from the U.S. are chosen for the analysis. The communities are selected due to their close proximity to wildlands and difference in community layout. Each community possess a unique geographical layout, such that effect of community characteristics can be drawn out. Suitable graphs are developed for each community by identifying

and classifying ignitable elements. The details on individual graphs formulated for each community is shown in Table 6.1. Since the focus of this study is to draw out a comparison between the selected communities, all elements in each community are assumed to be identical in nature i.e. possess same material properties.

Table 6.1: Details for each community layout

Location	Total Nodes	Total Ignitable Elements
Austin	11359	805
Jackson	11238	1605
Oakland	9326	845
Steamboat Springs	8068	1032

Each community has a unique footprint attributing to structure density, community layout, vegetation distribution and others. The individual community layouts are shown in Fig. 6.1. Based on vegetation alone communities can be classified into different types. In order to do a comparative study between the communities, individual vegetation (trees and shrubs) are not modeled exclusively. This is done to normalize the features of all communities such that the stochastic nature of vegetation does not affect the analysis. Although the proposed model can capture presence of discrete vegetation surrounding the houses, the community layout in this study is derived from openstreetmap.org, which had no information available on the location of discrete vegetation near the houses. To circumvent this problem in the future, GIS data can be used in conjunction with image pattern recognition algorithms to identify stray vegetation, which can be overlaid to obtain accurate representation of the community data. Once the vegetation is mapped out it will be incorporated into the community graph in the form of set of ignitable elements such that individual nodes would represent parts of vegetation and properties of vegetation would be assigned to nodes. The analysis of the updated graph would provide vulnerability estimate while considering the distribution of vegetation inside community.

The fire intervention framework discussed in Section 5.3 is applied to account for cumulative effect of vegetation around houses. The intervention framework is incorporated to model the resis-

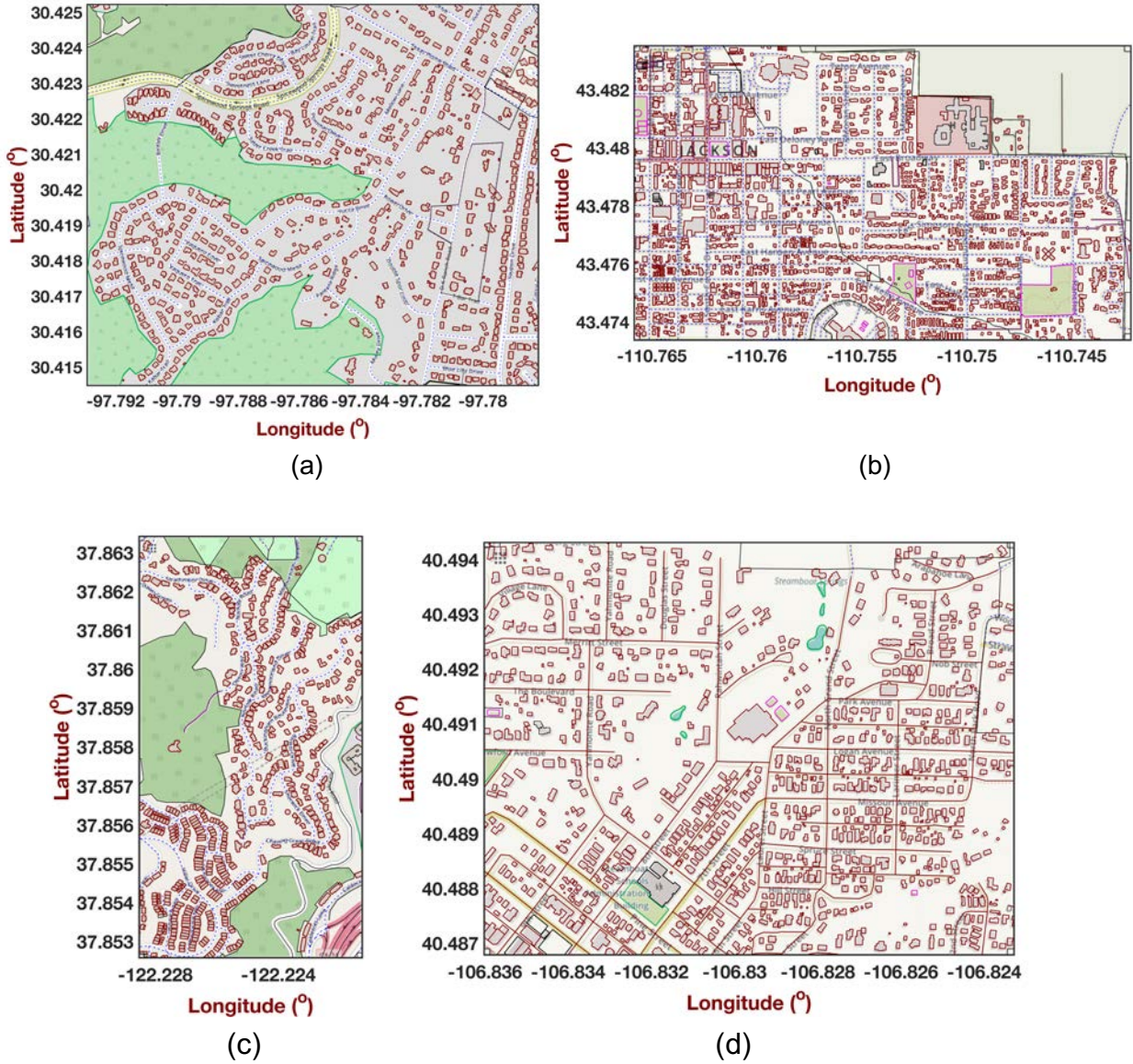


Figure 6.1: Community layouts for (a) Austin (Texas) (b) Jackson (Wyoming) (c) Oakland (California) (d) Steamboat (Colorado) (Map data ©OpenStreetMap contributors [107])

tance provided by the communities, which entails fire mitigation efforts by fire fighters and private home owners. An intervention strength of $\mu = 50\%$ is used for all cases, which indicates 50% of all elements in the communities are altered by adjusting the edge weights $P_{tr}^{(i,j)}$ to induce effect of fire mitigation. The location of these elements in each community is selected to represent the mean case. The wildlands govern vulnerability of a community significantly, understandably it would

govern the risk as well. Hence, a framework is implemented to account for the wildland vegetation surrounding the respective communities for each test case.

6.1.2 Wildland Ignition Probability

Wildland ignition probability has been the focus of numerous studies over the years. For this study, the Wildland Fire Assessment System (WFAS) developed by the USFS [134] was used. The WFAS performs daily fire danger forecasts with data from the National Digital Forecast Database for different locations across the US. The Fire danger rating level takes into account current and antecedent weather, fuel types, and both live and dead fuel moisture [40]. It primarily utilizes two performance indexes - (1) Burning Index (BI) and (2) Energy Release Component (ERC), in conjunction to determine fire danger levels at a location. The danger rating is normalized across different fuel models, indexes, and station locations. It is based on the primary fuel model cataloged for the station, the fire danger index selected to reflect staffing levels, and climatological class breakpoints. Staffing class are decided by local station managers from historical fire weather climatology and represent percentile values for the performance index selected for a specific day. Linear interpolation is used to determine probability of ignition ($P(Z)$), as given by Eq. 6.2, where $p_u^k(d)$ and $p_l^k(d)$ are appropriate upper and lower percentiles allotted on a daily basis by station managers and $v_u^k(d)$ and $v_l^k(d)$ are the performance index values corresponding to the percentiles selected. The slope $m(d)$ is given by Eq. 6.3 and the constant by Eq. 6.4.

Stn ID	Stn Name	Elev	Lat	Long	Mdl	Tmp	RH	Wind	PPT	ERC	BI	SC	KBDI	HUN	THOU	TEN	STL	ADJ	IC	(Staffing Specs)
*****	Alabama	*****																		
10402	BROWNSBORO	529	34.7	-86.3	7G	87	39	2	.00	25	15	1	188	15	21	8	3	M	9	ERC/ 40/ 45/90/97
10702	BANKHEAD NF	989	34.3	87.3	7G	82	62	1	.00	21	16	2	158	17	20	12	2	L	4	BI / 36/ 42/90/97
10990	LIRI	1200	34.4	85.6	8E	83	53	1	.00	19	17	2	88	15	21	11	3	M	6	BI / 30/ 35/90/97
11401	ONEONTA	1104	33.9	-86.3	7G	76	79	4	.04	4	0	0	132	17	22	35	1	L	0	ERC/ 40/ 45/90/97
12201	MOUNTAIN LONGLEAF	1050	33.7	85.7	8G	71	80	6	.00	9	11	2	42	20	24	17	1	L	0	ERC/ 50/ 61/90/97
12302	TERRAPIN CREEK	805	33.8	-85.5	7G	78	62	7	.00	10	15	3	46	20	26	13	2	L	6	BI / 33/ 39/90/97
12701	TALLGA	600	33.4	86.0	7G	73	89	1	.20	1	0	0	194	19	23	35	1	L	0	BI / 33/ 39/90/97
12801	SCHOOLHOUSE	932	33.1	86.0	7G	79	71	2	.00	11	11	2	46	20	24	14	2	L	2	BI / 33/ 39/90/97
12902	SHOAL CREEK	908	33.6	85.6	7G	69	91	1	.17	7	5	1	19	19	24	21	1	L	0	BI / 33/ 39/90/97

Figure 6.2: Sample wildfire ignition data from WFAS Archives

The wildfire ignition probability for a particular region is calculated based on the daily data obtained from WFAS archives. The staffing specs shown in Fig. 6.2 is used to calibrate Eq.

6.2. The parameters - $v_u^k(d)$, $v_l^k(d)$, $p_u^k(d)$ and $p_l^k(d)$ are obtained from the data sheet such that $v_u^k(d)$ and $v_l^k(d)$ represents the upper and lower performance index and $p_u^k(d)$ and $p_l^k(d)$ are the corresponding upper and lower percentiles. A dominant performance metric each day is selected based on which the calibration parameters are opted. There are 2 key performance metrics - ERC (Energy Release Component) and BI (Burning Index). Values between stations are estimated with an inverse distance-squared technique on a 10-km grid. Once Eq. 6.2 is suitably calibrated it is used to obtain the ignition probability corresponding to the observed value of the dominant performance index (I).

$$P(Z) = \frac{1}{100}(m(d).I(d) + c(d)) \quad (6.2)$$

$$m(d) = \frac{(v_u^k(d) - v_l^k(d))}{(p_u^k(d) - p_l^k(d))} \quad (6.3)$$

$$c(d) = v_u^k(d) - m(d).p_l^k(d) \quad (6.4)$$

The daily probability of wildland ignition for each of the selected communities for the years 2007, 2012 and 2017, and the months May to September are shown in Fig. 6.3, Fig. 6.4, Fig. 6.5 and Fig. 6.6.

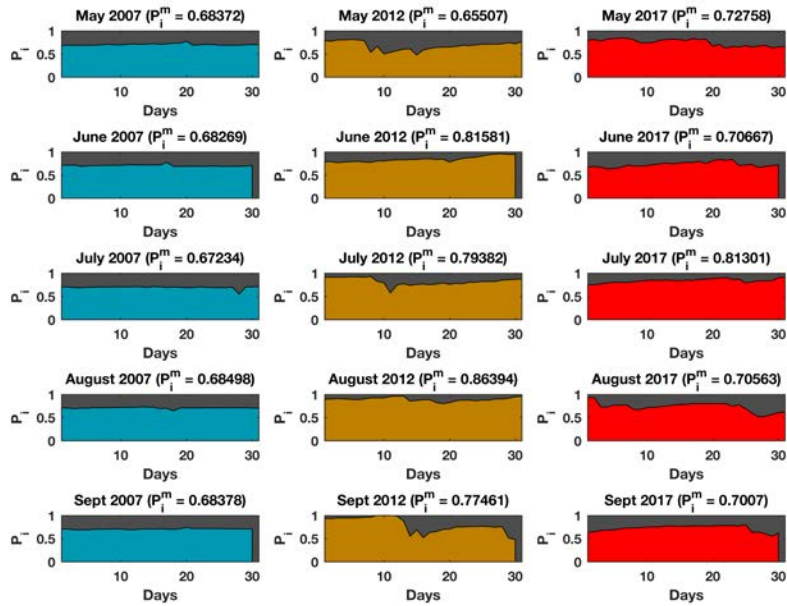


Figure 6.3: Probability of ignition (P_i) in months May-September for years 2007, 2012 and 2017 for Austin (Texas)

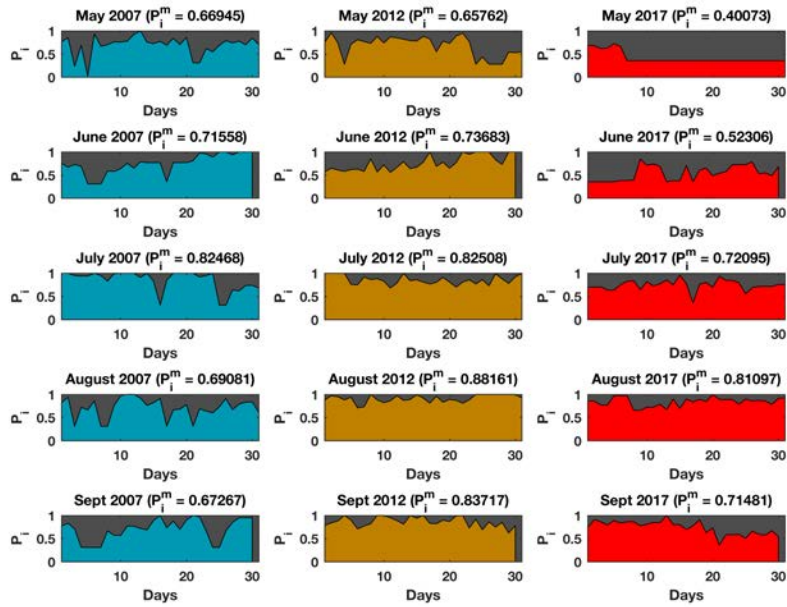


Figure 6.4: Probability of ignition (P_i) in months May-September for years 2007, 2012 and 2017 for Jackson (Wyoming)

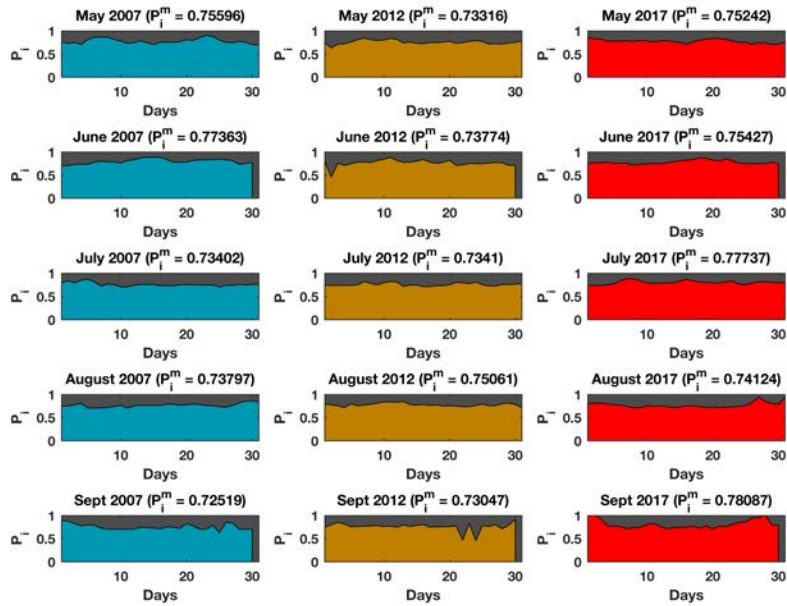


Figure 6.5: Probability of ignition (P_i) in months May-September for years 2007, 2012 and 2017 for Oakland (California)

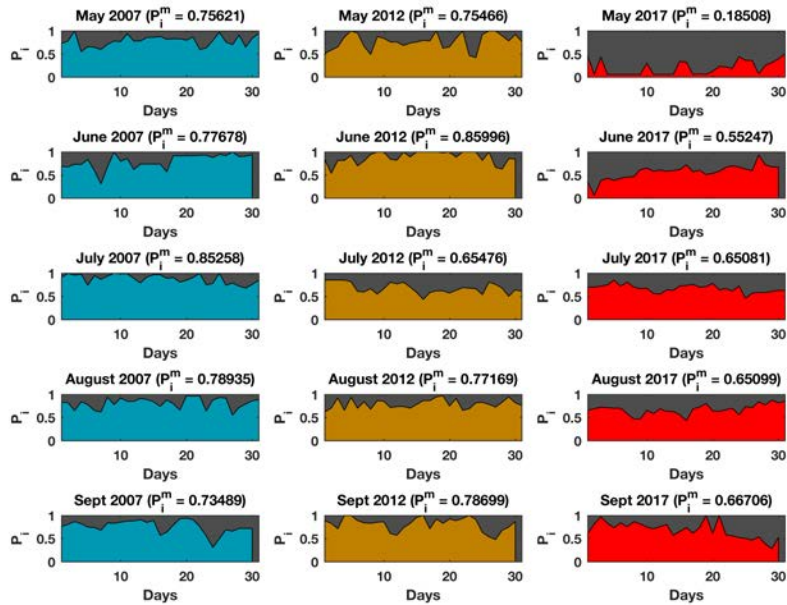


Figure 6.6: Probability of ignition (P_i) in months May-September for years 2007, 2012 and 2017 for Steamboat Springs (Colorado)

6.1.3 Community Susceptibility

The susceptibility of a community is defined as the mean vulnerability of all ignitable components within the community. The mean is one possible performance metric that is used in this study; however, it can be replaced by a weighted mean such that the weights for each ignitable component corresponds to its importance in a community. The definition of importance could vary depending on the focus of the analysis, but the alternative formulation could be used to account for high-value resources within a community. The vulnerability of each ignitable component in a community is evaluated based on the graph developed for the community layout based on the framework discussed in Chapter 4. An important component in evaluating the vulnerability of a community is to input the wind conditions correctly, as they are unique to each location. Daily Wind data is extracted from the archives of NOAA's National centers for environmental information. Based on the location, daily maximum sustained wind speed is used for evaluating vulnerability. Mean and peak wind speeds were disregarded in this study since the former would have given a conservative while the latter an overestimate value of the vulnerability. Since, sustained wind speed is calculated by averaging over a 1-min period, it provides a better estimate. Hourly data could also be used to capture changes in wind behavior so that more refined wildfire behavior is captured. However, the intent of this study is not to simulate a particular incident but to provide a generalized framework that can be utilized for any cases so as to highlight the underlying wildfire patterns while evaluating wildfire risk. Fig. 6.7, Fig. 6.8, Fig. 6.9 and Fig. 6.10 shows a sample of the community vulnerabilities obtained for the four regions selected in this study. The total vulnerability evaluated daily for each community for the intended years and months are shown in Fig. 6.11, Fig. 6.12, Fig. 6.13 and Fig. 6.14. The derivation of the final component i.e. the wildland propagation probability $P(Y(t)|Z(t))$ is discussed in the next section.

6.1.4 Wildland Propagation Probability

The wildland component $P(Y(t)|Z(t))$ can be calculated based on the wildland propagation framework discussed in Chapter 3. The wildland model can be used to determine the probability of



Figure 6.8: An example of Vulnerability map for Jackson (Wyoming)

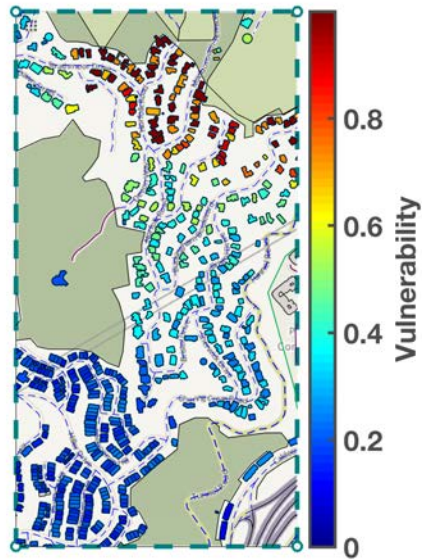


Figure 6.9: An example of Vulnerability map for Oakland (California)

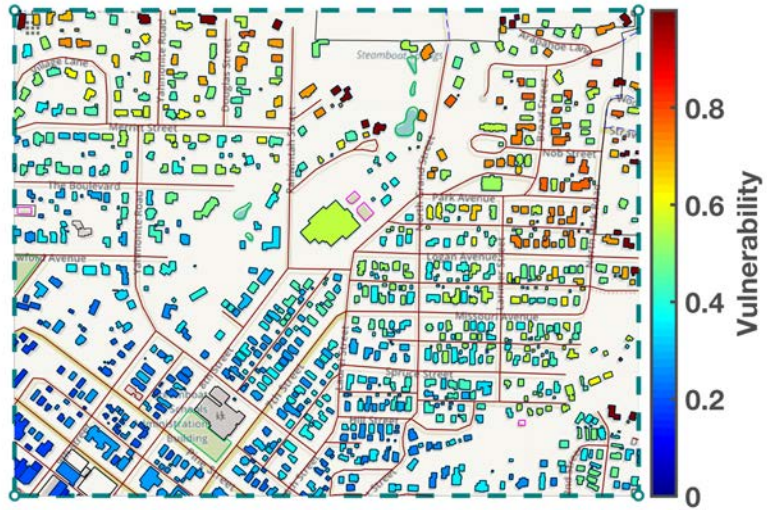


Figure 6.10: An example of Vulnerability map for Steamboat Springs (Colorado)

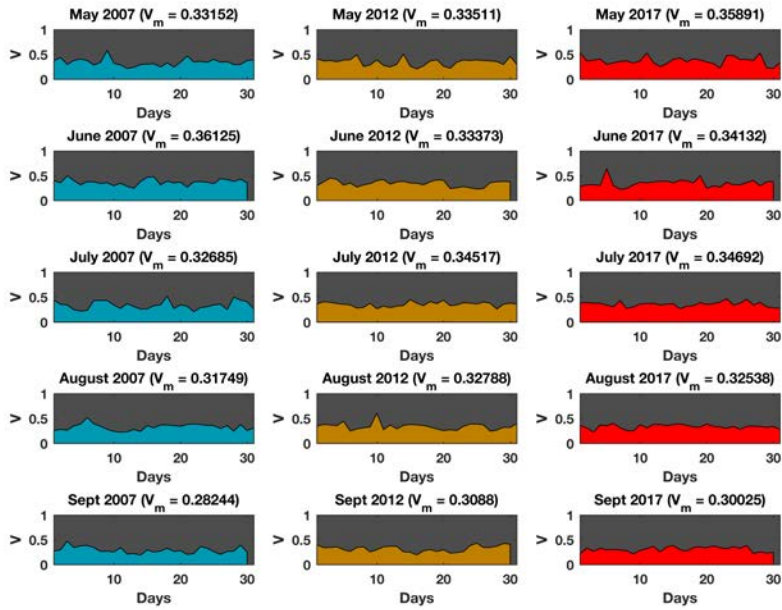


Figure 6.11: Community vulnerability (V) in months May-September for years 2007, 2012 and 2017 for Austin (Texas)

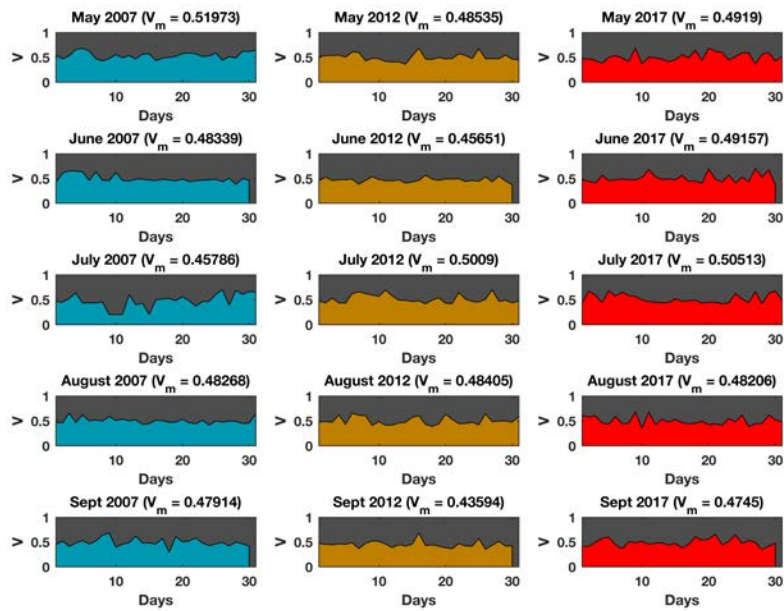


Figure 6.12: Community vulnerability (V) in months May-September for years 2007, 2012 and 2017 for Jackson (Wyoming)

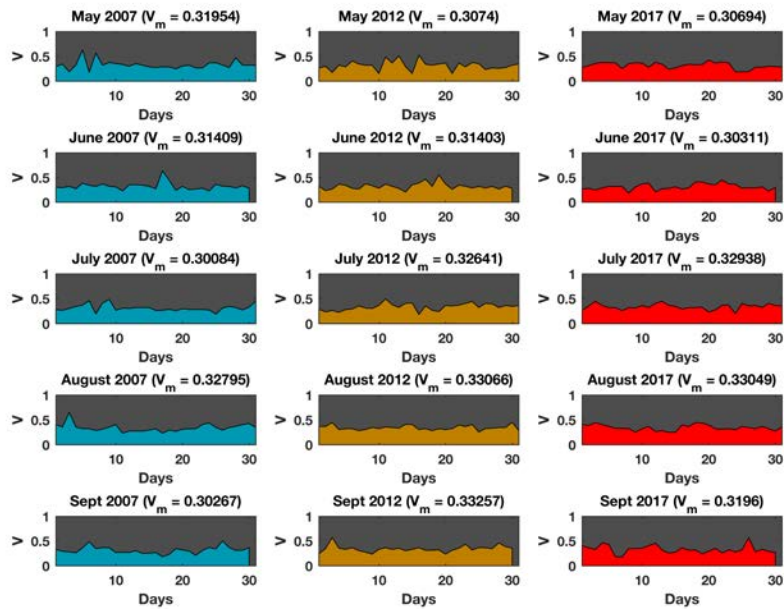


Figure 6.13: Community vulnerability (V) in months May-September for years 2007, 2012 and 2017 for Oakland (California)

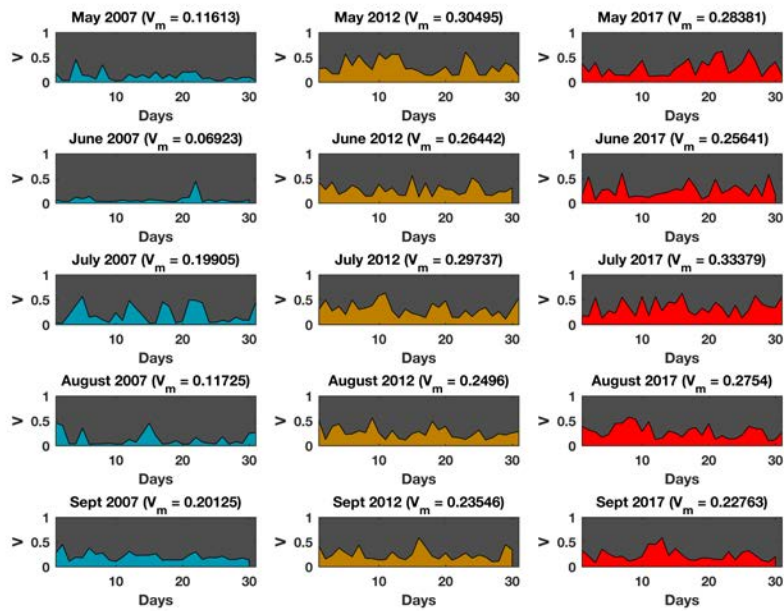


Figure 6.14: Community vulnerability (V) in months May-September for years 2007, 2012 and 2017 for Steamboat Springs (Colorado)

6.2 Case Study: Risk Analysis of Archetypal Communities in United States

The risk of each test community is calculated per day for the months May to September, as per the discussed framework. Fig. 6.15, Fig. 6.16, Fig. 6.17 and Fig. 6.18 show daily risk values for the months May-September for the years 2007, 2012 and 2017 for the four communities selected. The risk values for each day of the months are calculated based on the daily wind and ignition probability data obtained from the Fire Danger data (as discussed in Section 6.1.2). Mean risk values (R_m) for each month are also shown, which are defined as the average of risk for each day ($R(t)$), as given by Eq. 6.5. Based on the risk patterns observed for all communities it is evident that even if the chance of a wildfire ignition is high enough it may not necessarily result in high risk for communities. Unfavorable wind conditions result in high vulnerability of communities which are observed to affect the risk in several cases from the results. Some of the most destructive wildfires in history were accompanied by strong seasonal winds - (1) The Oakland wildfire (1991) by El Diablo winds [127], (2) The Thomas fire (2017) by Santa Ana winds [135], and (3) Australia Bushfires by Foehn winds [136]. The graph model is formulated in a way so as to incorporate all types of wind conditions ranging from mild to extreme events. For a given spatial resolution, the ignition transfer probabilities ($P_{tr}(i, j)$) can be updated based on the wind field pattern observed. For varying wind events no changes are required in the model formulation; however, the temporal resolution of the analysis would have to be increased, for instance using hourly wind data instead of daily wind data. Both probability of ignition and vulnerability of communities need to be considered to quantify wildfire risk. Based on the mean risk observed for different months of each community, Jackson is observed to have the highest overall risk and Steamboat to have the lowest, while Austin and Oakland showed intermediate risk relative to the other communities.

$$R_{(t)} = \frac{1}{t} \int_0^t R(t) dt \quad (6.5)$$

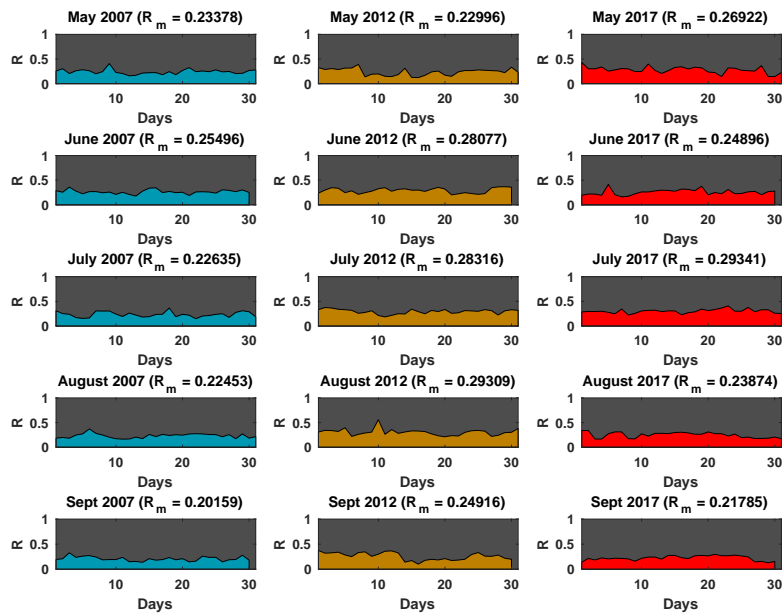


Figure 6.15: WUI fire risk in months May-September for years 2007, 2012 and 2017 for Austin (Texas)

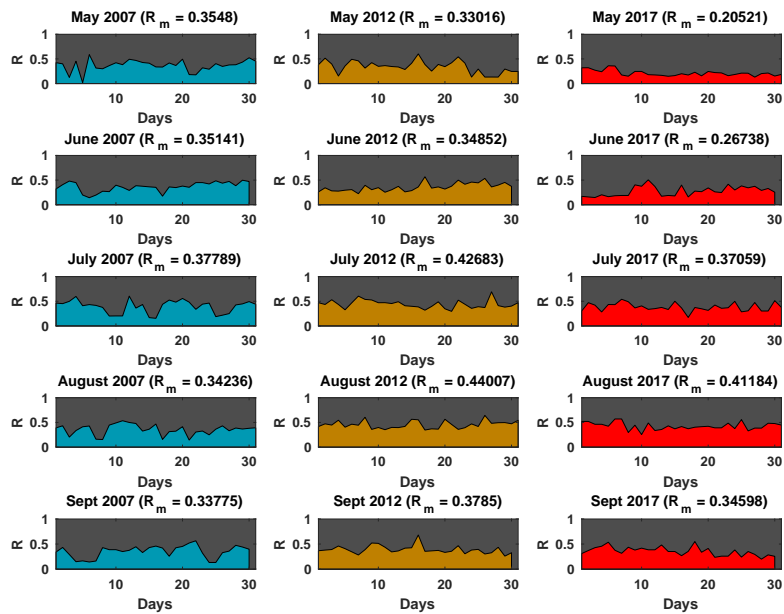


Figure 6.16: WUI fire risk in months May-September for years 2007, 2012 and 2017 for Jackson (Wyoming)

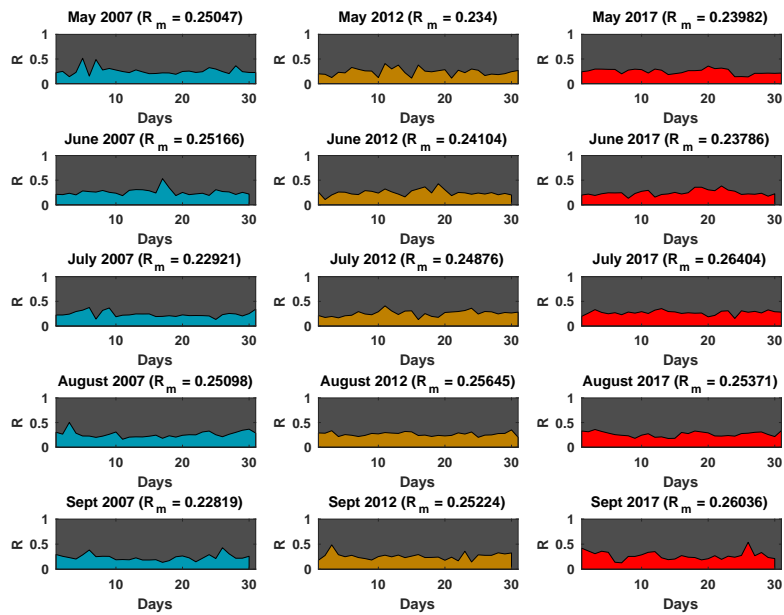


Figure 6.17: WUI fire risk in months May-September for years 2007, 2012 and 2017 for Oakland (California)

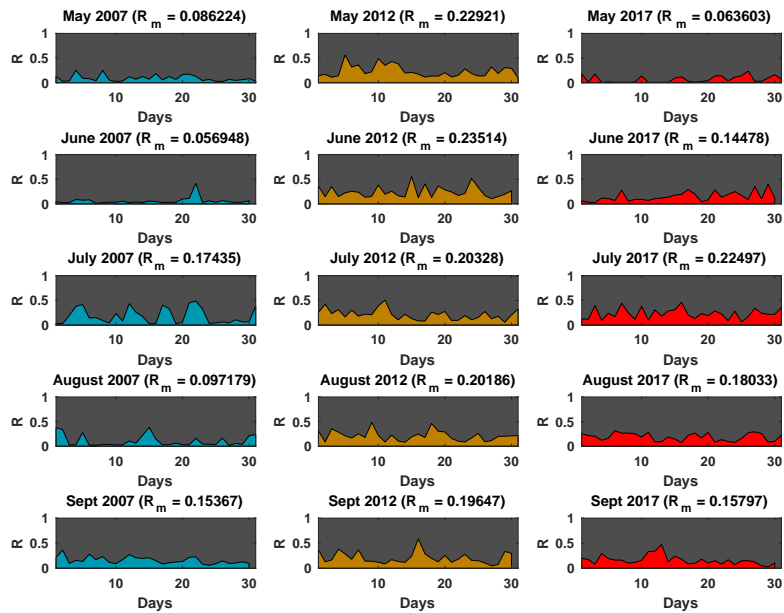


Figure 6.18: WUI fire risk in months May-September for years 2007, 2012 and 2017 for Steamboat (Colorado)

Steamboat exhibited both lower ignition probabilities (Fig. 6.6), as well as, lower community vulnerability (Fig. 6.14). The latter is specifically lower for steamboat due to the absence of significant wildland vegetation in the vicinity of the community, which limited the entry points for the wildfire. The discontinuous layout of the community further reduced the vulnerability. Among the four communities, Steamboat has the lowest amount of wildland vegetation (in terms of volume) near the communities that enable the wildfire to create internal sources in the communities. These internal sources allow the wildfire to reach deeper parts of the communities and spread more easily. Wildfire risk is function of both wildland ignition probability and community vulnerability. To understand the correlation of risk with these two key parameters, the Pearson correlation coefficient is calculated for each community separately (Table 6.2). For all communities, except Jackson, the correlation is observed to be stronger between risk and community vulnerability than risk and wildland ignition. This suggests that wildfire risk can be better regulated for these communities by controlling the community vulnerability. However, in case of Jackson the correlation between risk and wildland ignition is higher, which suggests that risk in this case is primarily governed by the wildlands. A different perspective would be that it would require much more effort to bring down the risk for Jackson below a certain threshold, since it is situated in a high fire vulnerability region. Hence, the risk can be quantified based on two types - communities where wildfire risk can be regulated with more measures in the community and those where wildlands should be the focus.

Table 6.2: Pearson correlation values between risk (R), vulnerability of community (V) and probability of wildland ignition (P_i), for each community

Correlation	Austin	Jackson	Steamboat	Oakland
R and P_i	0.5886	0.8304	0.5158	0.3075%
R and V	0.8407	0.3601	0.9534	0.8572%
V and P_i	0.0878	-0.1781	0.2409	-0.14%

As discussed in Chapter 5, wind conditions have a severe effect on the vulnerability of communities. Polar fragilities for the test communities are calculated to show their respective sensitivity

to wind direction (Fig. 6.19). These fragilities are formulated by varying the wind direction at an interval of 30° and calculating the mean vulnerability of community. Wind direction is measured anti-clockwise from the positive x-axis, such that a N-S wind is represented by $\theta = 270^\circ$ and S-N wind by $\theta = 90^\circ$. The individual data points in the polar fragilities represent the mean probability of fire reaching a house in the community from the wildland urban interface for a particular wind direction. For each wind direction, a new graph is formulated by updating the nodal probabilities, followed by most probable path (MPP) calculation to determine mean community vulnerability. For a community with a uniform fragility curve, which is defined as similar vulnerability across different wind directions, would suggest uniformity across community layout both in terms of fuel density and material property, while a non-uniform fragility curve would suggest bias in certain directions. For each community the dominant wind directions are observed to be different, which is to be expected given the different layouts of the communities (Fig. 6.1). Jackson is observed to have the least effect of wind direction, while Oakland is observed to have the most. During the 1991 Oakland wildfire, the situation was worsened by the seasonal Diablo winds which entered Oakland from the dominant direction shown in fragility curve ($\theta = 240^\circ$). The mean vulnerability for the 1991 wildfire is calculated to be 0.79. On September 2017, a fire ignited in the same location in wildlands of Oakland as it did in the infamous 1991 Tunnel fire [137]. However, this time the fire agencies were able to suppress the fire before it reached the internal parts of a community due to controlled wind conditions and prompt actions of the firefighters. The vulnerability is observed to be 0.25 which represents 68.3% reduction in vulnerability just due to the absence/presence of certain wind conditions. Ideally, the difference in building material used for reconstructing Oakland after the 1991 wildfire would also have an impact on reducing the vulnerability of the community. However, due to unavailability of data associated with the material changes the material of all households is assumed to be the same as pre 1991 wildfire. Hence, the analysis presented does not account for reduction in risk due to change in materials.

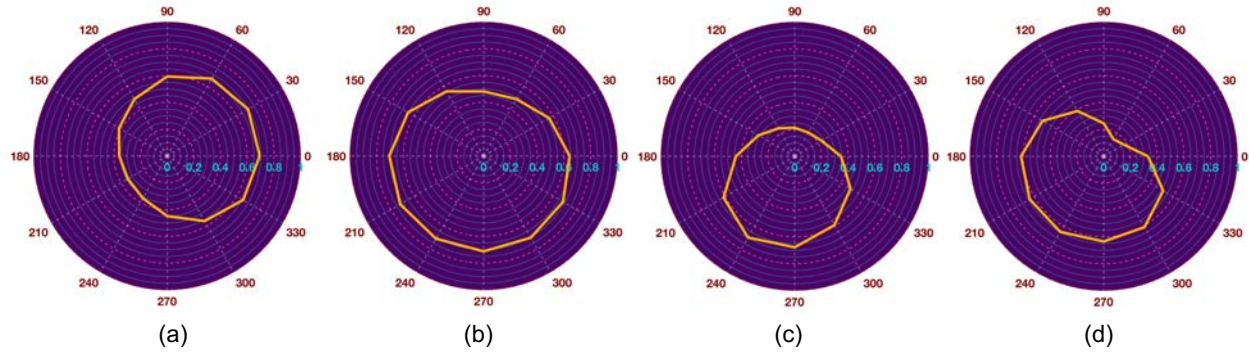


Figure 6.19: Polar fragilities for (a) Austin (Texas) (b) Jackson (Wyoming) (c) Oakland (California) (d) Steamboat Springs (Colorado) at wind speed $V_w = 15$ m/s

6.3 Intervention Strategy Optimization

6.3.1 Intervention Framework

The passive intervention framework, discussed in Section 5.3, takes into account the effect of fire intervention strategies applied at individual ignitable elements on WUI fire behavior. Some possibly effective strategies to reduce propagation of wildfire include installation of sprinkler systems and removal of unnecessary vegetation and mulch in the vicinity of households. The effects of such strategies were specifically prevalent in the 2016 McMurray wildfire, where majority of the houses that survived followed this practice. The effectiveness of such strategies is coming to light and is gaining attention all over the world. However, if one is to ask the question what fraction of households need to follow this strategy, or other effective strategies for that matter, to bring down the risk of overall community below a certain threshold, there does not exist any answers. There are currently no theoretical frameworks that can determine the efficacy of intervention measures on communities in a quantifiable manner. An optimization framework is discussed to identify the optimal number and location of households such that the community risk can be reduced below a certain threshold. Even though the main hindrance in practical application of such approaches is that the primary responsibility lies in the hands of individual household owners, perhaps in the future with some strong scientific evidence, a middle ground can be reached, and wildfire policies can be modified appropriately.

The passive intervention formulation describes the general mechanism of intervention strategies applied to graph theory model. The scaling factors α and β for the active and passive intervention strategies represent the cumulative effect of all strategies applied to a particular element. This formulation is used to conduct general investigations on the effects of intervention. The general formulation is extended in this chapter to provide a more comprehensive understanding on the effects of different intervention strategies on the community. There are several possible passive intervention strategies, but in this study the following four have been considered - (1) Vegetation in defensible space (2) Roofing material (3) Siding material (4) Presence of decking. These strategies have been a subject of extensive research by the Wildfire Research (WiRe) team from University of Colorado (CU), Boulder, CO. To quantify the effectiveness of each intervention measure, an effectiveness score, provided by the WiRe team, is assigned, as shown in Table 6.3. The scores shown in the table were provided by the Wildfire Research (WiRe) team from University of Colorado (CU), Boulder, CO. Each score represents the options available within a particular type of intervention strategy. For instance, in case of Defensible Space the scores $[0, 100]$ corresponds to the absence and presence of ignitable fuel within $10m$ of a household (ignitable element). The Roof type scores corresponds to ignitable wooden and non-ignitable roofing. The siding material scores correspond to non-ignitable and ignitable siding. For the decking, the scores correspond to the absence and presence of ignitable wooden decking. In this study, only two sub-categories of each intervention strategy are considered, however, any number of classifications can be considered within the scope of the proposed framework (as discussed below) even within a particular strategy.

Table 6.3: Effectiveness of different intervention measures

Index	Variable	Effectiveness Score (s_n)
1	Defensible Space	$[0,100]$
2	Roof type	$[0,200]$
3	Siding material	$[0,60]$
4	Decking	$[0,50]$

The ignition transfer probability, shown in Eq. 4.1, represents the edge weights between different ignitable elements of the wildfire graph G . To consider the effect of intervention measures the ignition equation is modified by introducing individual scaling factors corresponding to each mode of heat transfer, as shown in Eq. 6.6. β_c is the scaling factor corresponding to convection, β_r is the scaling factor corresponding to radiation and β_e is the scaling factor corresponding to ember mode of heat transfer. The modified equation is similar in concept to the intervention equation (Eq. 5.11), in which only a single scaling factor was used to model the effect of intervention measures. By dividing the scaling factors into individual components, the effect of intervention measures on individual modes can be accounted for.

$$P_{total}^{(i,j)} = (\beta_c \cdot P_{conv}^{(i,j)}) \cup (\beta_r \cdot P_{rad}^{(i,j)}) \cup (\beta_e \cdot P_{ember}^{(i,j)}) \quad (6.6)$$

Each of the scaling factor are formulated in a similar manner, as shown in their respective equation below (Eq. 6.7, Eq. 6.8 and Eq. 6.9). The scaling factor corresponding to a particular mode is calculated as a summation over all the intervention strategies that have an effect on that particular mode. l_c , l_r and l_e are sets of intervention strategies that impact the different modes. From the equations below it can be observed that all intervention strategies have an impact on the convection and ember mode, however, in case of radiation mode, the effect of roofing strategy is not considered. By segregating the effect the impact of intervention strategies can be captured much accurately. λ_c , λ_r and λ_e are the normalization constants for each mode of heat transfer to maintain the relative sensitivity between them. p_{l_c} , p_{l_r} and p_{l_e} are the normalized effectiveness score calculated as $s_n / (\max s_n)$. In this case, there are only two values in a tuple corresponding to each intervention type (Table 6.3). Hence, all normalized effectiveness scores are simplified to $[0, 1]$. Λ_{l_c} , Λ_{l_r} and Λ_{l_e} determine the presence or absence of a particular intervention strategy. The variables take only two values - 0 to represent absence and 1 to represent presence. Even if all four intervention strategies considered in this study are applied to a house, in reality, it would not reduce the ignition probability to zero. Therefore, a reduction factor R is introduced to ensure that

even after applying all intervention strategies the edge weights between elements $P_{tr}^{(i,j)}$ do not fall below a certain threshold. A value of $R = 0.80$ is used for all analysis in the study.

$$\beta_c = 1 - R \cdot \left[\sum_{l_c \in [1,3,4]} \lambda_{l_c} p_{l_c} \Lambda_{l_c} \right] \quad (6.7)$$

$$\beta_r = 1 - R \cdot \left[\sum_{l_r \in [1,3,4]} \lambda_{l_r} p_{l_r} \Lambda_{l_r} \right] \quad (6.8)$$

$$\beta_e = 1 - R \cdot \left[\sum_{l_e \in [1,2,3,4]} \lambda_{l_e} p_{l_e} \Lambda_{l_e} \right] \quad (6.9)$$

The equations for the normalization constants pertaining to different modes (λ_{l_c} , λ_{l_r} and λ_{l_e}) are given in Eq. 6.10, Eq. 6.11 and Eq. 6.12. The constants are obtained by normalizing the maximum effectiveness score value (s_{l_c} , s_{l_r} and s_{l_e}) among the intervention list (l_c , l_r and l_e) by the summation of scores of all intervention strategies within the list.

$$\lambda_{l_c} = \frac{\max_{\{l_c \in [1,3,4]\}}(s_{l_c})}{\sum_{l_c \in [1,3,4]} s_{l_c}} \quad (6.10)$$

$$\lambda_{l_r} = \frac{\max_{\{l_r \in [1,3,4]\}}(s_{l_r})}{\sum_{l_r \in [1,3,4]} s_{l_r}} \quad (6.11)$$

$$\lambda_{l_e} = \frac{\max_{\{l_e \in [1,2,3,4]\}}(s_{l_e})}{\sum_{l_e \in [1,2,3,4]} s_{l_e}} \quad (6.12)$$

6.3.2 Optimization Framework

The idea behind the proposed optimization framework is to determine optimal intervention strategy, which is represented as the set $\Lambda = \{\Lambda_{(1)}, \Lambda_{(2)}, \Lambda_{(3)}, \Lambda_{(4)}\}$, such that both, mean community vulnerability and intervention cost, which is the total cost of applying intervention strategies to complete or some parts of a community, are minimized. The optimization problem is formulated so as to minimize the fitness function shown in Eq. 6.13, which is a weighted linear combination

of normalized community vulnerability and normalized intervention cost. The two quantities are normalized so as to remove any bias since their minimum and maximum bounds are different. V_{avg} is the mean vulnerability of the community and V_{max} is the maximum vulnerability observed when no form of any intervention is applied to the community. C_{total} is the total cost of applying a particular intervention strategy to a community and C_{max} is the total cost of intervention when all interventions are applied to all elements of a community. The weight factors $\lambda_V \in [0, 1]$ and $\lambda_C \in [0, 1]$ represent the priority/importance given to each component (vulnerability and cost) under the constraint $\lambda_V + \lambda_C = 1$.

$$\min_{\Lambda} \left\{ Fitness = \lambda_V \cdot \frac{V_{avg}(\Lambda)}{V_{max}} + \lambda_C \cdot \frac{C_{total}(\Lambda)}{C_{max}} \right\} \quad (6.13)$$

The ‘Covariance Matrix Adaptation Evolution Strategy’ (CMA-ES) [138] is a stochastic method of optimization for continuous non-linear, non-convex functions. CMA-ES has been found to be flexible and efficient [139], and has been successfully used in other optimization problems [140]. CMA-ES is an Evolutionary type optimization, similar to Genetic algorithm, which means it is based on the basic principles of evolution (i.e. the interaction between generation, selection and mutation). The overall idea behind CMA-ES is the same as other evolution strategies except the method of generating population (‘population’ is referred to the different cases generated) the method of selection and the method of mutation differs. The CMA-ES algorithm exploits two different concepts – Maximum Likelihood Principle and Evolution Paths.

The role of Maximum Likelihood is to maximize the probability of selection of correct values and search domain. Initially a test population is chosen at the beginning of the algorithm by assuming a particular distribution. After the 1st iteration the Maximum Likelihood principle is used to update the parameters of the distribution i.e. the mean and the variance, such that the likelihood of the correct values of the previous iteration tends to increase. Similarly, to increase the likelihood of the correct search domain the covariance matrix of the distribution is updated. This process of updating not just the population but also the search domain is highly beneficial. The second key concept is exploiting the use of Evolution or Search Paths by recording them.

Evolution paths basically give an idea in which direction the favorable solutions can be found based on the results from the previous step. Thus, it gives a correlation between consecutive steps. These evolution paths are actually serving dual purpose. First, it is used in the adaptation process of the Covariance matrix instead of focusing on the variance of a single successful step. This enables a faster and a more efficient improvement in moving towards a favorable direction. The second is the use of evolution path to control the step size. The advantage of step size control is to avoid premature convergence, which is a common problem of concern in most evolutionary algorithms. Premature convergence is basically the convergence of the program on local solutions rather than the global. This takes place mainly due to lack of genetic variation among the population generated (i.e. all the members of the population have identical properties). To further increase the accuracy and robustness of CMA-ES certain modifications were made. Details on the optimization and its modifications are given in [140]. CMA-ES, alone, was used to minimize the formulated fitness function. However, due to high non-linearity in the problem the optimization was observed to be ineffective.

Lemma 6.3.1. *The optimal value of optimization variable Λ for minimization problem given in Eq. 5.20 for $\lambda_V = 1$ is $\Lambda = \{1, 1, 1, 1\}$ and for $\lambda_V = 0$ is $\Lambda = \{0, 0, 0, 0\}$*

Proof. For $\lambda_V = 1$ the weight factor for cost (λ_C) is 0, therefore, the fitness function becomes solely dependent on community vulnerability and the optimization is reduced to $\min \left[\frac{V_{avg}}{V_{max}} \right]$. It has already been shown in Fig. 5.11 that community vulnerability is inversely proportional to intervention strength, therefore, minimum vulnerability will be observed at maximum intervention strength, which corresponds to $\Lambda = \{1, 1, 1, 1\}$. Similarly, for $\lambda_V = 0$ the optimization is reduced to $\min \left[\frac{C_{total}}{C_{max}} \right]$ and the optimal strategy would correspond to minimum intervention strength, which is given by $\Lambda = \{0, 0, 0, 0\}$. □

Corollary 6.3.1.1. *Optimization can be conducted by discretizing the variable space into $2^n - 2$ spaces.*

Proof. For the optimization set $\Lambda = \{\Lambda_{(1)}, \Lambda_{(2)}, \Lambda_{(3)}, \Lambda_{(4)}\}$ the number of possible combinations ($2^{|\Lambda|}$) come out to be 16. All possibilities are listed in Fig. 6.20. Each combination represents an

intervention strategy applied to an ignitable element. Assuming a solution Λ' to be one of the 16 strategies applied to all homes. Based on the lemma 6.3.1 the potential solution will lie somewhere between the optimal solutions for $\lambda_V = 1$ and $\lambda_C = 0$. Therefore, Λ' can be an optimal solution for $1 > \lambda_V > 0$. In other words, optimal solutions for $1 > \lambda_V > 0$ would either be equal to or lie in the neighborhood of Λ' . If the cases $\Lambda' = \{1, 1, 1, 1\}$ and $\Lambda' = \{0, 0, 0, 0\}$ are excluded, since they represent the boundary cases for which optimal strategy is already known, 14 individual optimizations can be conducted by assuming different values of Λ' as the initial solution. \square

16	1	1	1	1
15	1	1	1	0
14	1	1	0	1
13	1	1	0	0
12	1	0	1	1
11	1	0	1	0
10	1	0	0	1
9	1	0	0	0
8	0	1	1	1
7	0	1	1	0
6	0	1	0	1
5	0	1	0	0
4	0	0	1	1
3	0	0	1	0
2	0	0	0	1
1	0	0	0	0

Intervention Measures

Figure 6.20: List of different intervention strategies Λ

CMA-ES is utilized to conduct the minimization by segregating the domain into 14 different sections. For each section, an independent optimization is conducted assuming a different initial solution. The list of initial solutions for the different sections are shown in Fig. 6.20. A test optimization is conducted on a part of Steamboat Springs (Colorado) community. The layout of

the community is the same as the one shown in Fig. 6.1(d). For different combinations of the importance factors (λ_V and λ_C) optimization is conducted by segregating the domain. The optimal cases found for each case are shown in Fig. 6.21. It is observed that at high wind speed cases ($> 10m/s$) for all combinations of importance factors the optimal case is always comprised of applying some form of intervention to all elements of the community, as opposed to selective elements only. However, as shown in Fig. 6.21, the optimal intervention strategy Λ can vary for different importance factor values. For instance, for $\lambda_V = 0.20$ (and $\lambda_C = 0.80$) the optimal strategy is $\Lambda = \{1, 0, 0, 0\}$, on the other hand, for $\lambda_V = 0.60$ (and $\lambda_C = 0.40$) the optimal strategy is $\Lambda = \{1, 1, 0, 0\}$.

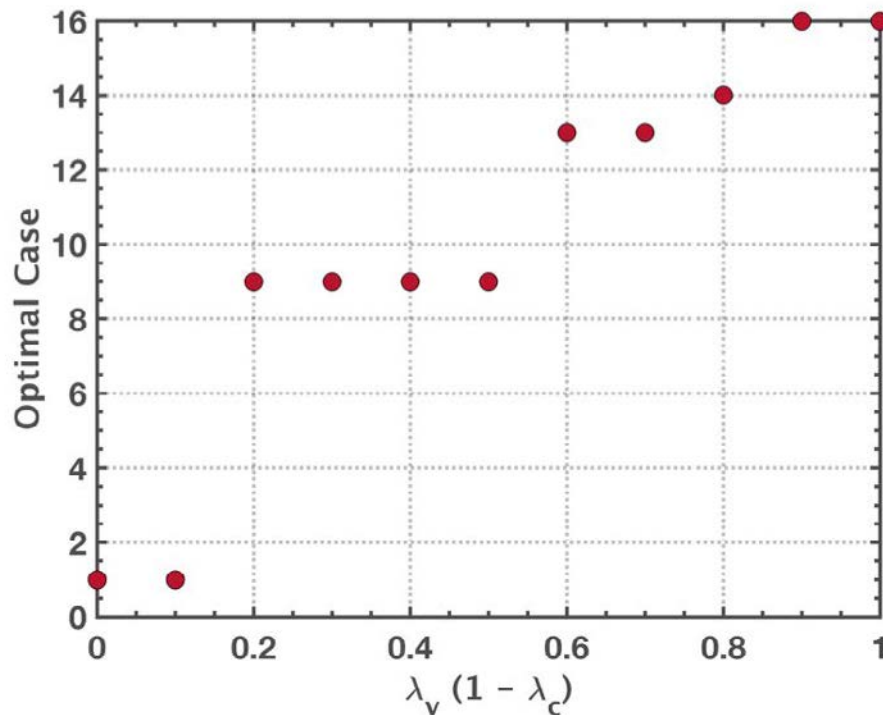


Figure 6.21: Optimal cases for different importance factor combinations for Steamboat Springs (Colorado)

6.3.3 Optimization Tests

The discussed intervention optimization was applied to the four communities shown previously in Section 6.1.1. Wind speed of 30 m/s and the wind directions for each community is

chosen based on Fig. 6.19, such that maximum vulnerability is observed in each case. Based on the results from the previous section, it is found that the optimal case is always found among the 16 possible intervention strategies applied at the same time to the entire community. Different intervention strategies are applied one at a time on the entire community and vulnerability analysis is conducted. Corresponding to the intervention strategy applied, the total cost of intervention is calculated. By combining the vulnerability and cost values for a specific combination of the importance factors, the fitness diagram is created. The corresponding vulnerability, total cost and fitness diagrams evaluated for each of the 4 communities are shown in Fig. 6.22, Fig. 6.23, Fig. 6.24 and Fig. 6.25. An important point to note is that the fitness diagram obtained for each of the analysis shown is for $\lambda_V = 0.50$ and $\lambda_C = 0.50$. As observed from the different diagrams, it is clear that effectiveness of each intervention strategy is different for each location. In order to achieve the same vulnerability different intervention strategies can be adopted for different communities. An optimal solution for one community might not be optimal for a different one. Furthermore, depending on the importance factors chosen this variation would be further accentuated. Hence, intervention strategies need to be customized based on the characteristics of a location and a one size fit all approach would be unsuitable. The results of the optimization show the need for individual community analysis since every community is unique.

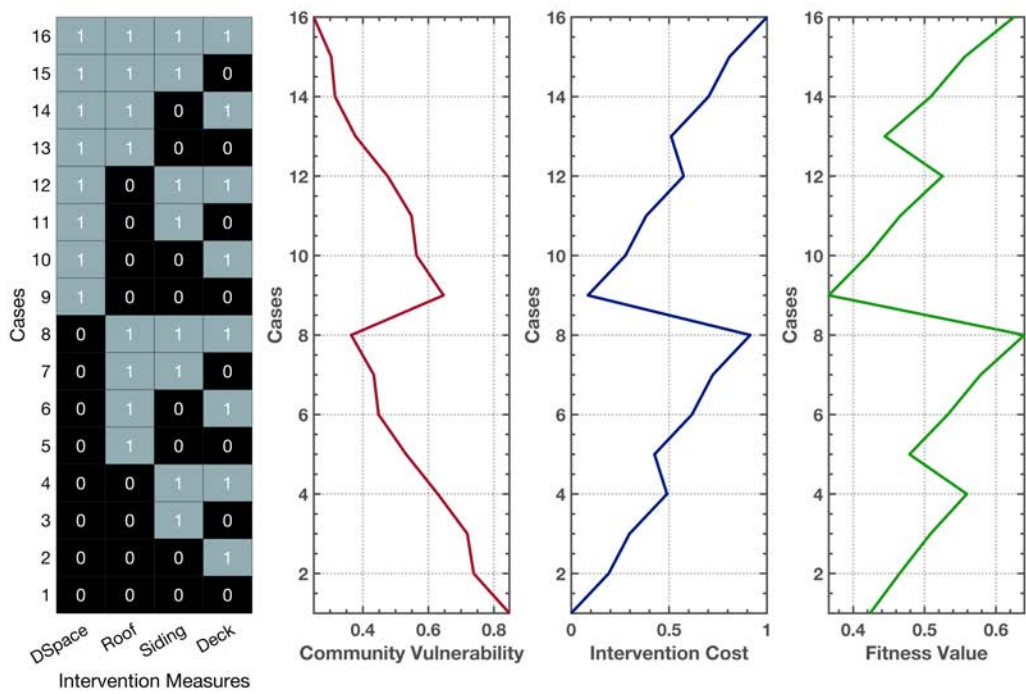


Figure 6.22: Vulnerability, intervention cost and total fitness digram shown for Austin

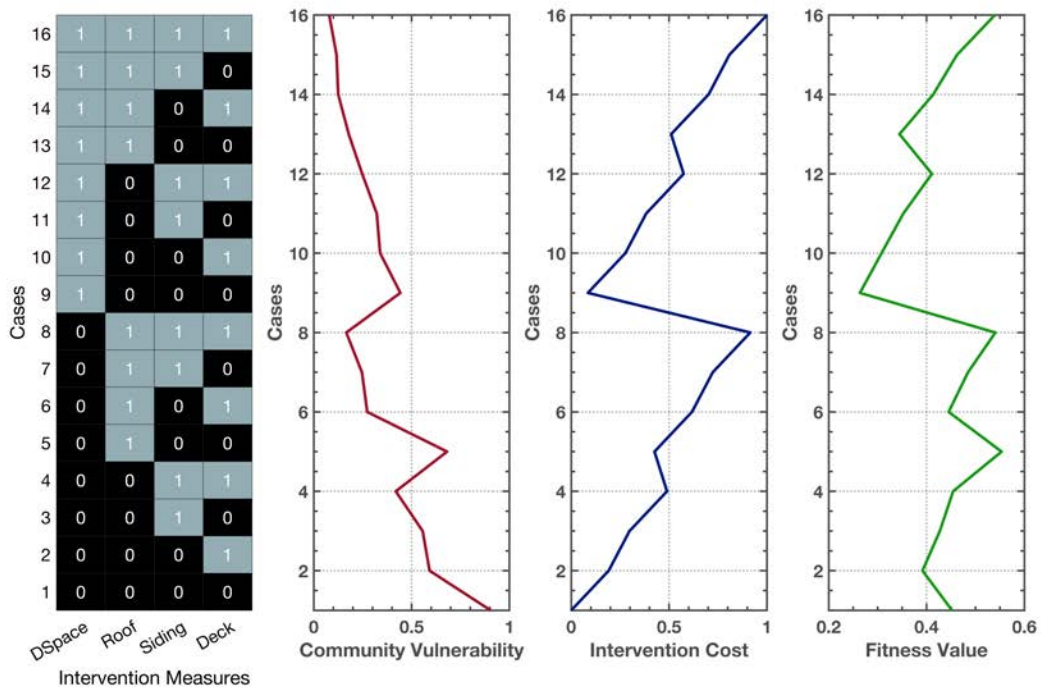


Figure 6.23: Vulnerability, intervention cost and total fitness digram shown for Jackson

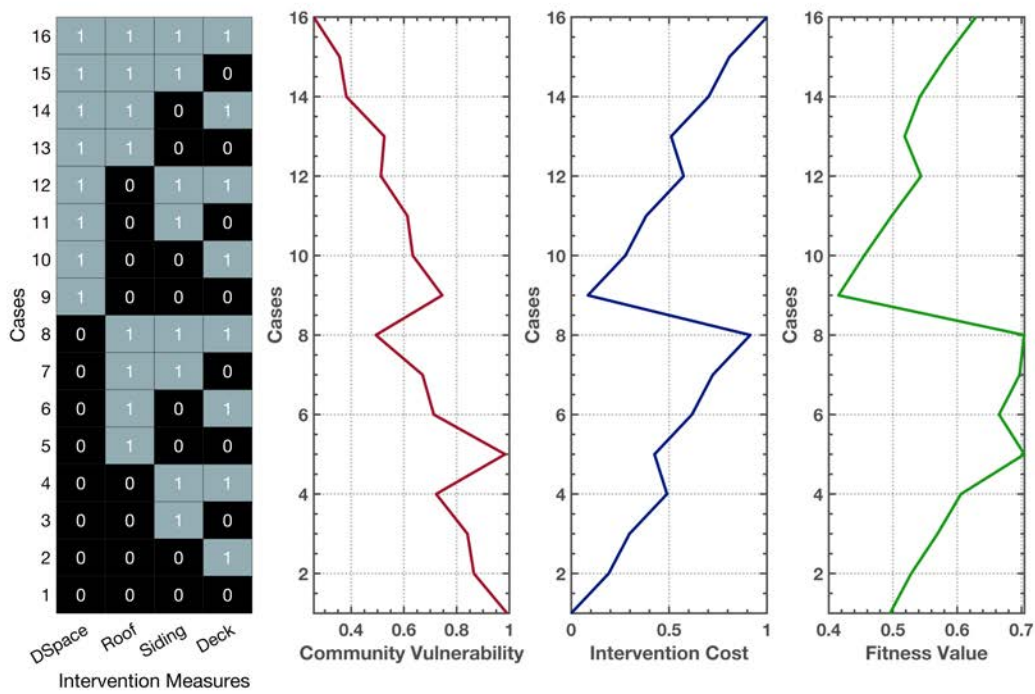


Figure 6.24: Vulnerability, intervention cost and total fitness digram shown for Oakland

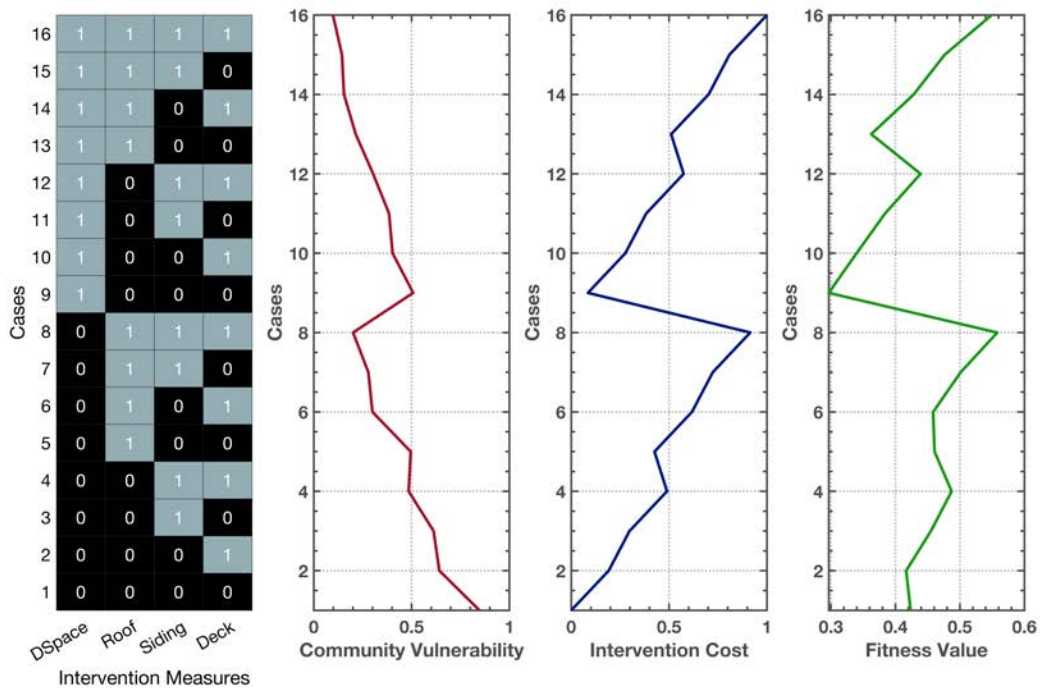


Figure 6.25: Vulnerability, intervention cost and total fitness digram shown for Steamboat

Chapter 7

Conclusions and Future Work

In light of the increasing potential risk to communities, effective strategies for wildfire management are required. Current strategies mainly entail fire suppression and fuel management in wildlands. There exists laws mandating mitigation requirements at the community level in certain places. For instance, the California 1992 Bates Bill, which was passed after the destruction from the 1991 Oakland Tunnel fire and the 1996 California Fire Plan, which is a cooperative effort between the State Board of Forestry and Fire Protection and California Board of Forestry, aimed at developing fire hazard maps. Researchers have identified that current tactics of severe fire suppression have led to significant rise in frequency of high intensity fires; thus, fire management focus needs to be shifted towards communities. Mitigation strategies geared towards complete containment of wildfires within the wildlands are nothing short of unrealistic. Therefore, the primary goal has to be on making communities resilient, with the purpose of minimizing potential losses. To better understand what factors govern the impact of WUI fires, tools to assess and quantify the risk to communities are required.

The observations from the analysis conducted in this study reaffirmed some of the long-stated findings from previous studies. We were able to quantify and understand the effects of intrinsic factors, which relate to factors that are naturally present in a community, and mitigation factors, which can be altered to regulate vulnerability of the community. The intrinsic factors were primarily identified as - (1) Wind speed (2) Wind direction (3) Community layout and (4) Wildland vegetation in the vicinity of the communities. High speed winds were found to strongly affect the generation of embers, which allowed the fire to spread easily. The discontinuities in the community layouts adversely affected fire propagation; however, the effect was minimal for high wind speeds. The wildlands surrounding the communities led to the creation of additional sources in the interior of communities, which caused significant increase in vulnerability. This increase was, however, a function of which structures the embers ignited. By igniting certain structures in the commu-

nity, the probability of wildfire propagation can be substantially increased. Certain structures have higher geographical contribution to fire spread than others.

To manage community vulnerability, mitigation factors such as presence of stray vegetation inside communities, layout and material properties of individual structures, and resources available for fire suppression, are critical. The effect of these factors was quantified in terms of mitigation strength, which was measured as the number of houses under some form of fire mitigation, and strategy efficiency, which was related to the selection of such houses. Both components were found to be strongly correlated to vulnerability; however, the effect of strategy was restricted to low to mid-range wind speeds only. Furthermore, depending on the wind conditions during a WUI fire, the community needs to have a certain level of resilience at the individual structural level, in order to have a fighting chance. These measures could include integration of fire-proof materials in household design, adoption of automatic sprinkler systems and/or management of stray vegetation in the household ignition zone. Essentially, a major responsibility of fire management lies within the hands of home owners; therefore, programs such as Fire Adapted Communities, Fire Adapted Communities Learning Network, Firewise Communities USA, and FireSmart Canada need to be implemented rigorously, which is going to require a paradigm shift in current fire management policies.

Using the formulated vulnerability model, wildfire risk for four different communities around the U.S. is evaluated using, local wind data, community buildings layout, and the probability of ignition in the wildland. It is observed that community risk is community specific and a function of different environmental and community parameters. A recently published study [141] found that California, Texas and Colorado experienced highest building losses due to wildfires among all states in the U.S. Interestingly, Wyoming is observed to have received significantly reduced losses. The analysis presented based on certain communities selected in the mentioned states present an antithesis to this observation. This leads to the conclusion that a generalized view point cannot be formulated for all communities based on cumulative analysis of large number of communities. Each community has a unique footprint as each community presents unique

characteristics, especially pertaining to their distinctive layout. There have been several valuable studies that have provided insightful information on the general trends of wildfire risk, but specific analysis of individual communities is also required such that custom intervention measures can be developed according to community properties. The results presented in this study highlight the importance of individual community risk analysis. This work lays the foundation for future studies that can aid in determining specific drivers for wildfire mitigation contingent on community characteristics.

This study was an attempt to start a dialogue in a new direction of quantifying wildfire risk to communities. There are assumptions and limitations in this study that hinder the "exact" applicability of the results to the evaluated communities. Due to the complexity of the wildfire problem the scope for this study had to be restricted. For instance, the formulated graph model was developed to be static in nature. The analysis did not include the presence of fences in backyards that have been shown to have an impact on fire propagation. The internal vegetation within the communities is not modeled exclusively. The proposed model is capable of incorporating the mentioned factors, however the purpose of this study is to lay the foundation. A generalized quantification framework for overall risk of communities is necessary to determine critical parameters for different types of communities. Even though the presented graph model is in its stage of infancy, once expanded, its application can be further extended to study other aspects of fire management, including but not limited to, sustainable urban planning and optimal firefighter mitigation strategies. The intervention strategy optimization provides a glimpse of the potential applications of the proposed graph model. By quantifying optimal strategies, changes in fire policies can be approached in a systematic fashion as it will allow policy makers, planners, and resource managers to develop long-term solutions to make communities more adaptable to wildfires. Specific design guidelines can be established, similar to design philosophies for other hazards, that are exclusive to each community and account for the mentioned critical variables.

Bibliography

- [1] C Whitlock. Land management: Forests, fires and climate. *Nature*, 432:28, 2004.
- [2] Editorial. Spreading like wildfire. *Nature Climate Change*, 7:755, 2017.
- [3] Editorial. Natural events and unnatural disasters. *Nature Plants*, 3, 2017.
- [4] J Bateman and G Davies. Greece wildfires a 'biblical disaster': At least 74 killed near athens as tourists forced to flee into sea. *The Telegraph*, 2018.
- [5] J Watts. Wildfires rage in arctic circle as sweden calls for help. *The Guardian*, 2018.
- [6] A L Westerling, H G Hidalgo, R Cayan, and T W Swetnam. Warming and earlier spring increase western u.s. forest wildfire activity. *Science*, 313:940, 2006.
- [7] T Schoennagel and et al. Adapt to more wildfire in western north american forests as climate changes. *Proceedings of National Academy of Science*, 114(18):4582–4590, 2017.
- [8] W M Jolly and et al. Climate-induced variations in global wildfire danger from 1979 to 2013. *Nature Communications*, 6:7537, 2015.
- [9] P E Dennison, S C Brewer, J D Arnold, and M A Moritz. Large wildfire trends in the western united states. *Geophysical Research Letters*, 41(8):2928–2933, 2014.
- [10] Natural Resources Canada. The state of canada's forests. Technical report, Canadian Forest Service, Ottawa, Canada, 2016.
- [11] S L Stephens and et al. Land use. managing forests and fire in changing climates. *Science*, 342(6154):41–42, 2013.
- [12] D E Calkin, J D Cohen, M A Finney, and M P Thomson. How risk management can prevent future wildfire disasters in the wildland-urban interface. *Proceedings of National Academy of Science*, 111(2), 2014.

- [13] M A Moritz and et al. Learning to coexist with wildfire. *Nature*, 515(7525):58–66, 2014.
- [14] M P North and et al. Environmental science. reform forest fire management. *Nature*, 349(6254):1280–1281, 2015.
- [15] S F Arno and J K Brown. Overcoming the paradox in managing wildland fire. *Western Wildlands (Montana Forest and Conservation Experiment Station, Missoula, MT)*, pages 40–46, 1991.
- [16] V C Radeloff and et al. Rapid growth of the us wildland-urban interface raises wildfire risk. *Proceedings of the National Academy of Sciences*, 115(13):3314–3319, 2018.
- [17] J K Balch and et al. Human-started wildfires expand the fire niche across the united states. *Proceedings of the National Academy of Sciences*, 114:2946–2951, 2016.
- [18] J Cohen and R D Stratton. Home destruction examination: Grass valley fire, lake arrowhead, ca. Technical Report R5-TP-026b, US Forest Service, Portland, OR, USA, 2008.
- [19] R Guidotti, H Chmielewski, V U Unnikrishnan, P Gardoni, T McAllister, and J W van de Lindt. Modeling the resilience of critical infrastructure: the role of network dependencies. *Sustainable and Resilient Infrastructure*, 1(3-4):153–168, 2016.
- [20] D Derya, B R Ellingwood, A B Liel, and S Dashti. Flood loss and recovery models for residential housing stock: A case study of the 2013 boulder, colorado floods. 12th International Conference on Structural Safety and Reliability, Vienna, Austria, 2017.
- [21] H Masoomi, J W van de Lindt, M R Ameri, T Q Do, and B M Webb. Combined wind-wave-surge hurricane-induced damage prediction for buildings. *Journal of Structural Engineering*, 145(1), 2019.
- [22] S Pilkington and H Mahmoud. Spatial and temporal variations in resilience to tropical cyclones along the united states coastline as determined by the multi-hazard hurricane impact level model. *Palgrave Communications*, 3(14), 2017.

- [23] H Masoomi and J W van de Lindt. Tornado community-level spatial damage prediction including pressure deficit modeling. *Sustainable and Resilient Infrastructure*, 2(4):179–193, 2017.
- [24] M Memari and et al. Minimal building fragility portfolio for damage assessment of communities subjected to tornadoes. *Journal of Structural Engineering*, 144(7), 2018.
- [25] T Maloney, B R Ellingwood, H Mahmoud, N Wang, Y Wang, and P Lin. Performance and risk to light-framed wood residential buildings subjected to tornadoes. *Structural Safety*, 70:35–47, 2018.
- [26] N Attary, J W van de Lindt, V U Unnikrishnan, A R Barbosa, and D T Cox. Methodology for development of physics-based tsunami fragilities. *Journal of Structural Engineering*, 143(5), 2017.
- [27] C Profita. Forest services says disaster funding bill will help fight wildfires this year. *OPB*, 2018.
- [28] B R Ellingwood. Earthquake risk assessment of building structures. *Reliability Engineering and Safety*, 74:251–262, 2001.
- [29] Y Li and B R Ellingwood. Hurricane damage to residential construction in the us: Importance of uncertainty modeling in risk assessment. *Engineering Structures*, 28:1009–1018, 2006.
- [30] I Bistinas and et al. Relationships between human population density and burned area at continental and global scales. *PLoS One*, page 8, 2013.
- [31] A D Syphard and et al. Unraveling the complexity of wildland urban interface fires. *Ecological Applications*, 17:1388–1402, 2007.
- [32] J Cohen. The wildland-urban interface fire problem. *Fremontia*, 38(2-3):16–22, 2010.

- [33] J D Cohen. Preventing disaster, home ignitability in the wildland-urban interface. *Journal of Forestry*, 98(3):15–21, 2000.
- [34] P H Gude, K Jones, R Rasker, and M C Greenwood. Evidence for the effect of homes on wildfire suppression costs. *International Journal of Wildland Fire*, 22:537–548, 2013.
- [35] J D Cohen and R Stratton. Home destruction within the hayman fire perimeter. Technical Report Gen. Tech. Rep. RMRS-GTR-114, U.S. Department of Agriculture, Forest Service, Rocky Mountain Research Station, CO, 2003.
- [36] J D Cohen. Relating flame radiation to home ignition using modeling and experimental crown fires. *Canadian Journal of Forest Research*, 34(8):1616–1626, 2004.
- [37] A D Syphard, J E Keeley, A B Massada, T J Brennan, and V C Radeloff. Housing arrangement and location determine the likelihood of housing loss due to wildfire. *PLoS One*, 7(3), 2013.
- [38] T D Penman, L Collins, A D Syphard, J E Keeley, and R A Bradstock. Influence of fuels, weather and the built environment on the exposure of property to wildfire. *PLoS One*, 9(10), 2014.
- [39] D Mollison. Spatial contact models for ecological and epidemic spread. *Journal of the Royal Statistical Society*, 39:283–326, 1977.
- [40] P Grassberger. On the critical behaviour of the general epidemic process and dynamical percolation. *Mathematical Biosciences*, 63:157–172, 1983.
- [41] M E J Newman. Spread of epidemic disease on networks. *Physical Review E*, 66, 2002.
- [42] M Kretzschmar, Y T H P van Duynhoven, and A J Severijnen. Modeling prevention strategies for gonorrhoea and chlamydia using stochastic network simulations. *American Journal of Epidemiology*, 144:306–317, 1996.

- [43] D T Haydon, M Chase-Topping, D J Shaw, L Matthews, J K Friar, J Wilesmith, and M E J Woolhouse. The construction and analysis of epidemic trees with reference to the 2001 uk foot-and-mouth outbreak. *Proceedings of the Royal Society B*, 270:121–127, 2003.
- [44] S Riley and et al. Transmission dynamics of the etiological agent of sars in hong kong: impact of public health interventions. *Science*, 300:1961–1966, 2003.
- [45] A S Klovdahl. Social networks and the spread of infectious diseases: the aids example. *Social Science and Medicine*, 21:1203–1216, 1985.
- [46] B R Ellingwood, H Cutler, P Gardoni, W G Peacock, J W van de Lindt, and N Wang. The centerville virtual community: a fully integrated decision model of interacting physical and social infrastructure systems. *Sustainable and Resilient Infrastructure*, 1(3-4):95–107, 2016.
- [47] G P Cimellaro, C Renschler, A Reinhorn, and L Arendt. Peoples: a framework for evaluating resilience. *The Bridge*, 10, 2016.
- [48] B R Ellingwood, J W van de Lindt, and T McAllister. A fully integrated model of interdependent physical infrastructure and social systems. *The Bridge*, 49(2), 2019.
- [49] M Memari, H Mahmoud, and B R Ellingwood. Post-earthquake fire performance of moment resisting frames with reduced beam section connections. *Journal of Constructional Steel Research*, 103:215–229, 2014.
- [50] M Memari and H Mahmoud. Framework for a performance-based analysis of fires following earthquakes. *Engineering Structures*, 171:794–805, 2018.
- [51] R C Rothermel. A mathematical model for predicting fire spread in wildland fuels. Technical Report Tech. Rep. INT-1 15, U.S. Department of Agriculture, Intermountain Forest and Range Experiment Station Research, 1972.

- [52] I Knight and J Coleman. A fire perimeter expansion algorithm based on Huygens' wavelet propagation. *International Journal of Wildland Fire*, 3:73–84, 1993.
- [53] P L Andrews. Behaveplus fire modeling system: past, present, and future. BehavePlus fire modeling system: past, present, and future, Bar Harbor, Maine, USA, 2007.
- [54] M A Finney. An overview of flammap fire modeling capabilities. Proceedings of the Fuels Management-How to Measure Success, pages 213–220, Portland, Ore, USA, 2006.
- [55] R D Stratton. Guidance on spatial wildland fire analysis: models, tools, and techniques. Technical Report General Technical Report RMRS-GTR-183, U.S. Department of Agriculture, Forest Service, Rocky Mountain Research Station, Ft. Collins, CO, USA, 2006.
- [56] M A Finney. Farsite: fire area simulator—model development and evaluation. Technical Report Tech. Rep. RMRS-RP-4, U.S. Department of Agriculture, Forest Service, Rocky Mountain Forest and Range Experiment Station, Ogden, Utah, USA, 1998.
- [57] M A Finney, I C Grenfell, and C W McHugh. A method for ensemble wildland fire simulation. *Environmental Modeling and Assessment*, 16(2):153–167, 2010.
- [58] I Altintas, J Block, H W Braun, R Callafon, M J Gollner, L Smarr, and A Trouve. Wifire: A real-time cyberinfrastructure for wildfire sensing and prediction. Large Wildland Fires Conference, pages 19–22, Missoula, MT, USA, 2014.
- [59] F A Albini. Spot fire distance from burning trees—a predictive model. Technical Report Gen. Tech. Rep. INT-56, U.S. Department of Agriculture, Forest Service, Intermountain Forest and Range Experiment Station, Ogden, UT, USA, 1979.
- [60] M C Rochoux, S Ricci, D Lucor, B Cuenot, and A Trouvé. Towards predictive data-driven simulations of wildfire spread. part i: Reduced-cost ensemble Kalman filter based on a polynomial chaos surrogate model for parameter estimation. *Natural Hazards and Earth System Sciences*, 14:2951–2973, 2014.

- [61] K McGrattan and et al. Fire dynamics simulator, user's guide. Technical report, National Institute of Standards and Technology, Gaithersburg, MD, 2013.
- [62] M A Finney. Fire growth using minimum travel time methods. *Canadian Journal of Forest Research*, 32(8):1420–1424, 2002.
- [63] A Stepanov and J M Smith. Modeling wildfire propagation with delaunay triangulation and shortest path algorithms. *European Journal of Operational Research*, 218(3):775–788, 2012.
- [64] M Hajian, E Melachrinoudis, and P Kubat. Modeling wildfire propagation with the stochastic shortest path: A fast simulation approach. *Environmental Modeling and Software*, 82(3):73–88, 2016.
- [65] A. Sekizawa and et al. Information system for supporting fire-fighting activities based on real time fire spread simulation. *Proceedings of Institute of Social Safety Science*, 11:117–120, 2000.
- [66] O Tsujihara, K Terada, and T Sawada. Development of simulation system of spreading fire occurring simultaneously in many places in an earthquake using petri-net. *Journal of Applied Computing in Civil Engineering*, 14:129–136, 2005.
- [67] W H Frandsen. Fire spread through porous fuels from the conservation of energy. *Combustion and Flame*, 16:9–16, 1971.
- [68] J K Brown. Field test of a rate-of-fire-spread model in slash fuels. Technical Report Research Paper INT-116, U.S. Department of Agriculture, Forest Service, Intermt. For. and Range Exp. Stn., Ogden, Utah, 1972.
- [69] J K Brown. Handbook for inventorying downed woody material. Technical Report General Technical Report INT-16, U.S. Department of Agriculture, Forest Service, Intermt. For. and Range Exp. Stn., Ogden, Utah, 1972.

- [70] A E Stevenson, D A Schermerhorn, and S C Miller. Simulation of southern california forest fires. Fifteenth Symp. (Int.) Combust. Proc. 1974, pages 147–155, Combust. Inst., Pittsburgh, PA, 1975.
- [71] F A Albini. Transport of firebrands by line thermals. *Combustion Science and Technology*, 32:277–288, 1983.
- [72] J C Sanderlin and R J Van Gelder. A simulation of fire behavior and suppression effectiveness for operation support in wildland fire management. Proceedings of the 1st International Conference on Mathematical Modeling, pages 619–630, University of Missouri, St. Louis, MO, 1977.
- [73] D G Anderson, E A Catchpole, N J DeMestre, and T Parkes. Modeling the spread of grass fires. *J. Aust. Math. Soc. (Ser. B)*, 23:451–466, 1982.
- [74] G D Richards. An elliptical growth model of forest fire fronts and its numerical solution. *Int. J. Numer. Meth. Eng.*, 30:1163–1179, 1990.
- [75] G D Richards. A general mathematical framework for modeling two-dimensional wildland fire spread. *Int. J. Wildland Fire*, 5(2):63–72, 1995.
- [76] I A French. Visualization techniques for the computer simulation of bushfires in two dimensions. Master’s thesis, University of New South Wales, Australian Defense Force Academy, Canberra, Australia, 1992.
- [77] J R Coleman and A L Sullivan. A real-time computer application for the prediction of fire spread across the landscape. *Simulation*, 67:230–240, 1996.
- [78] G D Richards and R W Bryce. A computer algorithm for simulating the spread of wildland fire perimeters for heterogeneous fuel and meteorological conditions. *Int. J. Wildland Fire*, 5(2):73–79, 1995.

- [79] J P Woycheese, P J Pagni, and D Liepmann. Brand propagation from large-scale fires. *J. Fire Prot. Eng.*, 10(2):32–44, 1999.
- [80] G P Forney. Smokeview (version 6), a tool for visualizing fire dynamics simulation data, volume i: User’s guide. Technical Report NIST Special Publication 1017-1, National Institute of Standards and Technology, Gaithersburg, Maryland, 2013.
- [81] M G Rollins. Landfire: a nationally consistent vegetation, wildland fire, and fuel assessment. *International Journal of Wildland Fire*, 18(3):235–249, 2009.
- [82] C Zhang and et al. Evaluation of a sensor-driven wildland fire spread modeling strategy using the fireflux experiment. 15th International Conference on Numerical Combustion, 2015.
- [83] Rollo, Luther, and Atkinson. Climate change and the effect of air pressure differences on building form in high risk bushfire areas. ANZSES conference, Geelong, 1999.
- [84] Cheney and Sullivan. Grassfires, fuel, weather and fire behavior. Technical report, CSIRO, Australia, 1997.
- [85] K Murphy, T Rich, and T Sexton. An assessment of fuel treatment effects on fire behavior, suppression effectiveness, and structure ignition on the angora fire, us. Technical Report Serv. Tech. Pap. R5-TP-025, United States Department of Agriculture, US, 2007.
- [86] H D Safford, D A Schmidt, and C H Carlson. Effects of fuel treatments on fire severity in an area of wildland–urban interface, angora fire, lake tahoe basin, california. *Ecol. Manage.*, 258:773–787, 2009.
- [87] S L Manzello, T G Cleary, J R Shields, and J C Yang. On the ignition of fuel beds by firebrands. *Fire Mater.*, 30:77–87, 2006.
- [88] S L Manzello, T G Cleary, J R Shields, and J C Yang. Ignition of mulch and grasses by firebrands in wildland–urban interface fires. *Int. J. Wildl. Fire*, 15:427, 2006.

- [89] S Manzano, J Shields, Y Hayashi, and D Nii. Investigating the vulnerabilities of structures to ignition from a firebrand attack. *Fire Saf. Sci.*, 9:143–154, 2008.
- [90] S L Manzano, A Maranghides, J R Shields, W E Mell, Y Hayashi, and D Nii. Mass and size distribution of firebrands generated from burning korean pine (*pinus koraiensis*) trees. *Fire Mater.*, 33:21–31, 2009.
- [91] S L Manzano, S H Park, and T G Cleary. Investigation on the ability of glowing firebrands deposited within crevices to ignite common building materials. *Fire Saf. J.*, 44:894–900, 2009.
- [92] A Maranghides and W Mell. A case study of a community affected by the witch and guejito fires. Technical Report Technical Note-1635, National Institute of Standards and Technology, Gaithersburg, MD, 2009.
- [93] J L Pellegrino, N P Bryner, and E L Johnsson. Wildland-urban interface fire research needs. Technical Report Workshop Summary Report, NIST, Gaithersburg, Maryland, 2013.
- [94] USDA and USDI. Protecting people and natural resources: a cohesive fuels treatment strategy. us healthy forests and rangelands plan. Technical report, USDA and USDI, 2006.
- [95] National Fire Protection Association (NFPA). Nfpa 1141: Standard for fire protection infrastructure for land development in wildland, rural and suburban areas. 2012.
- [96] National Fire Protection Association (NFPA). Nfpa 1142: Standard on water supplies for suburban and rural firefighting. 2012.
- [97] National Fire Protection Association (NFPA). Nfpa 1144: Standard for reducing structural ignition hazards from wildland fire. 2013.
- [98] National Fire Protection Association (NFPA). Nfpa 1143: Standard for wildland fire management. 2014.

- [99] ICC. International wildlan-urban interface code. Technical report, International Code Council, Country Club Hills, IL, 2012.
- [100] CBC. California build code, materials and construction methods for exterior wildfire exposure title 24, part 2, volume 1 of 2, chapter 7a (sacramento, ca: California code of regulations). 2009.
- [101] ASTM. Astm e-108-11: Standard test methods for fire tests of roof coverings. Technical report, ASTM International, West Conshohocken, PA, 2011.
- [102] ASTM. Astm e84-14, standard test method for surface burning characteristics of building materials. Technical report, ASTM International, West Conshohocken, PA, 2014.
- [103] ASTM. Astm e2726-12a: Standard test method for evaluating the fire-test-response of deck structures to burning brands. Technical report, ASTM International, West Conshohocken, PA, 2012.
- [104] ASTM. Astm d2898-10: Standard practice for accelerated weathering of fire- retardant-treated wood for fire testing. Technical report, ASTM International, West Conshohocken, PA, 2010.
- [105] UL. UI 790: Standard test methods for fire tests of roof coverings. Technical report, Underwriter Laboratories, Northbrook, IL, 2014.
- [106] I Karafyllidis and A Thanailakis. A model for predicting forest fire spreading using cellular automata. *Ecological Modeling*, 99(1):87–97, 1997.
- [107] OpenStreetMap contributors. Planet dump retrieved from <https://planet.osm.org> . <https://www.openstreetmap.org>, 2017.
- [108] J L Beverly, P Bothwell, J C R Conner, and E P K Herd. Assessing the exposure of the built environment to potential ignition sources generated from vegetative fuel. *International Journal of Wildfire*, 19:299–313, 2010.

- [109] E M Sparrow. A new and simpler formulation for radiative angle factors. *Journal of Heat Transfer*, 81:81–87, 1963.
- [110] N Kakuta, S Yokoyama, M Nakamura, and K Mabuchi. Estimation of radiative heat transfer using a geometric human model. *IEEE transactions on bio-medical engineering*, 48(3):324–331, 2012.
- [111] S Mazumder and M Ravishankar. General procedure for calculation of diffuse view factors between arbitrary planar polygons. *International Journal of Heat and Mass Transfer*, 55(23-24):7330–7335, 2012.
- [112] A Westhaver. Why some homes survived: Learning from the fort mcmurray wildfire disaster. Technical Report ICLR research paper series - no. 56, Institute for Catastrophic Loss Reduction, Toronto, Ontario, Canada, 2017.
- [113] J Martin and T Hillen. The spotting distribution of wildfires. *Applied Sciences*, 6:177, 2016.
- [114] T Hillen, B Greese, J Martin, and G de Vries. Birth-jump processes, with applications to wildfire spotting. *Journal of Theoretical Biology*, 9:104–127, 2015.
- [115] S L Manzello, A Maranghides, and W E Mell. Firebrand generation from burning vegetation. *International Journal of Wildfire*, 16:458–462, 2007.
- [116] H B Clements. Lift-off of forest firebrands. Technical Report Research Paper SE-159, USDA Forest Service, Southeastern Forest Experiment Station, Forest Service, USDA, Asheville, North Carolina, USA, 1977.
- [117] E W Dijkstra. A note on two problems in connection with graphs. *Numerische Mathematik*, 1:269–271, 1959.
- [118] J Y Yen. Finding the k shortest loopless paths in a network. *Management Science*, 17(11):712–716, 1971.

- [119] Wildland/Urban Interface Working Team. *Assessing wildfire hazards in the home ignition zone*. Natl. WUI Fire Program. Firewise Communities; NFPA, 2006.
- [120] J Xin and C Huang. Fire risk analysis of residential buildings based on scenario clusters and its application in fire risk management. *Fire Safety Journal*, 62:72–78, 2013.
- [121] C Bredeson. *Fire in oakland, california: Billion-dollar blaze*. *Enslow Publishers, Springfield, NJ, USA*, 1999.
- [122] P J Pagni. Causes of the 20 october 1991 oakland-hills conflagration. *Fire Safety Journal*, 21:331–339, 1993.
- [123] California Department of Forestry and Fire Protection. *Oakland/ berkeley hills fire of october 20, 1991, damage assessment survey*. Technical report, California Department of Forestry and Fire Protection, Berkeley, CA, USA, 1991.
- [124] P M Alexandre. Factors related to building loss due to wild res in the conterminous united states. *Ecological Applications*, 26(7):2323–2338, 2016.
- [125] P Bonacich. Power and centrality: A family of measures. *American Journal of Sociology*, 92:1170–1182, 1987.
- [126] L C Freeman. Centrality in social networks: Conceptual clarification. *Social Networks*, 1(3):215–239, 1979.
- [127] E Koo, P J Pagni, D R Weise, and J P Woycheese. Firebrands and spotting ignition in large-scale fires. *International Journal of Wildfire*, 19:818 – 843, 2010.
- [128] Partners in Protection. *FireSmart: protecting your community from wildfire (Second Edition)*. Capital Color Press Ltd. Edmonton, Alberta, 2003.
- [129] J P Woycheese. *Brand lofting and propagation from large-scale fires*. PhD thesis, University of California, Berkeley, 2000.

- [130] G K Dillon, J Menakis, and F Fay. Wildland fire potential: A tool for assessing wildfire risk and fuels management needs. Proceedings of the large wildland fires Conference (Proc. RMRS-P-73), pages 19–22, Missoula, Massachusetts, US, 2015.
- [131] NASF. Field guidance: identifying and prioritizing communities at risk. Technical report, National Association of State Foresters, 2003.
- [132] J H Scott, M P Thompson, and D E Calkin. Wildfire risk assessment framework for land and resource management. Technical Report General Technical Report RMRS-GTR-315, Rocky Mountain Research Station, Fort Collins, CO, U.S. Department of Agriculture, Forest Service, 2013.
- [133] M A Finney, C W McHugh, I C Grenfell, K L Riley, and K C Short. A simulation of probabilistic wildfire risk components for the continental united states. *Stochastic Environmental Research and Risk Assessment*, 25:973–1000, 2011.
- [134] L S Bradshaw, J E Deeming, R E Burgan, and Cohen J D. The 1978 national fire-danger rating system: technical documentation. Technical Report General Technical Report INT-169, Department of Agriculture, Forest Service, Southeaster Forest Experiment Station, Ogden, Utah, 1983.
- [135] P Vercammen, S Almasy, J Hanna, and M Park. Southern california fires growing quickly, forcing thousands to evacuate. *CNN*, 2017.
- [136] J J Sharples, G A Mills, R H D McRae, and R O Weber. Foehn like winds and elevated fire danger conditions in southeastern australia. *Journal of applied meteorology and climatology*, 49:1067–1095, 2010.
- [137] H Harris. Firefighters watch for hotspots at scene of oakland hills blaze. *East Bay Times*, 2017.
- [138] N Hansen. The cma evolution strategy: a tutorial. 2011.

- [139] N Hansen and S Kern. Evaluating the cma evolution strategy on multimodal test functions. International Conference on Parallel Problem Solving from Nature - PPSN VIII, Lecture Notes in Computer Science, vol 3242. Springer, Berlin, Heidelberg, 2004.
- [140] A Chulahwat and H Mahmoud. A combinatorial optimization approach for multi-hazard design of building systems with suspended floor slabs under wind and seismic hazards. *Engineering Structures*, 137:268–284, 2017.
- [141] H A Kramer, M H Mockrin, P M Alexandre, S I Stewart, and V C Radeloff. Where wildfires destroy buildings in the us relative to the wildland–urban interface and national fire outreach programs. *International Journal of Wildland Fire*, 27(5):329–341, 2018.

Appendix

LIST OF NOTATIONS

Parameter	Definition
\mathcal{E}	Total edge set of graph \mathcal{G}
$\mathcal{F}_{(.)}$	Set of surfaces for ignitable element $(.) = m, n$
\mathcal{G}	Graph of a community
$\mathcal{M}_{(x)}$	Adjacency list of x MPP
\mathcal{V}	Total node set of graph \mathcal{G}
$\mathcal{W}_{(k)}$	Node set of ignitable elements k
α	Intervention scaling factor for active strategies
β	Intervention scaling factor for passive strategies
$\epsilon_{(k)}^{(m)}$	Emissivity of surface k
η	Fire intervention (mitigation) strategy efficiency
$\Theta_{(k)}^{(m)}$	Inclination of source surface k
$\Theta_{(l)}^{(n)}$	Inclination of target surface l
$\theta_f^{(i)}$	Flame angle for node i
$\theta^{(i)}$	Wind direction at node i
$\theta_f^{(i)}$	Flame angle for node i
$\theta^{(i)}$	Wind direction at node i
λ_w	Scaling factor to account for wind effect
λ_t	Scaling factor to account for topography effect
μ	Fire intervention strength
$\phi^{(i,j)}$	Angle of edge joining node i to j w.r.t x-axis
A	Adjacency matrix
$A(x, y, t)$	State of cell at coordinates (x, y) at time t
$A_{(k)}^{(m)}$	Area of surface k
$A_w^{(m)}$	Area of ignitable element m
$a_{(i,j)}$	(i,j) entry of adjacency matrix A
$C^d(z)^n$	Total degree centrality of node z
$C_{d,i}^n(z)$	Indegree of node z
$C_{d,o}^n(z)$	Outdegree of node z
$C_{d,i}^w(m)$	Indegree of ignitable element m
$C_{d,o}^w(m)$	Outdegree of ignitable element m
$C_d(m)^w$	Total degree centrality of ignitable element m
$C_e^m(z)$	Eigenvector centrality of node z
$C_e^w(m)$	Eigenvector centrality of ignitable element m
$C_b^n(z)$	Betweenness centrality of node z

Parameter	Definition
$C_{b*}^n(z)$	Normalized betweenness centrality of node z
$C_{b*}^w(m)$	Normalized betweenness centrality of ignitable element m
$c^{(n)}$	Constant
$d_{(k,l)}^{(m,n)}$	Distance between surfaces k and l
d_{th}	Threshold distance for radiation
$d^{(i,j)}$	Distance between nodes i and j
$d_{conv}^{(i,j)}$	Convection threshold distance
$FTP^{(n)}$	Flux time product
$F_{cc}^{(i,j)}$	Wind correlation coefficient
$h_f^{(i)}$	Flame height
I	Fuel Density (in %)
K	Number of shortest paths
$N_{\mathcal{W}}$	Total number of ignitable elements in graph \mathcal{G}
$N_{\mathcal{M}(x)}$	Total members in adjacency list $\mathcal{M}(x)$
$N_{\mathcal{S}}$	Number of nodes in set \mathcal{S}
$N_{\mathcal{W}(m)}$	Number of nodes in ignitable element m
N^*	Normalization constant for betweenness centrality
n	Total number of nodes in graph \mathcal{G}
$P_{acc}^{(i,j)}$	Probability of access
$P_{tr}^{(i,j)}$	Probability of fire transfer from node i to j
$P_{cond}^{(i,j)}$	Probability of fire transfer by conduction from node i to j
$P_{MPP}^{(x)}$	Total probability of MPP x
$P_m^{(s)}$	Mean probability of K shortest paths for source node s
$P_i^{(s)}$	Probability of ignition for source node s
$Q_{cr}^{(n)}$	Critical flux for ignition
$q_{(l)}^{(m,n)}$	Total radiation heat flux on surface l
$q_{(k,l)}^{(m,n)}$	Radiation heat flux from surface k of element m to surface l of element n
$Rad[m, n]$	Radiation matrix between source element m and target element n
S	Ember spotting probability distribution function
$T^n(z)$	Transitivity of node z
$T^w(m)$	Transitivity of ignitable element m
T_f	Flame temperature

Parameter	Definition
T_a	Temperature of surroundings (Ambient temperature)
$t^{(n)}$	Minimum residence time for flames required for ignition
$t_r^{(l)}$	Residence time of each surface of ignited ignitable element m
$t_r^{(m)}$	
$V_n^{(i)}$	Fuel volume of source node i
$V^{(z)}$	Total vulnerability of node z
V_{avg}	Mean vulnerability of community
V_{total}	Total vulnerability calculated over a range of wind directions
$v_f^{(m,n)}$	View factor between surfaces of different ignitable elements
$v_f^{(k,l)}$	
v_w	Wind speed
$X_{conv}^{(i,j)}$	The event of ignition due to convection from node i to j
$X_{rad}^{(i,j)}$	The event of ignition due to radiation from node i to j
$X_{ember}^{(i,j)}$	The event of ignition due to ember spotting from node i to j